

INSTABILITIES OF SOME TIME-DEPENDENT FLOWS

by

Rory Thompson

A.B., San Diego State College
(1962)

M.S., San Diego State College
(1964)

SUBMITTED IN PARTIAL FULFILLMENT OF THE
REQUIREMENTS FOR THE DEGREE OF
DOCTOR OF PHILOSOPHY

at the

MASSACHUSETTS INSTITUTE OF TECHNOLOGY

September 1968

Signature of Author
Department of Meteorology, 19 August 1968

Certified by.....
Thesis Supervisor

Accepted by.....
Chairman, Departmental Committee on Graduate Students

Lindgren

WITHDRAWN
SEP FROM 1968
MIT LIBRARIES

INSTABILITIES OF SOME TIME-DEPENDENT FLOWS

by

Rory Thompson

Submitted to the Department of Meteorology

on August 19, 1968

in partial fulfillment of the requirements

for the degree of Doctor of Philosophy

ABSTRACT

The flow of fluid between two concentric cylinders is considered under three time-dependent forcings as an approach to instabilities of general time-dependent flows. The first is by gravity on a free surface; the annulus is rotating about an axis slightly tilted with respect to gravity, so there is a periodic motion. For certain geometries, there are resonances of inertial-gravity modes. These periodic motions cause a rectified mean azimuthal flow, including a central vortex for a cylinder, according to analysis of the viscous boundary layers. These mean flows can be unstable to shear oscillations, sometimes causing remarkable commotion which could disrupt geophysical modeling experiments. The theory is found to accord well with experiments.

The second type of forcing is periodic torsional motion

of the inner wall, with the outer wall held still. This causes periodic ring vortices for certain parameter ranges. These ring vortices are studied by several methods to ascertain the most practical ways to approach similar problems. Oscillations slow with respect to viscous diffusion time are essentially quasi-steady and give rise to essentially ordinary Taylor cells which turn on and off with each half-cycle. Faster oscillations give rise to more continuous Taylor cells which feed on the mean absolute centrifugal gradient. Critical Reynolds numbers are found by straight-forward numerical integrations and by harmonic expansions in time: purely periodic perturbations correspond to marginal growth rates. Experiments corroborate the results. Oscillations superposed on a mean rotation always destabilize.

The third type of forcing is similar to the second, except the inner cylinder is suddenly started. This illuminates what instability might mean on a flow that is changing anyway, and when a quasi-steady assumption can be used. In this case, one can be used even from small times, and the results fit experimental data of Chen and Christensen [1967] quite well.

Thesis Supervisor: Professor Louis N. Howard

Title: Professor of Mathematics

this thesis is dedicated to Luella

Table of Contents

- 1 Title Page
- 2 Abstract
- 4 Dedication
- 5 Table of Contents
- 8 Introduction
- 9 Literature review for general time dependence
- 10 Selection of problems
- 11 Chapter One -- The Slightly Tilted Cylinder
 - 11 Literature review
 - 11 for inviscid oscillations
 - 11 rectified boundary drifts
 - 12 shear instabilities with rotation
 - 12 slight tilt
 - 13 Notation and Equations
 - 16 Zero order interior solution
 - 17 eigenvalue expansions
 - 19 effects of finite Froude number
 - 21 resonances
 - 23 Zero order boundary solutions
 - 25 First order mean motion
 - 27 interior and ambiguity
 - 28 integration across the bottom boundary
 - 29 formulation of equations
 - 30 interior $v(0+,r)$
 - 34 radial flows in boundary

35	Shallow water
35	zero order
36	first order mean
37	Lagrangian drift
38	Side-Wall boundary layers
39	Shear instabilities on the mean azimuthal velocity
40	Ekman friction
41	Cartesian analog
42	bound on the shear parameter
43	Experiments
43	description of apparatus and operation
44	description of results
46	verification of theory
49	Chapter Two -- Periodic Centrifugal Instabilities
49	Literature review
53	Notation
53	Steady Taylor problem as example of numerical philosophy
54	Equations and basic flow
57	Solution of the initial value problem
59	boundary conditions
59	u,v forms
60	kinetic energy
62	critical Reynolds numbers
64	Quasi-steady and rapid oscillation limits

66	Mean Rotation superposed
66	Inner cylinder mean rotation
68	inertial waves
69	subharmonic resonance
71	Truncated spectral attempt
74	Experiments
74	description of apparatus and procedures
77	results for pure oscillation
77	results with superposed mean rotation
80	Inviscid oscillations
82	Chapter Three -- Suddenly Twisted Cylinder
82	Introduction
83	Scaling and estimate for critical
85	Quasi-steady approach
87	Numerical initial value solution
91	Proper finite-difference forms
92	'energy preserving' forms
93	disguised spectral forms
95	asymptotic approximations
96	Experimental comparison
97	After the critical time
99	approximate
100	analog set-up
104	Energy integral bounds
107	Acknowledgments
109	Bibliography
118	Biographical sketch

Instabilities of Some Time-Dependent Flows

Introduction

All geophysical flows are unsteady: the wind over water, the potential temperatures around a cumulus, and a long wave with a nascent cyclone imbedded, all change even as the perturbations grow, though usually on a longer time-scale. Yet, theories of wave growth or cyclogenesis classically assume the unperturbed flow to be steady. They generally do this for mathematical reasons: first, so the equations separate to leave a linear problem with constant coefficients in time, and second, to avoid difficulties with what it means to speak of instabilities on a flow which is changing anyway. So, how can one start toward understanding instabilities when the basic solution is not steady?

For certain ranges of parameters (such as the Reynolds number, the asymptotic behavior of the solution of the Navier-Stokes equations is not uniquely determined by the boundary conditions. E.g., the Benard problem of Boussinesq convection between parallel plates always has a conductive solution of no motion, but above a certain Rayleigh number, there also exist convective solutions which merge with the conductive solution as the Rayleigh number decreases to the critical parameter. This is known as "bifurcation". One

expects similar behavior for suitable non-dimensional parameters, even if some of them measure time-dependence. We have integral theorems such as Serrin's (1959a) which provide a basis in showing that there exist parameter ranges for which the basic flow is unique, but where are the limits of the ranges? Under what circumstances are the limits given by the linear theory, as Howard (1963) showed is true for the Benard problem?

The various fluid instabilities are so diverse that an attempt at a general theory would not be appropriate, though some general approaches to stability such as Serrin (1959a), Sorger (1966), and Ito (1961) have yielded weak but interesting uniqueness criteria for certain classes of flows. The classic sources of energy for a fluid instability are density differences (Benard, Rayleigh-Kelvin, and gravitational instabilities), shear (Kelvin-Helmholtz, Tollmien-Schlichting), and centrifugal forces (Taylor-Görtler), variously combined and complicated by rotation, magnetic fields, material temperature dependences, and various geometries. Of this wide choice, what problems can include time-dependence and yet be tractable?

There has been some work done on effects of time-dependence. Most of the relevant ones such as Lick (1965) and Currie (1967) which study turning on the heat in Benard convection, and D'Arcy (1951) which studies started concave flow, ignore the direct role of time, through assuming quasi-steadiness without particular investigation of when this may be appropriate, though it may hold over a time short compared to the time-scale of the basic flow. Sometimes this can be a bit disastrous. For instance, a stick

may be balanced upright on a hinge if it is oscillated vertically at the right frequency, even though a quasi-steady theory would indicate it to be always unstable. On the other hand, Benjamin and Ursell (1954) showed that when a cylinder containing an inviscid fluid with a free surface condition is shaken vertically with simple-harmonic acceleration, the fluid can be unstable even if the amplitude of the acceleration is much less than gravity, whereas a quasi-steady analysis always predicts stability. Yih (1967) considers horizontal oscillation of a plate with a viscous, shallow fluid on it in the long-wave limit, and likewise shows there exists instability. This does agree with quasi-steady theory.

So, what are suitable problems here? The easiest time-dependent centrifugal instabilities seem to be open, though Conrad and Criminale (1965) have done some quasi-steady work with certain weaknesses, and recently Sorger (1968, abstract only) has completed some Orr-Serrin bounds. The functions easiest to handle mathematically are simple harmonic plus steady [Chapter two of this thesis], and impulses [Chapter three]. Since it is desirable to approach time-dependence in easy stages, it is worth investigating Fultz's (1965) observation that weak periodic tide-like forces on a rotating fluid can cause considerable turmoil, unlike what a quasi-steady theory might suggest. This is the subject of Chapter One.

Forcing of the Fluid in a Slightly Tilted Rotating Cylinder or Annulus

The most common geophysical fluid dynamic laboratory models involve annuli (including cylinders), or perhaps spheres. Thus it is reasonable to study their responses to extraneous influences such as tides or imperfections of rotation. Kelvin (1880) found the oscillation modes for a rotating cylinder of fluid and described an experiment to excite axisymmetric modes with an axial plunger and disk, which was finally carried out by Fultz (1960). Baines (1967) theoretically studied axisymmetric forced oscillations of a finite rotating cylinder and found the asymptotic periodic flow contains pseudo-random patterns of internal shear for forcing slower than the rotation frequency. Aldridge (1967) experimentally studied axisymmetric modes of a rotating sphere excited by a small torsional oscillation.

Aldridge (1967) also studied the viscous boundary layer in his sphere and observed a rectified mean drift with a square law dependence on the oscillation amplitude. He also reported roll instabilities on the viscous boundaries with wavelengths and critical Reynolds number which suggest the instabilities are essentially time-dependent Görtler-Taylor vortices. Rectified currents in boundary layers have been studied for a long time, since at least Rayleigh (1884) and by many people. There are comprehensive reviews, e.g., by H. Schlichting (1968). Longuet-Higgins (1953) showed how two-dimensional, non-rotating gravity waves in shallow water cause a forward jet in the bottom boundary layer.

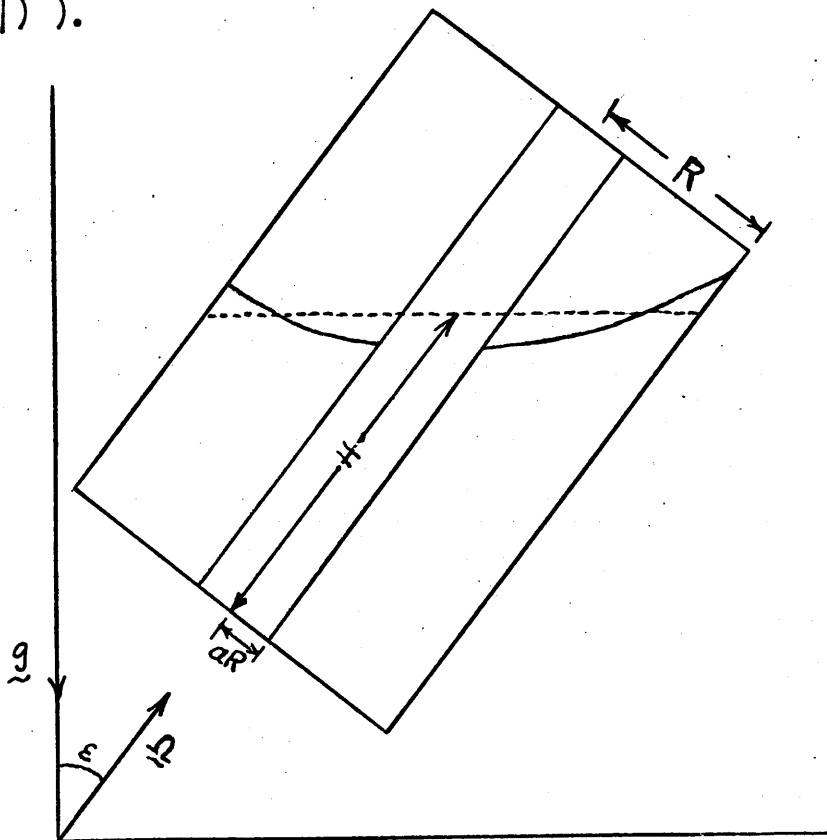
Instability of shear motion has been reviewed by Lin

(1949) and by Betchov and Criminale (1967), mostly for two-dimensional, non-rotating flows. Johnson (1963) gives a study of stability of one-dimensional parallel shear in a rotating, inviscid fluid, and gives a stability criterion for large wave numbers in a cylindrical shear layer.

The complicated steady motion due to precession of spheroids has been considered by Malkus (1964,1966) and Busse (1967), and of a cylinder by Johnson (1967). For rotating annuli, visible effects of the misalignment of the axis of rotation were reported by Fultz et al. (1959) and McDonald and Dicke (1967), but apparently the only previous studies of the effects have been by Fultz (1965) and Crow (1965). Fultz found that the water in a rotating, tilted rectangular box developed a powerful central vortex for a certain range of water depths. Crow found the same for a cylinder and showed that the depth of water corresponded to a resonance of inviscid fluid in a cylinder with an artificial pressure to keep the surface plane. In this thesis, the viscous boundary layers are considered carefully enough to show how vortices can arise, relieving the geostrophic ambiguity left by Crow, as well as considering all of the resonances, and improving the correspondence with experiments (also more thoroughly done) by considering the paraboloidal surface. The results also explain the puzzle proposed by Claes Rooth (private communication) as to why ink placed on the bottom of the cylinder often has intriguing scallop shapes which sometimes grow to form turbulence. A new observation is also made and explained that the ink will form concentric rings on the bottom.

Notation.

The cylinder is rotating at angular velocity Ω about its axis of symmetry at angle ϵ from vertical (so $\sin \epsilon = |\underline{g} \times \underline{\Omega}| / (|\underline{g}| |\underline{\Omega}|)$).



The outer radius is R , the inner is aR , the viscosity is ν , and the mean depth of the water is H . The usual cylindrical coordinates are taken rotating with the cylinder, so z is along its axis, r is radial, and θ is counterclockwise. The angular velocity Ω is chosen positive. So, the height around which to linearize is

$$H + \frac{\Omega^2}{2g} (r^2 - R^2 (1+a^2)/2) + \epsilon r \cos(\theta + \Omega t)$$

choosing θ counterclockwise from the projection of Ω onto horizontal. The deviation from this depth is denoted η^* . Let u be the radial velocity dr/dt , v be the tangential velocity $r d\theta/dt$, and w be the vertical velocity dz/dt . Let p be the

deviation pressure from hydrostatic, which latter includes centrifugal force and the rotating horizontal component of gravity as well as the vertical component.

In a frame rotating with the cylinder, the equations of motion for an incompressible, homogeneous fluid are:

$$\frac{\partial u}{\partial t} + u \frac{\partial u}{\partial r} + \frac{v}{r} \frac{\partial u}{\partial \theta} + w \frac{\partial u}{\partial z} - \frac{v^2}{r} = -\frac{\partial p}{\partial r} + \nu \left(\frac{\partial^2 u}{\partial r^2} + \frac{1}{r} \frac{\partial u}{\partial r} + \frac{1}{r^2} \frac{\partial^2 u}{\partial \theta^2} + \frac{\partial^2 u}{\partial z^2} - \frac{u}{r^2} - \frac{2\partial v}{r^2 \partial \theta} \right) + 2\Omega v,$$

$$\frac{\partial v}{\partial t} + u \frac{\partial v}{\partial r} + \frac{v}{r} \frac{\partial v}{\partial \theta} + w \frac{\partial v}{\partial z} + \frac{uv}{r} = -\frac{\partial p}{r \partial \theta} + \nu \left(\frac{\partial^2 v}{\partial r^2} + \frac{1}{r} \frac{\partial v}{\partial r} + \frac{1}{r^2} \frac{\partial^2 v}{\partial \theta^2} + \frac{\partial^2 v}{\partial z^2} - \frac{v}{r^2} + \frac{2\partial u}{r^2 \partial \theta} \right) - 2\Omega u,$$

$$\frac{\partial w}{\partial t} + u \frac{\partial w}{\partial r} + \frac{v}{r} \frac{\partial w}{\partial \theta} + w \frac{\partial w}{\partial z} = -\frac{\partial p}{\partial z} + \nu \left(\frac{\partial^2 w}{\partial r^2} + \frac{1}{r} \frac{\partial w}{\partial r} + \frac{1}{r^2} \frac{\partial^2 w}{\partial \theta^2} + \frac{\partial^2 w}{\partial z^2} \right),$$

$$\frac{\partial u}{\partial r} + \frac{u}{r} + \frac{\partial v}{r \partial \theta} + \frac{\partial w}{\partial z} = 0. \quad (1)$$

The boundary conditions are:

$$u = v = w = 0 \text{ at } z = 0,$$

$$u = v = w = 0 \text{ at } r = R \text{ and } r = aR \text{ [unless } a=0],$$

$$\frac{r\Omega^2 \mu}{2\rho} \left(\frac{\partial u}{\partial r} + \frac{\partial w}{\partial z} \right) - \frac{2u}{r} \frac{\partial w}{\partial z} + p + g(H - z + r \epsilon \cos(\theta + \Omega t)) + \frac{\Omega^2}{2} (r^2 - R^2(1+a^2)/2) = 0,$$

$$w = dz/dt,$$

$$\frac{r\Omega^2 \mu}{2} \left(\frac{\partial v}{\partial r} - \frac{v}{r} + \frac{1}{r} \frac{\partial u}{\partial \theta} \right) + \mu \left(\frac{\partial v}{\partial z} + \frac{1}{r} \frac{\partial w}{\partial \theta} \right) = 0,$$

$$\frac{\Omega^2 r}{2} (-pp + \epsilon g \eta^* + 2u \frac{\partial u}{\partial r}) + \mu \left(\frac{\partial u}{\partial z} + \frac{\partial w}{\partial r} \right) = 0.$$

The last four boundary conditions all hold at the surface,

$$z = H + \epsilon r \cos(\theta + \Omega t) + \frac{\Omega^2}{2g} (r^2 - R^2(1+a^2)/2) + \eta^*.$$

Surface tension is neglected. Now scale t by Ω^{-1} , r and z by R ,

u, v , and w by $\epsilon \Omega R$, p by $\epsilon R \Omega^2$, and η^* by ϵFR , where $F = \Omega^2 R/g$.

Also define $E = \nu/\Omega^2 R$. Then the non-dimensional equations of motion are:

$$\frac{\partial u}{\partial t} + \epsilon \left[u \frac{\partial u}{\partial r} + \frac{v}{r} \frac{\partial u}{\partial \theta} - \frac{v^2}{r} + w \frac{\partial u}{\partial z} \right] = -\frac{\partial p}{\partial r} + 2v + E \left[\frac{\partial^2 u}{\partial r^2} + \frac{1}{r} \frac{\partial u}{\partial r} + \frac{1}{r^2} \frac{\partial^2 u}{\partial \theta^2} + \frac{\partial^2 u}{\partial z^2} - \frac{u}{r^2} - \frac{2\partial v}{r^2 \partial \theta} \right],$$

$$\frac{\partial v}{\partial t} + \epsilon \left[u \frac{\partial v}{\partial r} + \frac{v}{r} \frac{\partial v}{\partial \theta} + \frac{uv}{r} + w \frac{\partial v}{\partial z} \right] = -\frac{1}{r} \frac{\partial p}{\partial \theta} - 2u + E \left[\frac{\partial^2 v}{\partial r^2} + \frac{1}{r} \frac{\partial v}{\partial r} + \frac{1}{r^2} \frac{\partial^2 v}{\partial \theta^2} + \frac{\partial^2 v}{\partial z^2} - \frac{v}{r^2} + \frac{2\partial u}{r^2 \partial \theta} \right],$$

$$\frac{\partial w}{\partial t} + \epsilon \left[u \frac{\partial w}{\partial r} + \frac{v}{r} \frac{\partial w}{\partial \theta} + w \frac{\partial w}{\partial z} \right] = -\frac{\partial p}{\partial z} + E \left[\frac{\partial^2 w}{\partial r^2} + \frac{1}{r} \frac{\partial w}{\partial r} + \frac{1}{r^2} \frac{\partial^2 w}{\partial \theta^2} + \frac{\partial^2 w}{\partial z^2} \right],$$

$$\frac{\partial u}{\partial r} + \frac{u}{r} + \frac{1}{r} \frac{\partial v}{\partial \theta} + \frac{\partial w}{\partial z} = 0, \quad (2)$$

with boundary conditions of

$$u = v = w = 0 \quad \text{at } z = 0,$$

$$u = v = w = 0 \quad \text{at } r = 1 \text{ and } r = a \quad [\neq 0],$$

$$-rFE \left(\frac{\partial u}{\partial z} + \frac{\partial w}{\partial r} \right) - 2E \frac{\partial w}{\partial z} + p = \eta,$$

$$w = -r \sin(\theta + t) + F \frac{\partial \eta}{\partial t} + Fur +$$

$$\varepsilon [u \cos(\theta + t) - v \sin(\theta + t) + Fu \frac{\partial \eta}{\partial r} + Fv \frac{\partial \eta}{\partial \theta}],$$

$$rF [E^{-1}(p - \eta) - \frac{\partial u}{\partial r}] + \frac{\partial u}{\partial z} + \frac{\partial w}{\partial r} = 0,$$

$$-F [r^2 \frac{\partial v}{\partial r} + \frac{\partial u}{\partial \theta}] + \frac{\partial v}{\partial z} + \frac{1}{r} \frac{\partial w}{\partial \theta} = 0,$$

with the last four equalities holding at

$$z = \frac{F}{2} [r^2 - (1+a^2)/2] + \varepsilon [r \cos(\theta + t) + F\eta] + H/R.$$

Expand the non-dimensional variables in the small parameter

ε , so $u = u_0 + \varepsilon u_1 + O(\varepsilon^2)$, etc., and separate the

coefficients of ε to get the zero order (linear) equations

(3) and the first order equations (16).

$$\frac{\partial u_0}{\partial t} = -\frac{\partial p_0}{\partial r} + 2v_0 + E \left(\nabla^2 u_0 - \frac{u_0}{r^2} - \frac{2}{r^2} \frac{\partial v_0}{\partial \theta} \right),$$

$$\frac{\partial v_0}{\partial t} = -\frac{\partial p_0}{r \partial \theta} - 2u_0 + E \left(\nabla^2 v_0 - \frac{v_0}{r^2} + \frac{2}{r^2} \frac{\partial u_0}{\partial \theta} \right),$$

$$\frac{\partial w_0}{\partial t} = -\frac{\partial p_0}{\partial z} + E \nabla^2 w_0,$$

$$\frac{\partial u_0}{\partial r} + \frac{u_0}{r} + \frac{\partial v_0}{r \partial \theta} + \frac{\partial w_0}{\partial z} = 0,$$

$$\nabla^2 \equiv \frac{\partial^2}{\partial r^2} + \frac{1}{r} \frac{\partial}{\partial r} + \frac{1}{r^2} \frac{\partial^2}{\partial \theta^2} + \frac{\partial^2}{\partial z^2}.$$

(3)

The zero-order inviscid boundary conditions are

$$w_0 = 0 \quad \text{at } z = 0,$$

$$u_0 = 0 \quad \text{at } r = 1 \text{ and at } r = a \quad [\neq 0],$$

$$\text{and } p_0 = \eta \quad \text{and } w_0 = -r \sin(\theta + t) + F \frac{\partial \eta}{\partial t} + Fur$$

$$-2E \frac{\partial u_0}{\partial z}$$

$$\text{at } z = F(2r^2 - 1 - a^2)/4 + H/R.$$

The zero-order viscous boundary conditions are

$$u_0 = v_0 = 0 \text{ at } z = 0,$$

$$v_0 = w_0 = 0 \text{ at } r = 1 \text{ and } r = a \text{ [unless } a = 0 \text{],}$$

$$\text{and } rF[E(r-\eta)\frac{\partial u}{\partial r}] + \frac{\partial u}{\partial z} + \frac{\partial w}{\partial r} = 0 \text{ at } z = F(2r^2 - 1 - a^2)/4 + H/R,$$

$$\frac{\partial v}{\partial z} + \frac{1}{r} \frac{\partial w}{\partial \theta} - F[r^2 \frac{\partial (v/r)}{\partial r} + \frac{\partial u}{\partial \theta}].$$

Zero-order Interior Solution

In the interior, E is negligible [$0(10^{-5})$] in the experiments discussed later], so set $E = 0$ in (3) for the interior behavior. The equations are linear, so only keeping the driven components of flow, write

$$w_0 = w(r, z) \sin(\theta + t), \quad \eta_0 = \eta(r) \cos(\theta + t), \quad u_0 = u(r, z) \sin(\theta + t),$$

$$p_0 = p(r, z) \cos(\theta + t), \text{ and } v_0 = v(r, z) \cos(\theta + t), \text{ so}$$

$$u = -\frac{\partial p}{\partial r} + 2v$$

$$-v = p/r - 2u$$

$$w = -\frac{\partial p}{\partial z}$$

(4)

$$\frac{\partial u}{\partial r} + \frac{u}{r} - \frac{v}{r} + \frac{\partial w}{\partial z} = 0$$

are the interior equations, with boundary conditions

$$w = 0 \text{ at } z = 0,$$

$$u = 0 \text{ at } r = 1 \text{ and } r = a \text{ [}\neq 0\text{]},$$

$$p = \eta \text{ and } w = -r - F\eta + Fru \text{ at } z = F(2r^2 - 1 - a^2)/4 + H/R.$$

Equations (4) imply

$$w = -\frac{\partial p}{\partial z}$$

$$u = (\frac{\partial p}{\partial r} + 2p/r)/3,$$

$$v = (2\frac{\partial p}{\partial r} + p/r)/3,$$

which can be substituted into the continuity equation to yield:

$$\frac{\partial^2 p}{\partial \lambda^2} + \frac{1}{\lambda} \frac{\partial p}{\partial \lambda} - \frac{p}{\lambda^2} = 3 \frac{\partial^2 p}{\partial z^2} \tag{5}$$

with boundary conditions

$$\begin{aligned} \frac{\partial p}{\partial z} &= 0 \text{ at } z = 0, \\ \frac{\partial p}{\partial \lambda} + 2p/r &= 0 \text{ at } r = 1 \text{ and } r = a \text{ [unless } a = 0], \\ \frac{\partial p}{\partial z} &= r + Fp/3 - Fr \frac{\partial p}{\partial \lambda} / 3 \text{ at } z = F(2r^2 - 1 - a^2)/4 + H/R. \end{aligned}$$

By the usual separation techniques, one solves

$$Z''(z) + \frac{\lambda^2}{3} Z = 0 \text{ and } r R''(r) + rR' + (\lambda^2 r^2 - 1)R = 0.$$

The solutions are of the form

$$RZ = [J_1(\lambda r) - \frac{\lambda J_1'(\lambda) + 2J_1(\lambda)}{\lambda Y_1'(\lambda) + 2Y_1(\lambda)} Y_1(\lambda r)] \cos(\frac{\lambda}{\sqrt{3}} z),$$

with λ to solve

$$\begin{aligned} [a\lambda J_1'(a\lambda) + 2J_1(a\lambda)] [\lambda Y_1'(\lambda) + 2Y_1(\lambda)] = \\ [\lambda J_1'(\lambda) + 2J_1(\lambda)] [a\lambda Y_1'(a\lambda) + 2Y_1(a\lambda)]. \end{aligned}$$

For $a = 0$, the solutions are of the form

$$RZ = J_1(\lambda r) \cos(\frac{\lambda}{\sqrt{3}} z),$$

with λ to solve

$$\lambda J_1'(\lambda) + 2 J_1(\lambda) = 0. \tag{6}$$

For $\lambda^2 < 0$, there is no non-zero $\mu = i\lambda$ which satisfies $\mu I_1'(\mu) + 2I_1(\mu) = 0$, since $I_1(x) = J_1(ix)$ is monotonic. Using the Bessel function tables of Abramowitz and Stegun (1965) for initial estimates, the first five roots of (6) were found by use of the polynomial approximations to J_1 of E.E.Allen (1954) to be

$$\begin{aligned} \lambda_1 = 2.7346426, \lambda_2 = 5.691402, \lambda_3 = 8.76658, \\ \lambda_4 = 11.87525, \text{ and } \lambda_5 = 14.99735. \end{aligned}$$

For $a \neq 0$, there is also such an asymptotically equally

spaced sequence of λ 's, and in fact, $\lambda_n \sim n\pi/(1-a)$, for $(1-a)/n$ small. Note this asymptotic relation already holds for $a = 0$. The motions corresponding to these eigenvalues are plainly inertial waves, which will be influenced by gravity through the surface boundary condition. There is also one $\mu = i\lambda$ for $a \neq 0$, giving an additional eigenfunction

$$RZ = [I_1(\mu r) - \frac{\mu I_1'(\mu) + 2I_1(\mu)}{\mu K_1'(\mu) + 2K_1(\mu)} K_1(\mu r)] \cosh \frac{\mu z}{\sqrt{a}}, \quad (7)$$

where μ satisfies

$$[a\mu K_1'(a\mu) + 2K_1(a\mu)][\mu I_1'(\mu) + 2I_1(\mu)] = [a\mu I_1'(a\mu) + 2I_1(a\mu)][\mu K_1'(\mu) + 2K_1(\mu)]. \quad (8)$$

This μ can be found approximately by considering the shapes of the graphs for $sI_1'(s) + 2I_1(s)$ and $sK_1'(s) + 2K_1(s)$. By considering the values at $a\mu$ and μ as μ increases, plainly the left side of (8) is positive but the right side is negative until $a\mu > \mu^* \approx 1.329$. Plainly also, the left is always < 1 , and very much so for $a \ll 1$, but the right is > 1 for $a\mu > \mu^{**} \approx 2.113$, so as $a \rightarrow 0$, $\mu \rightarrow 1.329/a$. For $a \rightarrow 1$, one can expand in Taylor series around μ^* to get $\mu \approx \pi \sqrt{3 \frac{1-a}{a}}$. If one needs μ for only one given a , probably the most practical way to find it accurately is by using (8) with tables. E.g. for $a = 0.9$, $\mu \approx 1.81$. From (7), this mode is seen to resemble a Kelvin wave in decaying exponentially away from the walls, as well as downward. Since \sinh has but one real zero, there are no resonances for this mode.

Each of the modes satisfy the homogenous bottom and side boundary conditions; a sum is necessary to satisfy the non-

homogenous surface condition boundary condition. Unfortunately, as well as being inhomogenous, it is inseparable, so some sort of expansion is necessary. F is small in the experiments, so can be used as the expansion parameter. First consider the case $a = 0$ (i.e., a cylinder), so

$$p = \sum_{n=1}^{\infty} A_n \cos\left(\frac{\lambda_n}{\sqrt{3}} z\right) J_1(\lambda_n r) \quad (9)$$

where λ_n satisfies

$$\lambda_n J_1'(\lambda_n) + 2 J_1(\lambda_n) = 0.$$

The surface boundary condition has yet to be satisfied. Using a Taylor expansion in F , this condition is

$$\frac{\partial p}{\partial z} + \frac{F}{4} (2r^2 - 1) \frac{\partial^2 p}{\partial z^2} = r + \frac{Fp}{r} - \frac{1}{3} Fr \frac{\partial p}{\partial r} + O(F^2) \quad (10)$$

at $z = H/R$. Perhaps such an expansion is questionable for the higher modes (those for which $nF > 1$), but these will not be studied much, since they are more susceptible to friction, less effected by F , and of less interest anyway.

The coefficients in the expression (9) for p will be found by a Galerkin technique of making the error in satisfying the condition (10) orthogonal to each of the functions $J_1(\lambda_n r)$. That is, to make

$$\sum_{n=1}^{\infty} A_n \left\{ -\frac{\lambda_n}{\sqrt{3}} \sin\left(\frac{\lambda_n H}{\sqrt{3} R}\right) J_1(\lambda_n r) - \frac{F \lambda_n^2}{12} \cos\left(\frac{\lambda_n H}{\sqrt{3} R}\right) (2r^2 - 1) J_1(\lambda_n r) \right. \\ \left. - \frac{F}{3} \cos\left(\frac{\lambda_n H}{\sqrt{3} R}\right) J_1(\lambda_n r) + \frac{F \lambda_n}{\sqrt{3}} \cos\left(\frac{\lambda_n H}{\sqrt{3} R}\right) r J_1'(\lambda_n r) \right\} = r, \quad (11)$$

multiply each side by $r J_1(\lambda_n r)$ and integrate over $[0, 1]$. The

resulting linear system determines the response $\{A_n\}$ unless the determinant is zero, in which case there is a resonance.

The case $F = 0$ is easy, for then the equations are
$$\sum_{n=1}^{\infty} A_n \left\{ -\frac{\lambda_n}{\sqrt{3}} \sin\left(\frac{\lambda_n H}{\sqrt{3}R}\right) \int_0^1 r J_1(\lambda_n r) J(\lambda_n r) dr \right\} = \int_0^1 r^2 J_1(\lambda_n r) dr, \text{ for } k=1(1)\infty.$$

Then using equation (6.49) page 89 of Tranter (1956) and noting that

$$\frac{\partial}{\partial t} (t^2 J_2(t)) = t^2 J_1(t),$$

the equations for $F = 0$ are simply

$$A_k \left\{ -\frac{\lambda_k}{\sqrt{3}} \sin\left(\frac{\lambda_k H}{\sqrt{3}R}\right) J_1^2(\lambda_k) \frac{1 + \frac{3\lambda_k^2}{2}}{2} \right\} = J_2(\lambda_k), \text{ for } k=1(1)\infty.$$

Clearly the determinant is zero iff one of the coefficients of $\{A_k\}$ is zero, and otherwise the response is determinate:

$$p = - \sum_{n=1}^{\infty} 2\sqrt{3} J_2(\lambda_n).$$

While the pressure formally has a dense set of singular depths (multiples of $H/R = 1.992, .957, .625, .458, \text{ etc.}$) one does not expect to see the higher modes, since viscosity will damp them more, especially since

$$\frac{2\sqrt{3} J_2(\lambda_n)}{(\lambda_n + \frac{3}{2}\lambda_n) J_1^2(\lambda_n)} = 1.32, -0.50, 0.30, -0.18, 0.06, \text{ etc.}$$

goes rapidly to zero as n increases, so the resonances get narrower as well as shallower as n increases. The zero-order solutions for $F=0$ are thus:

$$p_0 = - \varepsilon \sum_{n=1}^{\infty} \left[\frac{2\sqrt{3} J_2(\lambda_n)}{\lambda_n^2 + 3} \frac{J_2(\lambda_n)}{J_1^2(\lambda_n)} \right] J_1(\lambda_n r) \cos \frac{\lambda_n z}{\sqrt{3}} \cos(\theta + t),$$

abbreviated

$$\begin{aligned} p_0 &= \sum A_n J_1(\lambda_n r) \cos\left(\frac{\lambda_n z}{\sqrt{3}}\right) \cos(\theta + t), \\ u_0 &= \sum \frac{A_n \lambda_n}{6} [3J_0(\lambda_n r) + J_2(\lambda_n r)] \cos\left(\frac{\lambda_n z}{\sqrt{3}}\right) \sin(\theta + t), \\ v_0 &= \sum \frac{A_n \lambda_n}{6} [3J_0(\lambda_n r) - J_2(\lambda_n r)] \cos\left(\frac{\lambda_n z}{\sqrt{3}}\right) \cos(\theta + t), \\ w_0 &= \sum \frac{A_n \lambda_n}{\sqrt{3}} J_1(\lambda_n r) \sin\left(\frac{\lambda_n z}{\sqrt{3}}\right) \sin(\theta + t). \end{aligned} \quad (11)$$

The above are dimensionless; dimensionalizing, one has, e.g.,

$$u = -\epsilon \Omega R \sum_{n=1}^{\infty} \frac{\lambda_n J_2(\lambda_n)}{\sqrt{3}(\lambda_n)^2 J_2(\lambda_n) \sin(\frac{\lambda_n H}{\sqrt{3}R})} [3J_0(\frac{\lambda_n R}{R}) + J_2(\frac{\lambda_n R}{R})] \cos(\frac{\lambda_n z}{\sqrt{3}}) \sin(\Omega t + \theta),$$

so the magnitudes depend only on $(\epsilon R \Omega)$ and H/R . One expects the qualitative behavior of the system for $F = 0$ to carry over for $F > 0$, at least for small F 's. So, the main task is to determine how much the first few resonance depths change with F .

The first step is to solve for just the first coefficient. We write $p \approx A_1 \cos(\frac{\lambda_1 z}{\sqrt{3}}) J_1(\lambda_1 r)$ and make the error in the surface boundary condition (10) orthogonal to $J_1(\lambda_1 r)$:

$$\int_0^1 r J_1(\lambda_1 r) \left\{ A_1 \left[-\frac{\lambda_1}{\sqrt{3}} \tan(\frac{\lambda_1 H}{\sqrt{3}R}) J_1(\lambda_1 r) - F \frac{\lambda_1^2}{12} (2r^2 - 1) J_1(\lambda_1 r) + \frac{1}{3} F J_1(\lambda_1 r) + \frac{F \lambda_1 r J_1'(\lambda_1 r)}{3} \right] - r \right\} dr = 0.$$

I.e., we truncate the system (11) to the first element to get

$$A_1 \left\{ \left[-\frac{\lambda_1}{\sqrt{3}} \sin(\frac{\lambda_1 H}{\sqrt{3}R}) + F \frac{\lambda_1^2}{12} \cos(\frac{\lambda_1 H}{\sqrt{3}R}) + \frac{1}{3} F \cos(\frac{\lambda_1 H}{\sqrt{3}R}) \right] J_1^2(\lambda_1) \frac{1 + \frac{3}{2} \lambda_1^2}{2} - F \frac{\lambda_1^2}{2} \int_0^1 r^3 J_1^2(\lambda_1 r) dr \cos(\frac{\lambda_1 H}{\sqrt{3}R}) + F \frac{\lambda_1}{2} \cos(\frac{\lambda_1 H}{\sqrt{3}R}) J_1^2(\lambda_1) \left(1 - \frac{3}{4}\right) \right\} = J_2(\lambda_1).$$

Numerically, the integral evaluates to 0.130. This gives a first approximation to the singularity as

$$-1.576 \tan(1.576H/R) - F(0.459) = 0,$$

or for F small,

$$(H/R)_{crit} \sim 1.995 - 0.618F.$$

The coefficients required for the Galerkin approximation to (11) were found using the 7-point and 9-point Gaussian integration schemes, to yield

$$A_1[-.2048s_1 -.0597Fc_1] + A_2[.0454Fc_1] + A_3[-.0111Fc_1] + \dots = .4805$$

$$A_1[.0454Fc_2] + A_2[-.1898s_2 + .0135Fc_2] + A_3[.0775Fc_2] + \dots = -.1713$$

$$A_1[-.0111Fc_3] + A_2[.0775Fc_3] + A_3[-.1859s_3 + .0541Fc_3] + \dots = .0910$$

(12)

etcetera, where $s_1 = \sin\left(\frac{\lambda_1}{\sqrt{R}}\right)$, etcetera. First approximations to the second and third resonances are found by setting the diagonal terms equal to zero. This yields the above estimate for the first harmonic, and gives for the second

$$(H/R)_{crit} = \pi + \tan^{-1} (.071F),$$

or

$$(H/R)_{crit} = .958 + .072F, 1.915 + .072F, \text{ etc.}$$

The first approximation to the third harmonic yields

$$(H/R)_{crit} = 1.621 + .291F, 1.241 + .291F, 1.862 + .291F, \text{ etc.}$$

To get a second approximation, one can find the zeros of the determinant of the whole third-order minor above numerically, to avoid difficulty in combining the disparate trigonometric terms. One may use the values of the other two trigonometric functions at the first approximation to the harmonic to improve the estimate. Note the corrections to π/m are no longer independent of n . Carrying out the computations with $F = .145$ yielded the estimates

$$\begin{aligned} (H/R)_1 &\approx 1.905 \\ (H/R)_2 &\approx .968 \\ (H/R)_3 &\approx .67, 1.25 \end{aligned} \tag{13}$$

where the error estimate is about one in the last place given. These are compared with experiments later, and are found to be excellent: certainly within experimental error, and definite improvements over the $F = 0$ estimates.

Zero-Order Boundary Solutions

While E very small allows viscosity to be ignored throughout most of the fluid, the high order terms become important in regions of relative height $E^{\frac{1}{2}}$ from the top and bottom. Rescaling (3) in the usual fashion for boundary layers, the boundary equations [$z = O(E^{\frac{1}{2}})$] are:

$$\begin{aligned}\frac{\partial u_0}{\partial t} &= -\frac{\partial p_0}{\partial r} + \frac{\partial^2 u_0}{\partial s^2} + 2v_0, \\ \frac{\partial v_0}{\partial t} &= -\frac{\partial p_0}{r\partial\theta} + \frac{\partial^2 v_0}{\partial s^2} - 2u_0,\end{aligned}\tag{14}$$

$$0 = -\frac{\partial p_0}{\partial s}$$

$$\frac{\partial u_0}{\partial r} + \frac{u_0}{r} + \frac{\partial v_0}{r\partial\theta} + \frac{\partial w_0}{\partial s} = 0$$

$$\frac{\partial u_0}{\partial s} = \frac{\partial v_0}{\partial s} = 0, \quad w_0 = -r - F\eta_0 - Fur \quad \text{at } s = 0 \text{ for the top,}$$

$$u_0 = v_0 = w_0 = 0 \quad \text{at } s = 0 \text{ for the bottom,}$$

and the solution merges with the interior.

These problems might be called time-dependent Ekman layer problems. The top boundary layer requires $\frac{\partial u_0}{\partial s}$ and $\frac{\partial v_0}{\partial s}$ to change by $O(1)$ across a distance $O(E^{\frac{1}{2}})$, which means the top boundary layer will only negligible change the stresses from the interior values. In any case, the strong motions near a resonance will not show up, because they automatically satisfy the free stress condition, for the normal velocity of the resonant mode is by definition zero at the mean surface. Then continuity causes the rest of the stress to vanish, for the normal derivatives of u_0 and v_0 will behave like the second derivative of the normal velocity, which

vanishes at the mean surface.

Across the bottom boundary layer, u_0 and v_0 , and hence the stresses, change by $O(1)$, so must be considered more explicitly. In the same fashion as the steady Ekman problem, and writing $\frac{\partial}{\partial x} \rightarrow i$, one gets

$$\frac{\partial^4 u}{\partial y^4} - 2i \frac{\partial^2 u}{\partial y^2} + 3u = -\frac{2}{\lambda} \frac{\partial p}{\partial x} - i \frac{\partial p}{\partial x},$$

which has characteristic roots $\pm(1-i)/\sqrt{2}$ and $\pm(1+i)\sqrt{3}/2$.

Boundedness as $y \rightarrow \infty$ excludes the roots with positive real parts, so imposing $u = v = 0$ at $y = 0$ gives

$$u = -\frac{i}{3} \left(\frac{\partial p}{\partial x} + \frac{2p}{\lambda} \right) + \frac{i}{2} \left(\frac{\partial p}{\partial x} + \frac{p}{\lambda} \right) e^{-\frac{1+i}{\sqrt{2}} y} - \frac{i}{6} \left(\frac{\partial p}{\partial x} - \frac{p}{\lambda} \right) e^{-\frac{\sqrt{3}}{2} (1+i) y}$$

$$v = \frac{1}{3} \left(2 \frac{\partial p}{\partial x} + \frac{p}{\lambda} \right) - \frac{1}{2} \left(\frac{\partial p}{\partial x} + \frac{p}{\lambda} \right) e^{-\frac{1+i}{\sqrt{2}} y} + \frac{1}{6} \left(\frac{\partial p}{\partial x} - \frac{p}{\lambda} \right) e^{-\frac{\sqrt{3}}{2} (1+i) y}$$

and imposing continuity and $w = 0$ at $y = 0$ gives

$$w = \nabla_x^2 p \left[\frac{i}{3} z + E^{\frac{1}{2}} \left\{ \frac{-1+i}{2\sqrt{2}} e^{-\frac{(1+i)y}{\sqrt{2}}} - \frac{-1+i}{2\sqrt{2}} - \frac{1+i}{6\sqrt{6}} e^{-\frac{\sqrt{3}}{2} (1+i)y} + \frac{1+i}{6\sqrt{6}} \right\} \right].$$

Note the extra term due to non-steadiness soon swamps the (modified) Ekman convergence, as one proceeds into the interior.

Restoring the factor e^{it} and taking real parts, one has in the bottom boundary:

$$u_0 = \sum \frac{a_n \lambda_n}{c} \left\{ (3J_0 + J_2) \sin(\theta + t) - 3J_0 e^{-\frac{y}{\sqrt{2}}} \sin(\theta + t + \frac{y}{\sqrt{2}}) - J_2 e^{-\frac{\sqrt{3}}{2} y} \sin(\theta + t - \frac{\sqrt{3}}{2} y) \right\}$$

$$v_0 = \sum \frac{a_n \lambda_n}{c} \left\{ (3J_0 - J_2) \cos(\theta + t) - 3J_0 e^{-\frac{y}{\sqrt{2}}} \cos(\theta + t + \frac{y}{\sqrt{2}}) + J_2 e^{-\frac{\sqrt{3}}{2} y} \cos(\theta + t - \frac{\sqrt{3}}{2} y) \right\}$$

$$w_0 = \sum \frac{a_n \lambda_n}{\sqrt{3}} J_1(\lambda_n \lambda) \left\{ z \sin(\theta + t) - \frac{E^{\frac{1}{2}}}{\sqrt{2}} e^{-\frac{y}{\sqrt{2}}} \left[\cos(\theta + t + \frac{y}{\sqrt{2}}) + \sin(\theta + t + \frac{y}{\sqrt{2}}) \right] \right. \\ \left. + \frac{E^{\frac{1}{2}}}{3\sqrt{6}} e^{-\frac{\sqrt{3}}{2} y} \left[-\cos(\theta + t - \frac{\sqrt{3}}{2} y) + \sin(\theta + t - \frac{\sqrt{3}}{2} y) \right] + E^{\frac{1}{2}} \left(\frac{1}{\sqrt{2}} + \frac{1}{3\sqrt{6}} \right) \cos(\theta + t) + E^{\frac{1}{2}} \left(\frac{1}{\sqrt{2}} - \frac{1}{6} \right) \sin(\theta + t) \right\}. \quad (15)$$

Feeding this transient Ekman suction back into the interior

had only the effect of rotating the pattern by $E^{\frac{1}{2}}$, allowing the transport of momentum to counteract friction. Equations (15) will be used in the first-order forcing in the boundary layer.

First-Order Mean Motion

The first-order equations of motion are

$$\begin{aligned} \frac{\partial u_1}{\partial t} + u_0 \frac{\partial u_0}{\partial r} + \frac{v_0}{r} \frac{\partial u_0}{\partial \theta} + w_0 \frac{\partial u_0}{\partial z} - \frac{v_0^2}{r} &= -\frac{\partial p_1}{\partial r} + 2v_1 + E(\nabla^2 u_1 - \frac{u_1}{r^2} - \frac{2\partial v_1}{r^2 \partial \theta}), \\ \frac{\partial v_1}{\partial t} + u_0 \frac{\partial v_0}{\partial r} + \frac{v_0}{r} \frac{\partial v_0}{\partial \theta} + w_0 \frac{\partial v_0}{\partial z} + \frac{u_0 v_0}{r} &= -\frac{\partial p_1}{r \partial \theta} - 2u_1 + E(\nabla^2 v_1 - \frac{v_1}{r^2} + \frac{2\partial u_1}{r^2 \partial \theta}), \\ \frac{\partial w_1}{\partial t} + u_0 \frac{\partial w_0}{\partial r} + \frac{v_0}{r} \frac{\partial w_0}{\partial \theta} + w_0 \frac{\partial w_0}{\partial z} &= -\frac{\partial p_1}{\partial z} + E \nabla^2 w_1, \\ \frac{\partial u_1}{\partial r} + \frac{u_1}{r} + \frac{\partial v_1}{r \partial \theta} + \frac{\partial w_1}{\partial z} &= 0 \end{aligned} \tag{16}$$

$u_1 = v_1 = w_1 = 0$ at $z = 0$ and at $r = 1$ and $r = a$ [unless 0],

$$w = F \frac{\partial \eta_0}{\partial z} + F u_0 \frac{\partial \eta_0}{\partial r} + F v_0 \frac{\partial \eta_0}{r \partial \theta} + u_0 \cos(\theta+t) + F u_1 r \quad \text{at } z = F[r^2(1+a^2)]/2$$

$$-v_0 \sin(\theta+t) + \frac{1}{2} r + E[1 \cos(\theta+t) + F \eta_0]$$

The mean motion only will be considered, denoted by \bar{a} superbar. Since θ and t only occur in the combination $(\theta+t)$, a time average is also a θ -average, i.e., a steady state has been reached. Write

$$\begin{aligned} \bar{u}(r,z) &= \overline{u_0 \frac{\partial u_0}{\partial r}} + \overline{\frac{v_0}{r} \frac{\partial u_0}{\partial \theta}} + \overline{w_0 \frac{\partial u_0}{\partial z}} - \overline{\frac{v_0^2}{r}}, \\ \bar{v}(r,z) &= \overline{u_0 \frac{\partial v_0}{\partial r}} + \overline{\frac{v_0}{r} \frac{\partial v_0}{\partial \theta}} + \overline{\frac{w_0 \partial v_0}{\partial z}} + \overline{\frac{u_0 v_0}{r}}, \\ \bar{w}(r,z) &= \overline{u_0 \frac{\partial w_0}{\partial r}} + \overline{\frac{v_0 \partial w_0}{r \partial \theta}} + \overline{w_0 \frac{\partial w_0}{\partial z}}. \end{aligned} \tag{17}$$

These are known from (15), though cumbersome, except that

$\mathcal{H}(r, z) = 0$ in the interior, from $\overline{\sin(\theta+t) * \cos(\theta+t)} = 0$,
etc.

The first-order mean equations are:

$$\begin{aligned} \mathcal{L}(r, z) &= -\frac{\partial \bar{p}_1}{\partial r} + 2\bar{v}_1 + E(\nabla^2 \bar{u}_1 - \frac{\bar{u}_1}{r^2}), \\ \mathcal{H}(r, z) &= -2\bar{u}_1 + E(\nabla^2 \bar{v}_1 - \frac{\bar{v}_1}{r^2}), \\ \mathcal{M}(r, z) &= -\frac{\partial \bar{p}_1}{\partial z} + E \nabla^2 \bar{w}_1, \\ \frac{\partial \bar{u}_1}{\partial r} + \frac{\bar{u}_1}{r} + \frac{\partial \bar{w}_1}{\partial z} &= 0, \end{aligned} \tag{18}$$

$\bar{u}_1 = \bar{v}_1 = \bar{w}_1 = 0$ at $z = 0$ and at $r = 1$ and $r = a$ [unless 0],

$$\begin{aligned} \bar{w}_1 &= -(r \cos(\theta+t) + F \frac{\partial \bar{w}_0}{\partial z})(w_0 - F \frac{\partial \bar{w}_0}{\partial z} - F r u_0) + F \frac{\partial \bar{w}_1}{\partial z} + F r \bar{u}_1 \\ &+ \overline{u_0 \cos(\theta+t) - v_0 \sin(\theta+t)} + F u_0 \frac{\partial \bar{w}_0}{\partial r} + F v_0 \frac{\partial \bar{w}_0}{\partial \theta} = F r \bar{u}_1, \end{aligned}$$

at $z = H/R + F[r^2/2 - \frac{(1+a^2)}{4}]$.

Standard boundary-layer theory suggests splitting the problem into two parts: interior and boundary layers. The interior equations are:

$$\begin{aligned} \mathcal{L}(r, z) &= -\frac{\partial \bar{p}_1}{\partial r} + 2\bar{v}_1, \\ 0 &= -2\bar{u}_1, \\ \mathcal{M}(r, z) &= -\frac{\partial \bar{p}_1}{\partial z}, \\ \frac{\partial \bar{u}_1}{\partial r} + \frac{\bar{u}_1}{r} + \frac{\partial \bar{w}_1}{\partial z} &= 0, \end{aligned} \tag{19}$$

where $\bar{w}_1 = 0$ at $z = H/R + F(r^2 - \frac{1+a^2}{4})/2$, and other boundary conditions to match the boundary solutions. In the surface boundary layer, it was earlier found that \mathcal{L} and \mathcal{H} change by at most $O(E^{\frac{1}{2}})$. Thus equations (22) below have only trivial solutions, to $O(E^{\frac{1}{2}})$, for free stress surface conditions, so the boundary condition $\bar{w}_1 = F r \bar{u}_1$ effectively

holds at the top of the interior. In the interior,

$$\bar{u}_1 = 0 \tag{20}$$

then implies $\frac{\partial \bar{w}_1}{\partial z} = 0$ from (19.4), which with the top boundary condition implies

$$\bar{w}_1 = 0. \tag{21}$$

Eliminating p between (19.1) and (19.3) gives

$$\frac{\partial \bar{v}_1}{\partial z} = \frac{1}{2} \frac{\partial \mathcal{H}}{\partial z} - \frac{1}{2} \frac{\partial \mathcal{M}}{\partial z},$$

but leaves \bar{v}_1 ambiguous by any axially symmetric geostrophic flow. Since we are particularly interested in such, this is inconvenient. Of course, one could also say there is such an ambiguity in the zero-order flow, but there we can argue that any non-driven flow will decay from Ekman friction. Here that is not evident.

The cases of principal interest are resonances, when the nth component of the formulas (15) dominate, so

$$\begin{aligned} \mathcal{H} &\sim \frac{A_m^2 \lambda_m^3}{72\pi} \int_0^{2\pi} \left\{ (3J_0(\lambda_m r) + J_2(\lambda_m r)) \left(-2J_1 - \frac{2J_2}{\lambda_m r}\right) \cos^2\left(\frac{\lambda_m z}{\sqrt{3}}\right) \sin^2(\theta+t) \right. \\ &\quad + (3J_0 - J_2) \left(-4J_1 + (3J_0 - 3J_2)/\lambda_m r\right) \cos^2\left(\frac{\lambda_m z}{\sqrt{3}}\right) \cos^2(\theta+t) \\ &\quad \left. + 2J_1 (3J_0 + J_2) \sin^2\left(\frac{\lambda_m z}{\sqrt{3}}\right) \sin^2(\theta+t) \right\} d\theta, \\ \mathcal{M} &\sim \frac{A_m^2 \lambda_m^3}{24\sqrt{3}\pi} \int_0^{2\pi} \left\{ (3J_0 + J_2) (J_0 - J_1/\lambda_m r) \sin(2\lambda_m z/\sqrt{3}) \sin^2(\theta+t) \right. \\ &\quad + (3J_0 - J_2) (J_1/\lambda_m r) \sin(2\lambda_m z/\sqrt{3}) \cos^2(\theta+t) \\ &\quad \left. + J_1^2 \sin(2\lambda_m z/\sqrt{3}) \sin^2(\theta+t) \right\} d\theta, \\ \frac{\partial \mathcal{H}}{\partial z} &\sim \frac{A_m^2 \lambda_m^4}{72} \left\{ 2(3J_0 + J_2) (J_1 + J_2/\lambda_m r) + (3J_0 - J_2) \left(3\left[\frac{J_0 - J_2}{\lambda_m r}\right] + 4J_1\right) \right. \\ &\quad \left. + 2J_1 (3J_0 + J_2) \sin(2\lambda_m z/\sqrt{3}) \right\} \end{aligned}$$

Since the nth resonance is such that $\sin(\lambda_n H/\sqrt{3} R) = 0$,

$\cos^2(\lambda_{\infty} H / \sqrt{3} R) = 1$, and

$$\int_0^{H/R} \frac{\partial \bar{v}_1}{\partial z} dz = \int_0^{H/R} \frac{\partial \bar{v}_1}{\partial r} dz = 0.$$

Thus, the vertical average of $\bar{v}_1 = \bar{v}_1(0+, r)$. Let's go to the bottom boundary to get this value.

Physically, we look for (\bar{u}, \bar{w}) -rolls in the boundary, driven by radiation pressure. \bar{v}_1 is coupled at the tops of these rolls by Coriolis force. Suppress writing r , and apply scaling of the usual boundary variety to get the mean first-order flow in the boundary:

$$\begin{aligned} \mathcal{L}(\bar{v}_1) &= 2\bar{v}_1 + \frac{\partial^2 \bar{u}_1}{\partial \bar{y}^2} - \frac{\partial \bar{p}_1}{\partial \bar{r}} \\ \mathcal{N}(\bar{v}_1) &= -2\bar{u}_1 + \frac{\partial^2 \bar{v}_1}{\partial \bar{y}^2} \\ 0 &= -\frac{\partial \bar{p}_1}{\partial \bar{y}} \end{aligned} \quad (22)$$

$$\frac{\partial \bar{u}_1}{\partial \bar{r}} + \frac{\bar{u}_1}{\bar{r}} + \frac{\partial \bar{w}_1}{\partial \bar{y}} = 0$$

$$\bar{u}_1 = \bar{v}_1 = \bar{w}_1 = 0 \quad \text{at } \bar{y} = 0$$

$$\bar{u}_1 \text{ and } \bar{w}_1 \rightarrow 0 \text{ for } \bar{y} \gg 1.$$

Now \mathcal{L} and \mathcal{N} can be found from the result (15) of the boundary layer analysis, and equations (22) are of a well-behaved linear form, so one should be able to solve them analytically. Several months of effort were convincing that the same answer will never recur, so the easier, and therefore more reliable, technique of numerical solution was taken up. Unfortunately, this turned out to require a good part of the floating point software for the PDP-1 computer, so also took several months, but at least the answers are reproducible.

The system (22) is a two boundary value problem on an infinite interval. Two methods come to mind, namely shooting and relaxation. The first is more convenient for determining

the eigenvalues $\frac{\partial \bar{p}}{\partial n}$ which allow solution. Reformulate the w-boundary conditions via the continuity equation

$$0 = \int_0^\infty \frac{\partial \bar{w}_1}{\partial r} dr = \left(\frac{\partial}{\partial r} + \frac{1}{r}\right) \int_0^\infty \bar{u}_1 dr$$

so

$$\int_0^\infty \bar{u}_1 dr = S/r,$$

i.e., no vertical flux out implies the total horizontal flux is constant. For a cylinder, this must be finite (in fact, zero) for $r = 0$, so the boundary conditions and equations are

$$U + c = \frac{\partial^2 \bar{u}_1}{\partial r^2} + 2\bar{v}_1$$

$$N = \frac{\partial^2 \bar{v}_1}{\partial r^2} - 2\bar{u}_1$$

(23)

$$\bar{u}_1(0) = \bar{v}_1(0) = 0,$$

\bar{u} and $\frac{\partial \bar{v}}{\partial r} \rightarrow 0$ for $r \gg 1$,
 $\int_0^\infty \bar{u} dr = 0,$

where $\frac{\partial \bar{p}}{\partial n}$ is written c to emphasize its independence of r , and is determined by the five boundary conditions on the fourth order equation. This system can be numerically solved fairly easily by simultaneously computing three solutions:

$$y_1' = y_2, y_2' = U+c - 2y_3, y_3' = y_4, y_4' = N + 2y_1,$$

$$y_5' = y_6, y_6' = U+c - 2y_7, y_7' = y_8, y_8' = N + 2y_5,$$

$$y_9' = y_{10}, y_{10}' = U+c - 2y_{11}, y_{11}' = y_{12}, y_{12}' = N + 2y_9,$$

$$y_{13}' = y_1, y_{14}' = y_5, y_{15}' = y_9,$$

where $y_n(0) = 0$ for $n = 1$ to 15 except $y_6(0) = y_{12}(0) = 1$.

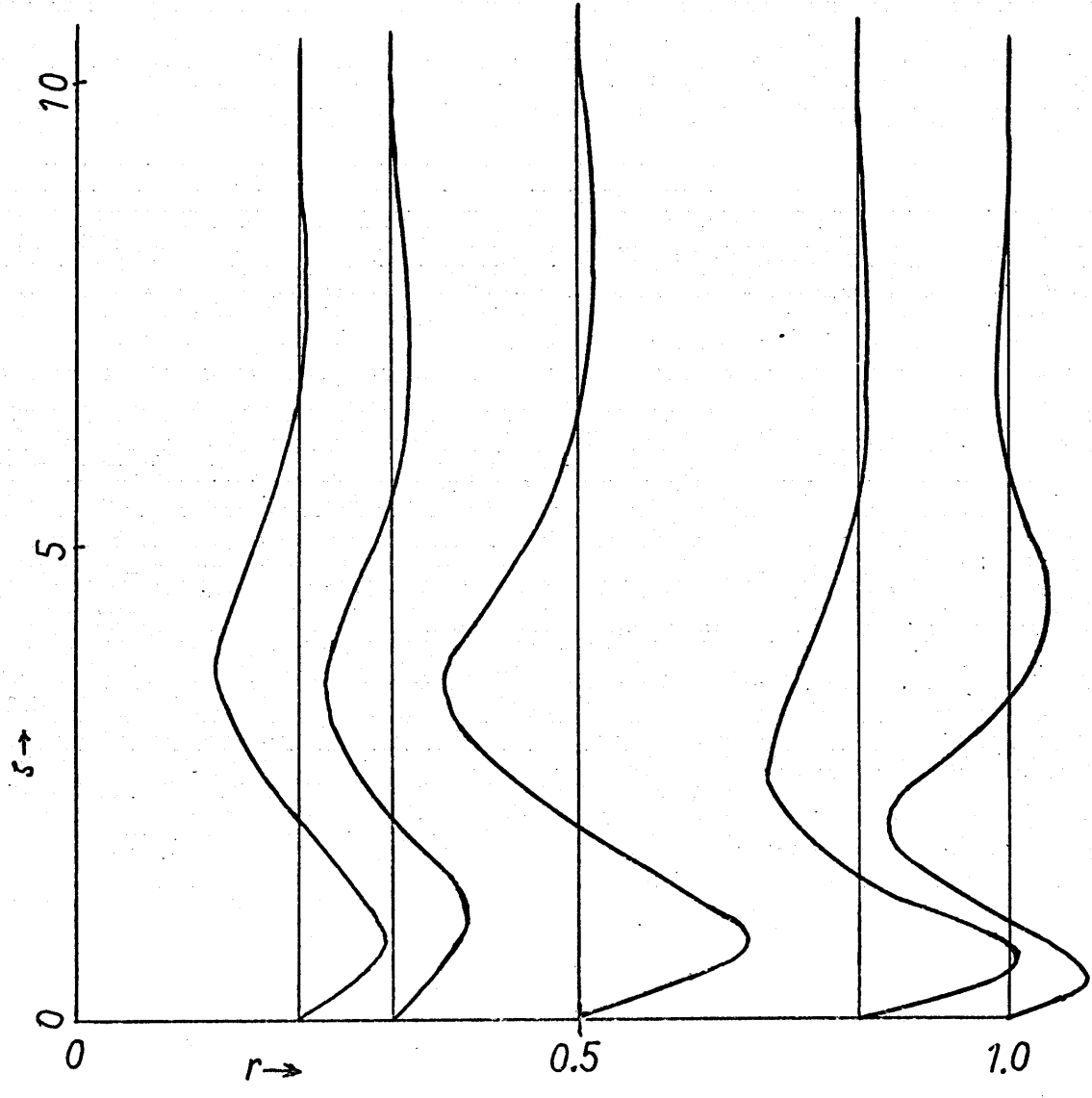
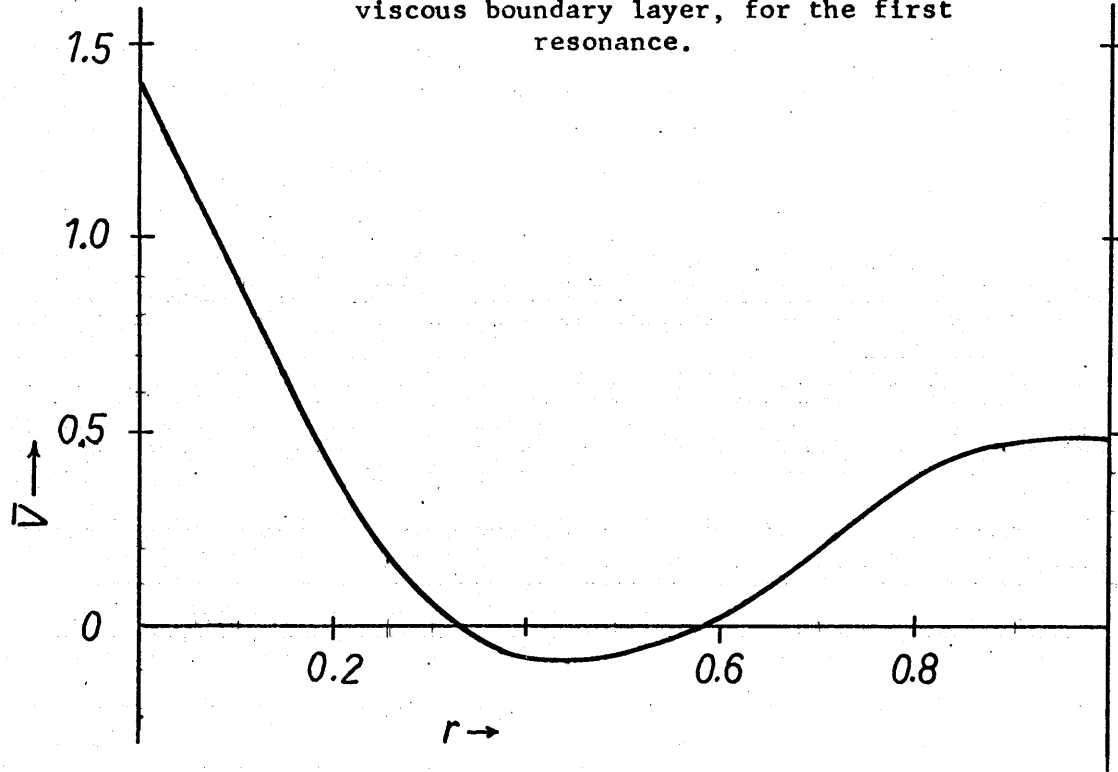
One integrates this set to infinity [using a Kutta-Merson scheme with automatic step-size control to keep down the error.] and checks whether the other boundary conditions can be satisfied. They can be if there is a linear combination of the three solution vectors which satisfies $\frac{\partial \bar{u}}{\partial r} = \frac{\partial \bar{v}}{\partial r} = W = 0$ as $r \rightarrow \infty$, which is so if the determinant

$$\begin{vmatrix} y_2 & y_6 & y_{10} \\ y_4 & y_8 & y_{12} \\ y_{13} & y_{14} & y_{15} \end{vmatrix} = 0.$$

If not, use the value of the determinant to search for a better value for c , by bisecting the interval within which the zero is known to lie. Given c , \bar{v}_1 at the outer edge of the boundary layer is given by $(\mathcal{L} + c)/2$, and is plotted for the first three resonances in figure (2). Note that a first-order vortex occurs at the origin in each case. The exponentially growing possible solutions to the equations limited the integration to $J \leq 12$. Fortunately, \mathcal{L} and \mathcal{H} had already effectively reached their asymptotic values before then, so the limitation was not serious. The values of \mathcal{L} and \mathcal{H} were found with as little hand algebra as possible, which meant long but straightforward programs taking much computer time. The Bessel functions were evaluated with error less than 2×10^{-7} using the approximations of E.E. Allen (1952). The trigonometric and exponential functions were evaluated with error less than 2×10^{-8} using the approximations of Hastings (1958). The integrals over θ were approximated by a twelve-point formula, and the vertical derivatives were approximated by central differences. Using the determinant above avoided having to find the actual initial conditions necessary to hit the boundary conditions at infinity. This was highly necessary while shooting, for the undesired exponentially growing solutions rendered the solution highly unstable, as numerical experiments confirmed. Thus, to find the actual

Figure 2a.

non-dimensional mean azimuthal velocity at the top of the viscous boundary layer, for the first resonance.



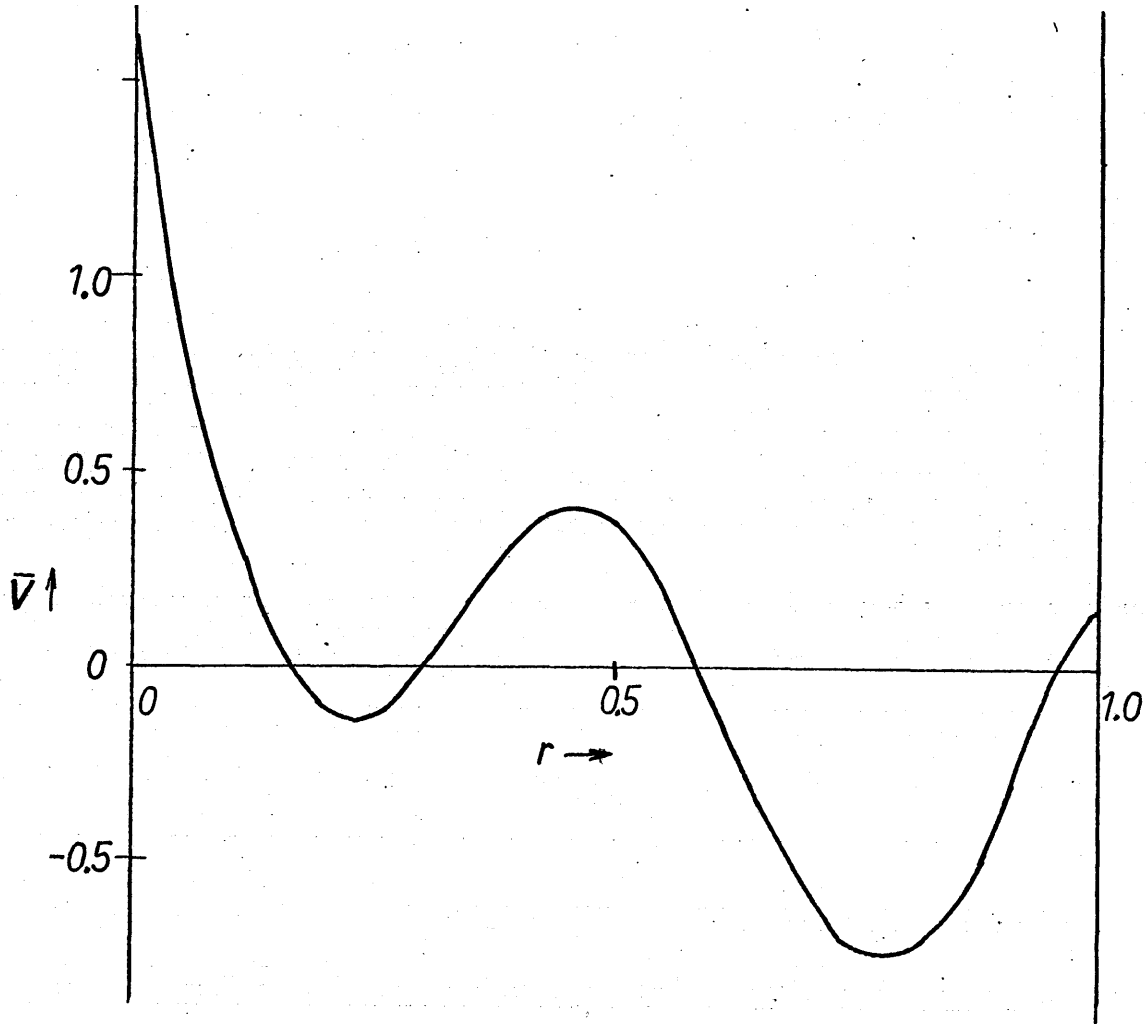


Figure 2b.
Second resonance.

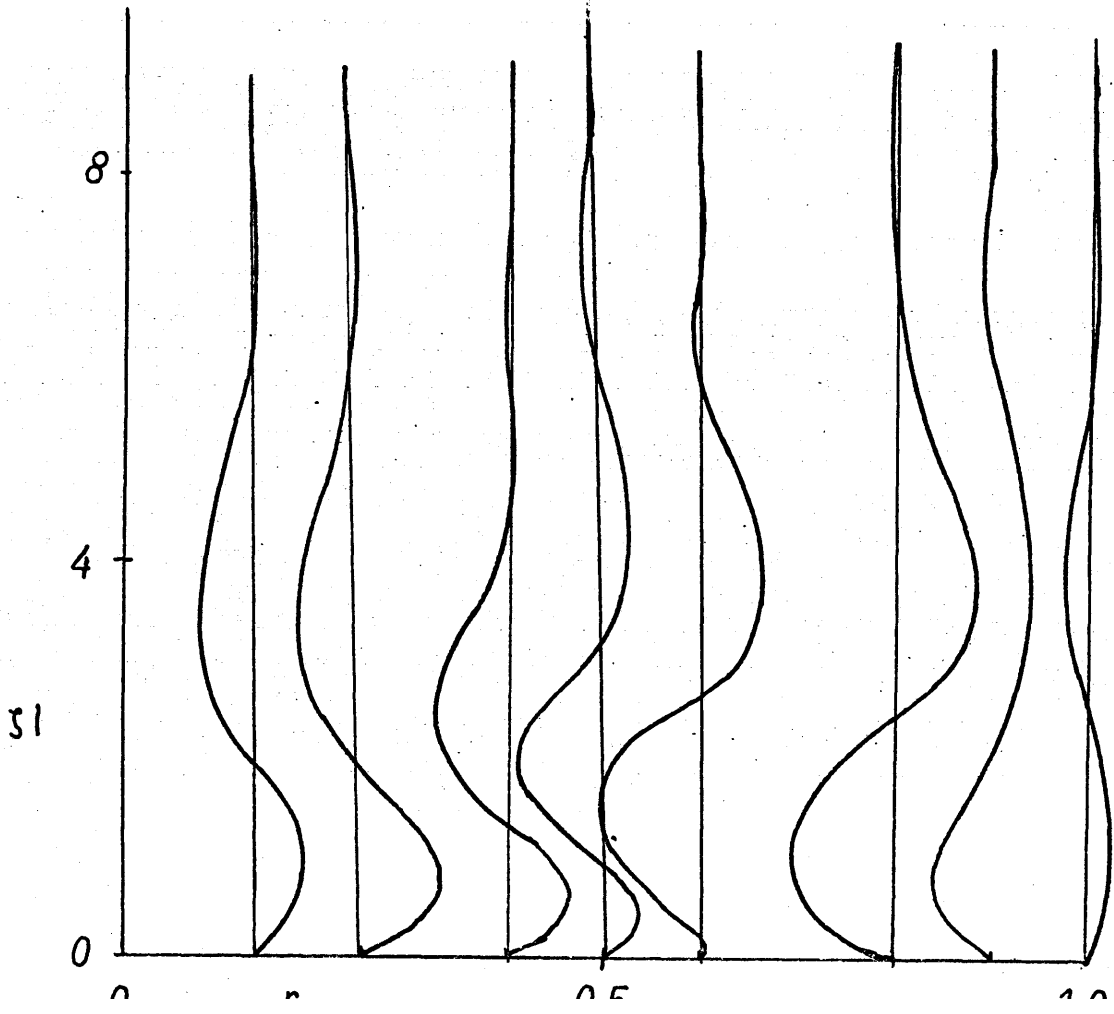


Figure 3b.
Second resonance.

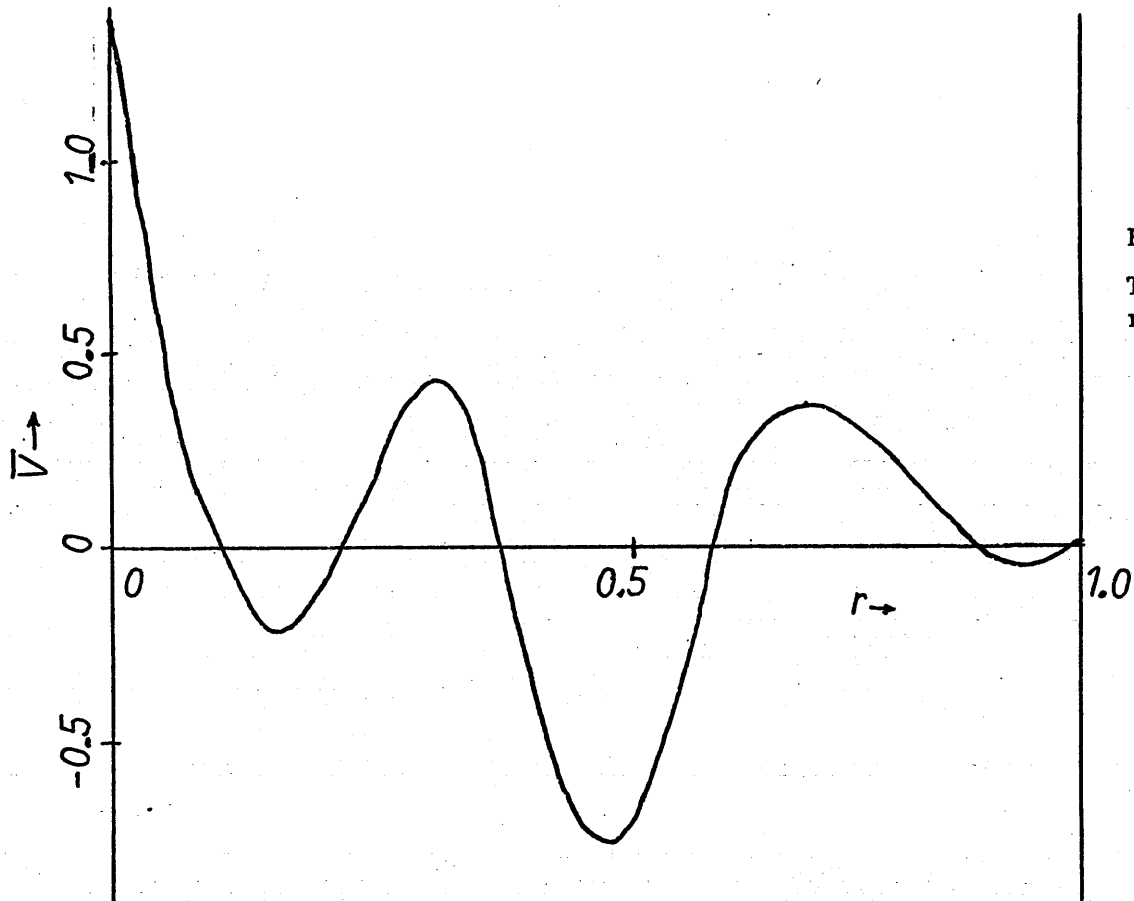


Figure 2c.
Third resonance.

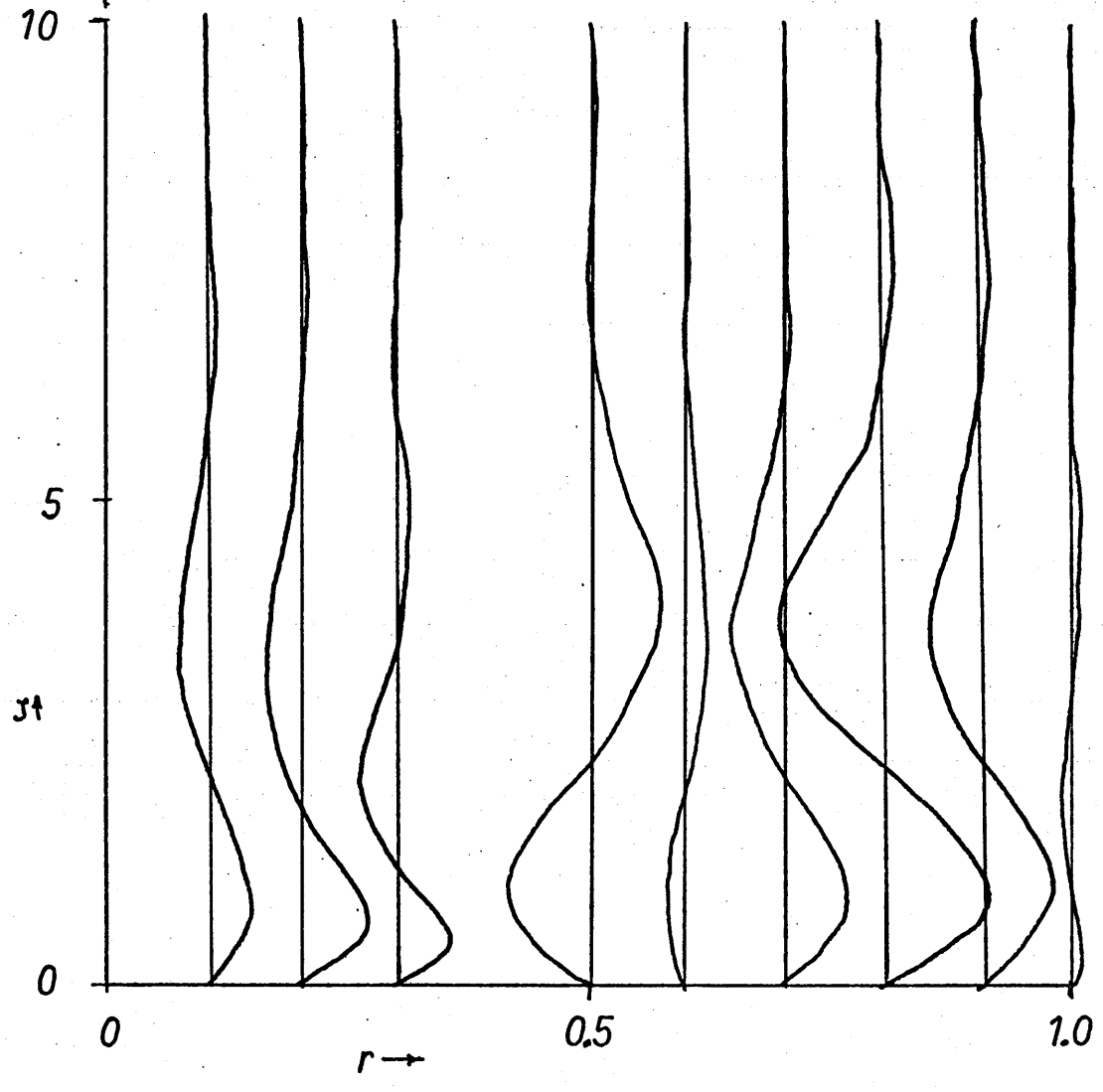


Figure 3c
Third resonance

velocities in the boundary layer, another technique is necessary. Now that the eigenvalues $c(r, \lambda_n)$ are known, a relaxation technique may be used. The same programs to compute u and v were used, along with the usual second-order approximations to the second differences and boundary conditions in system (23). Liepmann relaxation in alternating directions was used, with a visual display to check for satisfactory convergence. Starting from random initial guesses, the convergence was slow due to what appeared to be a close analog to slowly-decaying geostrophic oscillations with sweep number in the place of time. Over-relaxation just increased the frequency. So, a small amount of damping (slight increase in the magnitude of the middle coefficient in the differencing scheme) was introduced and then relaxed to zero itself. This very effectively killed the oscillations. The resultant non-dimensional radial mass fluxes in the boundary are sketched in figure (3) for the first three resonances. Features of special interest about the depicted mass flux in the boundary layer are that they represent somewhat distorted Ekman spirals and the (closed) flows occur in n gyres for the n th resonance. These gyres, or ring vortices, will result in sweeping anything on the bottom into rings. They are sketched in figure (3) for the first three resonances.

Shallow Water

The above treatment has been focused on the resonances, which occur for depths comparable to the radius. While these are the most important cases, the limit of shallow water is also of interest, especially since it is easier, at least if one takes $RF/H = 0$.

While the sums over Bessel functions still hold, they do not converge rapidly, so it is easier to start over. In fact, to compute the Lagrangian drift later, it is easier to use Cartesian coordinates. Proceeding as before, except scaling z by H and hence u and v by $\varepsilon \Omega R^2/H$, the zero-order interior equations are

$$\begin{aligned}\frac{\partial u_0}{\partial t} &= -\frac{\partial p_0}{\partial x} + 2V_0, \\ \frac{\partial v_0}{\partial t} &= -\frac{\partial p_0}{\partial y} - 2u_0, \\ 0 &= -\frac{\partial p_0}{\partial z} \\ \frac{\partial u_0}{\partial x} + \frac{\partial v_0}{\partial y} + \frac{\partial w_0}{\partial z} &= 0\end{aligned}\tag{24}$$

with boundary conditions of

$$u_0 = 0 \quad \text{at } r = 1 \text{ and } r = a \quad [\neq 0],$$

$$w_0 = 0 \quad \text{at } z = 0$$

$$w_0 = -x \sin t - y \cos t \quad \text{at } z = 1.$$

The solution is

$$\begin{aligned}w_0 &= -z (x \sin t + y \cos t) \\ u &= (-4xy \cos t + (14y^2 + 10x^2 - 10) \sin t)/16, \\ v &= ((14x^2 + 10y^2 - 10) \cos t - 4xy \sin t)/16.\end{aligned}\tag{25}$$

Thus, there are no resonances.

The structure of the bottom boundary layer is needed.

The equations of motion there are

$$\begin{aligned}\frac{\partial u_0}{\partial t} &= \frac{\partial u_0(\infty)}{\partial t} + \frac{\partial^2 u_0}{\partial \zeta^2} + 2V - 2V(\infty), \\ \frac{\partial v_0}{\partial t} &= \frac{\partial v_0(\infty)}{\partial t} + \frac{\partial^2 v_0}{\partial \zeta^2} + 2U(\infty) - 2U_0,\end{aligned}\quad (25)$$

with $u_0(0) = v_0(0) = 0$; $u_0 \rightarrow u_0(\infty)$, $v_0 \rightarrow v_0(\infty)$ as $\zeta \rightarrow \infty$. It seems easiest to solve this by the method of undetermined coefficients, since we know from the form of the solutions (15) before that

$$\begin{aligned}u(x, y, t, \zeta) - u(x, y, t, \infty) &= A e^{-\frac{\zeta}{\sqrt{2}}} \sin(t + \frac{\zeta}{\sqrt{2}}) + B e^{-\frac{\zeta}{\sqrt{2}}} \cos(t + \frac{\zeta}{\sqrt{2}}) \\ &\quad + C e^{-\frac{\zeta}{\sqrt{2}}} \sin(t - \frac{\zeta}{\sqrt{2}}) + D e^{-\frac{\zeta}{\sqrt{2}}} \cos(t - \frac{\zeta}{\sqrt{2}}), \\ v(x, y, t, \zeta) - v(x, y, t, \infty) &= E e^{-\frac{\zeta}{\sqrt{2}}} \sin(t + \frac{\zeta}{\sqrt{2}}) + F e^{-\frac{\zeta}{\sqrt{2}}} \cos(t + \frac{\zeta}{\sqrt{2}}) \\ &\quad + G e^{-\frac{\zeta}{\sqrt{2}}} \sin(t - \frac{\zeta}{\sqrt{2}}) + H e^{-\frac{\zeta}{\sqrt{2}}} \cos(t - \frac{\zeta}{\sqrt{2}}),\end{aligned}$$

for coefficients which are functions of x and y only. Since these solutions must satisfy the equations of motion (25),

$$F = A, \quad E = -B, \quad H = -C, \quad G = D.$$

Four more are given by $u(0) = v(0) = 0$,

which imply

$$\begin{aligned}16u_0 &= (-4xy) \cos t + (14y^2 + 10x^2 - 10) \sin t \\ &\quad + (10 - 12r^2) e^{-\frac{\zeta}{\sqrt{2}}} \sin(t + \frac{\zeta}{\sqrt{2}}) + 2(x^2 - y^2) e^{-\frac{\zeta}{\sqrt{2}}} \sin(t - \frac{\zeta}{\sqrt{2}}) \\ &\quad + 4xy e^{-\frac{\zeta}{\sqrt{2}}} \cos(t - \frac{\zeta}{\sqrt{2}}),\end{aligned}\quad (25b)$$

$$\begin{aligned}16v_0 &= (14x^2 + 10y^2 - 10) \cos t - 4xy \sin t \\ &\quad + (10 - 12r^2) e^{-\frac{\zeta}{\sqrt{2}}} \cos(t + \frac{\zeta}{\sqrt{2}}) + 4xy e^{-\frac{\zeta}{\sqrt{2}}} \sin(t - \frac{\zeta}{\sqrt{2}}) - 2(x^2 - y^2) e^{-\frac{\zeta}{\sqrt{2}}} \cos(t - \frac{\zeta}{\sqrt{2}}).\end{aligned}$$

These give, upon rescaling w_0 by $E^{\frac{1}{2}}$ as before,

$$\begin{aligned}16 \frac{\partial w_0}{\partial \zeta} &= -16 \left(\frac{\partial u_0}{\partial x} + \frac{\partial v_0}{\partial y} \right) \\ &= -16(y \cos t + x \sin t) + 24e^{-\frac{\zeta}{\sqrt{2}}} [y \cos(t + \frac{\zeta}{\sqrt{2}}) + x \sin(t + \frac{\zeta}{\sqrt{2}})] \\ &\quad + 8e^{-\frac{\zeta}{\sqrt{2}}} [y \cos(t - \frac{\zeta}{\sqrt{2}}) + x \sin(t - \frac{\zeta}{\sqrt{2}})],\end{aligned}$$

which can be integrated to give w . Since the stresses must be formed numerically anyway, the integration may as well also be numerical. The x and y derivatives may be exactly evaluated by second-order differences, since there are only quadratic coefficients. Then, one shoots for the eigenvalues for the boundary equations as before, and gets \bar{v}_1 at the outer edge of the boundary layer. The result for $y = 0$ is

$$\bar{v}_1(r, 0+) = +.123 r - .084 r^3. \quad (26)$$

This allows one to determine the Eulerian mean velocity throughout the interior, since v is independent of z . This mean azimuthal velocity ought to be experimentally measurable, and has been by Heyer (1967). However, the velocities are so slow [$O(\epsilon^2)$] that one needs to consider the difference between the Lagrangian mean velocity of an integrative tracer and the Eulerian mean velocity given above. The Lagrangian velocity of a particle originally at point \underline{a} is $\underline{v}(\underline{a}, t)$, and is the Eulerian velocity \underline{u} at the current location of the particle, $\underline{a} + \delta \underline{x}$. Expanding in ϵ and using a Taylor series,

$$\begin{aligned} \epsilon \underline{v}_0(\underline{a}, t) + \epsilon^2 \underline{v}_1(\underline{a}, t) &= \epsilon \underline{u}_0(\underline{a} + \delta \underline{x}, t) + \epsilon^2 \underline{u}_1(\underline{a} + \delta \underline{x}, t) \\ &= \epsilon \underline{u}_0(\underline{a} + \epsilon \int_0^t \underline{v}_0 dt + O(\epsilon^2), t) + \epsilon^2 \underline{u}_1(\underline{a} + O(\epsilon), t) \\ &= \epsilon \underline{u}_0(\underline{a}, t) + \epsilon^2 (\underline{u}_1(\underline{a}, t) + \int_0^t \underline{u}_0 dt \cdot \nabla \underline{u}_0) + O(\epsilon^3), \end{aligned}$$

so we have the formula given by Longuet-Higgins (1953):

$$\bar{v}_1 = \bar{u}_1 + \int_0^t \underline{u}_0 dt \cdot \nabla \underline{u}_0. \quad (27)$$

The latter increment to the Eulerian mean velocity is easily found from formulas (25b) to be

$$-\frac{21}{32} r^3 + 5r/8$$

in a tangential direction, so the mean Lagrangian tangential velocity, after dimensionalizing, is

$$[+.748(r/R) - .740(r/R)^3] \quad (28)$$

Side Wall Boundary Layers

So far, the effects of the side-walls have been ignored. This is because they are ignorable to a considerable extent, since the Coriolis force does not couple with \bar{V}_1 here as it does on the bottom.

The full viscous zero-order equations are given as (3). Considering the side boundary layers, write $s = \delta(r-1)$, and expand in δ . The continuity equation and $u = 0$ at $s = 0$ force rescaling u by δ also. The viscous terms do not enter the equations in δ until $= E^{\frac{1}{2}}$, so the interior equations hold outside an E layer, and there is no need to consider an $E^{\frac{1}{3}}$ or $E^{\frac{1}{4}}$ layer. When $\delta = E^{\frac{1}{2}}$, consider

$$\begin{aligned} 0 &= -\frac{\partial p_0}{\partial s}, \\ \frac{\partial v_0}{\partial t} &= -\frac{\partial p_0}{r \partial \theta} + \frac{\partial^2 v_0}{\partial s^2}, \\ \frac{\partial w_0}{\partial t} &= -\frac{\partial p_0}{\partial z} + \frac{\partial^2 w_0}{\partial s^2}, \\ \frac{\partial u_0}{\partial s} + \frac{\partial v_0}{r \partial \theta} + \frac{\partial w_0}{\partial z} &= 0, \end{aligned} \tag{29}$$

with $u_0 = v_0 = w_0 = 0$ at $s = 0$, and all merge with the interior.

Since p_0 is independent of s , the v and w equations are simple diffusion equations, and $\frac{\partial v_0}{\partial t} = -\frac{\partial p_0}{r \partial \theta}$, so writing $v_0 = A \cos(\theta + t)$, $w_0 = B \sin(\theta + t)$ as the speeds just outside the boundary layers,

$$V_0 = A(1 - e^{-\frac{t}{\sqrt{2}}} \cos \frac{t}{\sqrt{2}}) \cos(\theta + t) - A e^{-\frac{t}{\sqrt{2}}} \sin \frac{t}{\sqrt{2}} \sin(\theta + t),$$

$$W_0 = B(1 - e^{-\frac{t}{\sqrt{2}}} \cos \frac{t}{\sqrt{2}}) \sin(\theta + t) + B e^{-\frac{t}{\sqrt{2}}} \sin \frac{t}{\sqrt{2}} \cos(\theta + t),$$

The continuity equation may be integrated to give u

$$u_0 = (A - \frac{\partial B}{\partial z}) \sin(\theta + t) \left[1 + \frac{1}{\sqrt{2}} e^{-\frac{t}{\sqrt{2}}} (\cos \frac{t}{\sqrt{2}} - \sin \frac{t}{\sqrt{2}}) - \frac{1}{\sqrt{2}} \right] \\ - (A - \frac{\partial B}{\partial z}) \cos(\theta + t) \left[\frac{1}{\sqrt{2}} e^{-\frac{t}{\sqrt{2}}} (\cos \frac{t}{\sqrt{2}} + \sin \frac{t}{\sqrt{2}}) - \frac{1}{\sqrt{2}} \right].$$

If we now consider the (steady) mean velocity, the zero-order $E^{\frac{1}{2}}$ layer above will reflect in the forcing. If we subtract the interior forcing from the mean velocity, we will have effectively the steady side-wall problem considered by Howard (1968), since the $E^{\frac{1}{2}}$ deviation forcing will act as forced mean velocities $(\bar{u}, \bar{v}, \bar{w})$ at the outer edge of the $E^{\frac{1}{2}}$ layer, which can be taken as the inner boundary for an $E^{\frac{1}{3}}$ layer. Howard shows how this $E^{\frac{1}{3}}$ layer will balance out \bar{u} and \bar{w} , while an $E^{\frac{1}{4}}$ layer will allow \bar{v} to match the interior. E.g., $\bar{v}_1 \neq 0$ at $r = 1$ in figures 2 is no difficulty.

Possible Shear Instability.

The last section showed that there will be mean tangential velocities \bar{v}_1 in the interior, and consequently shears. Thus there is a possibility of shear instabilities.

Since the cylinder is rotating and the sinuous flow will not be rapid, the Taylor-Proudman theorem will hold for the perturbations, even if the mean shear does depend on z . Thus, it is reasonable to average v with respect to z and consider the motion as two-dimensional. Now, a scaling argument shows that for such a system, the Ekman friction far dominates lateral friction, so the latter will be neglected. This gives a barotropic shear problem which seems more relevant to geophysical fluid dynamics than the classical shear problems.

The perturbations are nearly non-divergent:

$$\frac{\partial u}{\partial r} + \frac{u}{r} + \frac{\partial v}{r \partial \theta} = \frac{E^{\frac{1}{2}} \zeta}{2}$$

where the vorticity is defined by

$$\zeta = \frac{\partial v}{\partial r} + \frac{v}{r} - \frac{\partial u}{r \partial \theta}.$$

The Ekman vorticity equation is

$$\frac{\partial \zeta}{\partial t} + R_0 \frac{\bar{v}}{r} \frac{\partial \zeta}{\partial \theta} + R_0 \frac{\partial \zeta}{\partial r} u + \frac{1}{2} R_0 E^{\frac{1}{2}} Z \zeta = -E^{\frac{1}{2}} \zeta$$

where \bar{v} has been rescaled to $O(1)$ in energy measure, the Rossby number

$$R_0 = \frac{|\bar{v}|}{\Omega R} \approx A_m^2 \varepsilon^{\frac{1}{2}} \sqrt{2 \int_0^1 r v_m^2(0+, r) dr},$$

with A_m the amplification factor near a resonance from equations (12), and Z the mean vorticity $\frac{\partial \bar{v}}{\partial r} + \frac{\bar{v}}{r}$. Since the perturbation flow is nearly non-divergent, write

$$u = -\frac{\partial \psi}{r \partial \theta} + E^{\frac{1}{2}} u_1, \quad v = \frac{\partial \psi}{\partial r} + E^{\frac{1}{2}} v_1.$$

Substituting into the vorticity equation and back into the continuity equation gives

$$u = -\frac{\partial \psi}{r \partial \theta} + E^{\frac{1}{2}} \frac{\partial \psi}{\partial r} + O(E), \quad v = \frac{\partial \psi}{\partial r} + E^{\frac{1}{2}} \frac{\partial \psi}{r \partial \theta} + O(E),$$

$$\zeta = \nabla^2 \psi + O(E).$$

Substitute these into (30) to get

$$\frac{\partial}{\partial t} \nabla^2 \psi + R_0 \frac{\bar{v}}{r} \frac{\partial \nabla^2 \psi}{\partial \theta} + R_0 \frac{\partial z}{\partial r} \left(-\frac{\partial \psi}{r \partial \theta} + E^{\frac{1}{2}} \frac{\partial \psi}{\partial r} \right) + \frac{1}{2} R_0 E^{\frac{1}{2}} z \nabla^2 \psi = -E^{\frac{1}{2}} \nabla^2 \psi + O(E). \quad (31)$$

Both experiment and balance of equation (31) suggest R_0 is $O(E^{\frac{1}{2}})$, so writing $R_0 = S E^{\frac{1}{2}}$ and $\tau = E^{\frac{1}{2}} t$ in (31) and dropping terms of $O(E^{\frac{1}{2}})$,

$$\frac{\partial \nabla^2 \psi}{\partial \tau} = -S \frac{\bar{v}}{r} \frac{\partial \nabla^2 \psi}{\partial \theta} + S \left[(\nabla^2 - \frac{1}{r^2}) \bar{v} \right] \frac{\partial \psi}{\partial \theta} - \nabla^2 \psi. \quad (32)$$

For growth of a shear instability, one needs tilted troughs, so one cannot separate r and θ easily. Since rotation has dropped out except in E , one looks for insight in the corresponding 'f-plane' cartesian equation

$$\frac{\partial \nabla^2 \psi}{\partial \tau} = -S \bar{v} \frac{\partial \nabla^2 \psi}{\partial y} + S (\nabla^2 \bar{v}) \frac{\partial \psi}{\partial x} - \nabla^2 \psi, \quad (32c)$$

with ψ periodic in x and y . Figure (2) of \bar{v} at several resonances suggests the

$$\bar{v} = \sqrt{2} \cos x$$

is an appropriate cartesian form. An upper bound for $\inf S$ can be found from any admissible ψ which gives $\frac{\partial KE}{\partial \tau} \geq 0$. Since this is a barotropic shear problem, a good estimate requires 'tilted troughs', and one expects on physical grounds that an excellent approximation should come from the trial form:

$$\psi = \left\{ \begin{array}{l} \sin x \sin(ky - \beta x), \quad 0 < x < \pi, \\ \sin x \sin(ky + \beta x - 2\beta\pi), \quad \pi < x < 2\pi, \\ \text{periodic extension,} \quad \text{other } x. \end{array} \right\}.$$

For this trial form and \bar{v} ,

$$\begin{aligned}
\frac{\partial KE}{\partial \varepsilon} &= \frac{\partial}{\partial \varepsilon} \iint \frac{1}{2} |\nabla \psi|^2 = - \iint \psi \frac{\partial}{\partial \varepsilon} \nabla^2 \psi \\
&= S \iint \bar{v} \psi \frac{\partial}{\partial y} \nabla^2 \psi - S \iint (\nabla^2 \bar{v}) \psi \frac{\partial \psi}{\partial x} - \iint \psi \nabla^2 \psi \\
&= \frac{8}{3} \beta \pi k \sqrt{2} S - (k^2 + \beta^2 + 1) \pi^2,
\end{aligned}$$

so at marginal growth,
$$S = \frac{3(\beta^2 + k^2 + 1)\pi}{8\sqrt{2}\beta k}$$

which has a minimum of
$$S = \frac{3\pi}{4\sqrt{2}}$$

at $\beta = k = \infty$. The latter implies a y - or θ -wavelength much shorter than the x -wavelength imposed by the mean shear. This corresponds to the experimental observation of wave-number about thirty around on the second mode, and to the marked tilt of the troughs which develop. Returning to the dimensional form, there will be instability if

$$\sqrt{2 \int_0^1 v_m^2(0+, r) r dr} (A_m^2 \varepsilon^2) E^{-\frac{1}{2}} > \frac{3\pi}{4\sqrt{2}}, \quad (33)$$

but not if much below, unless another resonance is active. the A_m 's are given by inverting the infinite set of equations (12) near the n th resonance. From equations (12),

$$\begin{aligned}
A &= 2.34 \left| \sin(1.65 H/R) \right|^{-1}, \\
A &= 0.90 \left| \sin(3.25 H/R) \right|^{-1}, \\
A &= 0.49 \left| \sin(4.7 H/R) \right|^{-1},
\end{aligned} \quad (34)$$

etc., where F has been set to .145 for the resonances, but to 0 for the coefficients. The error in the coefficients is only $O(F)$.

The mean square amplitudes for the first three v 's are .33, .44, and .31, so the instability bounds are

$$\varepsilon_1 = .059 \left| \sin(1.65 H/R) \right|,$$

$$\begin{aligned}\epsilon_2 &= .132 \left| \sin(3.25 H/R) \right| , \\ \epsilon_3 &= .29 \left| \sin(4.7 H/R) \right| ,\end{aligned}\tag{34a}$$

using $E = 1.5 \times 10^{-5}$ to match the experiment. The instability bounds predicted by (34a) are given in figure 4. Note that if ϵ is greater than any of the right sides above, instability is predicted. Thus, there are wedges of instability reaching down to zero tilt. However, as the tilt increases, shears may occur when no one component is dominant, so there may be instabilities for $\epsilon \Omega R$ large, even if ϵ is not large enough to cause one component to go unstable.

When comparing the experimental results given in figure 4 with the instability bounds given above, remember that the experimental v 's are in cylindrical coordinates, and are not exactly sinusoidal. Nonetheless, the results compare well enough to conclude that the observed instabilities are due to the vertically averaged barotropic shears, with Ekman friction.

Experimental Verification

It is time to show that the theory developed so far has some relation to reality. The turntable used was the 1-meter table in the Fluid Dynamics Laboratory of the Woods Hole Oceanographic Institution, described in Turner and Frazel (1958). This turntable is carefully engineered to maintain constant angular velocity, which is continuously adjustable over a large range. Tilting was accomplished by a hand winch from a guard-rail to the four foot steel plate upon which the turntable stood, allowing accurate measurement of small angles. The cylinder used was clear plexiglass of radius 14.5 cm, depth 29 cm, and quite accurately circular and right. A flat clear plastic sheet was used as a lid to get rid of torque from the air.

The flow was made visible with dye and dust. A television attached to the turntable showed the zero-order waves rotating backward on the rotating frame of reference, but otherwise did not have sufficient resolution, and was restricted to one view, so was not used further.

A typical run consisted of filling the cylinder to the desired depth with hot and cold water mixed to room temperature, centering it on the turntable as closely as feasible, then speeding the turntable to a fixed voltage on a dial. The angular velocity this corresponded to varied

from day to day, so the actual frequency was determined with a stop-watch. It was not realized then that F would be important, and setting a particular angular velocity was not easy. The fluid was allowed to spin up for at least twenty minutes, then potassium permanganate crystals were dropped through small holes in the lid to check for completed spin-up. The permanganate dye was used to trace bottom boundary motions, and fluorescent dye was used in the interior. As soon as spin-up was completed [except in three cases of resonances], the turn-table was slowly tilted and left for at least ten minutes, usually thirty. Then observations were made, mostly of the ink on the bottom though interesting cases were followed in the interior. Then the table was carefully tilted further. The results are plotted in figure 4 . If nothing much was observed (besides the zero-order periodic motion), a circled dot is entered. If rings of ink were observed, a circled R is entered, with the number of rings, counting center dots and ink at the edge as rings. It may be worth noting that these rings were not due to the location of the dye crystals, for they normally sharpened up long after the crystals had dissolved and occasionally clear areas formed over a crystal, except for its thin plume going either in or out. At higher tilts, the rings became unstable to wavy disturbances, with wave number 30 and up for outer rings and wave numbers 2 to 4 for inner rings. These are entered as circled I's with the number of rings. Near resonances, the instability was violent enough that visible rings did not have time to form before powerful vortices

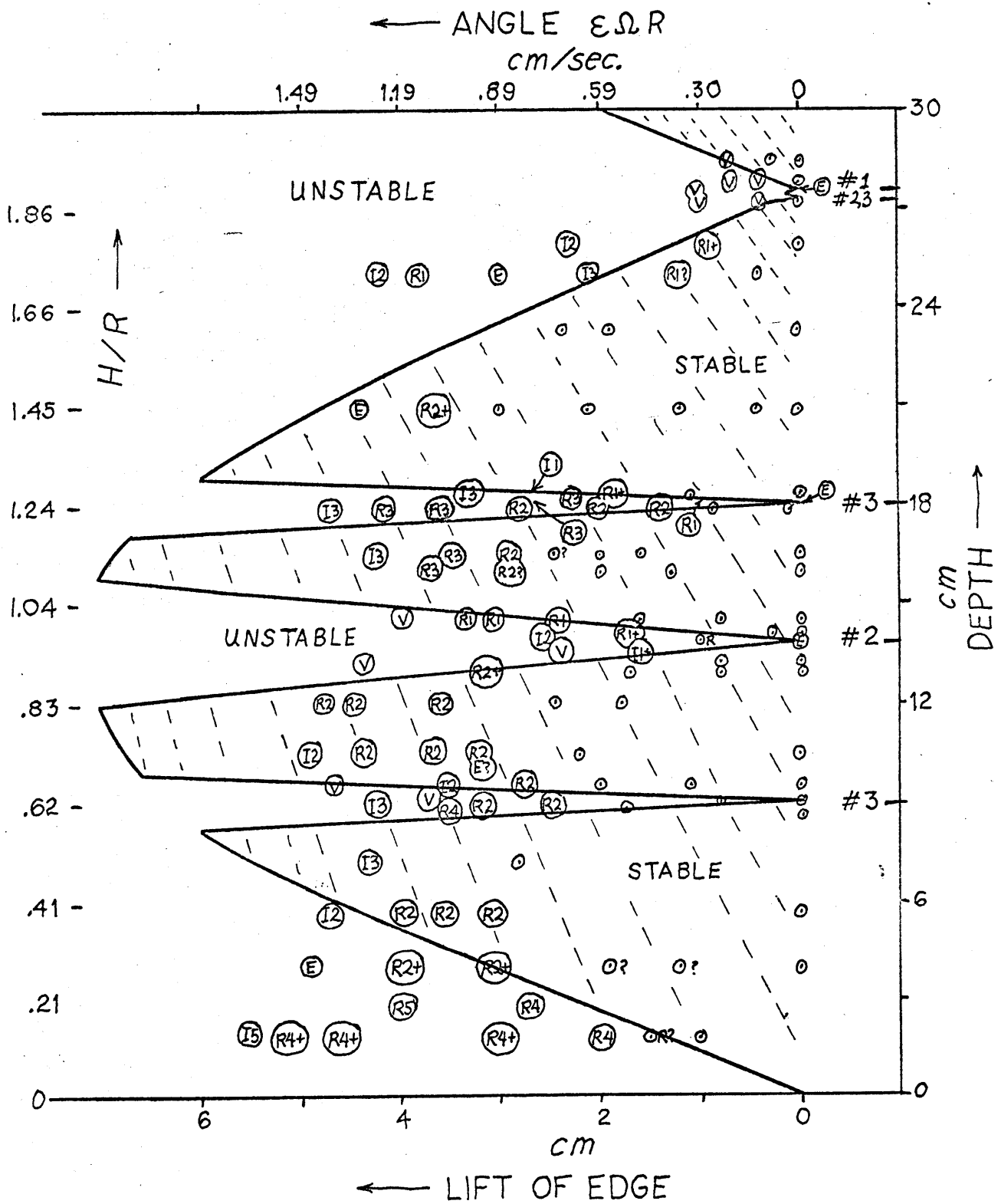


fig. 4

formed, which are entered as circled V 's. These are presumably what Fultz and Crow observed, since they form most strongly near the first resonance. It may be worth noting that these vortices are not necessarily the first-order vortex at the origin derived upon finding the theoretical \bar{V}_1 , though their continued existence may depend on similar causes, because these vortices form from the instability on the inner ring when this grows slowly enough to observe in detail. Occasionally a ring of ink along the wall will develop cusps which may grow and spread into the interior. These are entered as circled E 's and were observed at zero lift of the edge at three resonances. They look as if they might be caused by an instability on a shear a little way in from the wall, with the ink collected in the the corner because it is heavier. However, they may be due to a Görtler-Taylor centrifugal instability of the zero-order flow up and down over the concave corner. This idea is discussed in the next chapter.

Looking at the completed diagram, we see there is a general agreement with the theory: there are resonances which get weaker as n increases, there are rings of convergence and divergence in the bottom boundary, with generally one ring for the second resonance and two for the third. The vortices (zero rings) go with the first. Now let us look at the quantitative predictions.

The experiments were mostly run about 30 rpm, so $F = .145$. Thus the zero-order interior theory gave resonances at $H/R = 1.905, .968, \text{ and } .67, 1.25$ for the first, second, and

third resonances. With $R = 14.5$ cm, this forecasts $H = 27.60$ cm, 14.05 cm, and 9.72 , 18.1 cm. The observed E 's for zero tilt are taken as the experimental tips of the wedges of instability, and occurred at depths 27.5 cm, 13.9 cm, and 18.0 cm. There is also a wedge around 9.2 cm, though its center is not well defined. These seem like excellent confirmations and are within the experimental error, which is mostly due to various F 's being used. The widths and depths of the stable region seem in agreement with the (a posteriori) prediction of figure .

A rather crude experiment with an annulus with outer radius 35.4 cm and inner radius 21 cm was also tried on a similar turntable that could not be tilted. The annulus was not deep enough to try the first harmonic, but the invisible tilt automatically in the table was sufficient to cause considerable current and edge vortices at 13 cm, surprisingly close to the predicted second resonance at $H = \frac{\sqrt{2}}{2}(35.4 - 21)$ cm = 12.4 cm, considering the crudeness of the experiment. These currents and vortices were not observed at four other random depths, so this was encouraging.

A later exploratory trial with a smaller but much better built annulus showed a few sluggish vortices at the first resonance but not at the others. Since the vortices retained the same size as before (a few cm) they filled over half of the gap, suggesting they found it difficult to form, since incipient vortices were visible to the desirous eye at the second resonance. However, what may be much more interesting is that a relatively strong meridional circu-

lation developed near the first and second resonances, though there was a lid, and spin-up had been complete before tilting, ink in the bottom layer flowed out to the outer corner and from there, spiraled up and forward through the interior to near the upper inner corner. However, the water next to the inner wall remained clear while the ink formed into a central and outer ring (for the second resonance, at $H \approx (R_2 - R_1)\sqrt{3}/2$). Such circulations could conceivably exist in nature or in an experimental model.

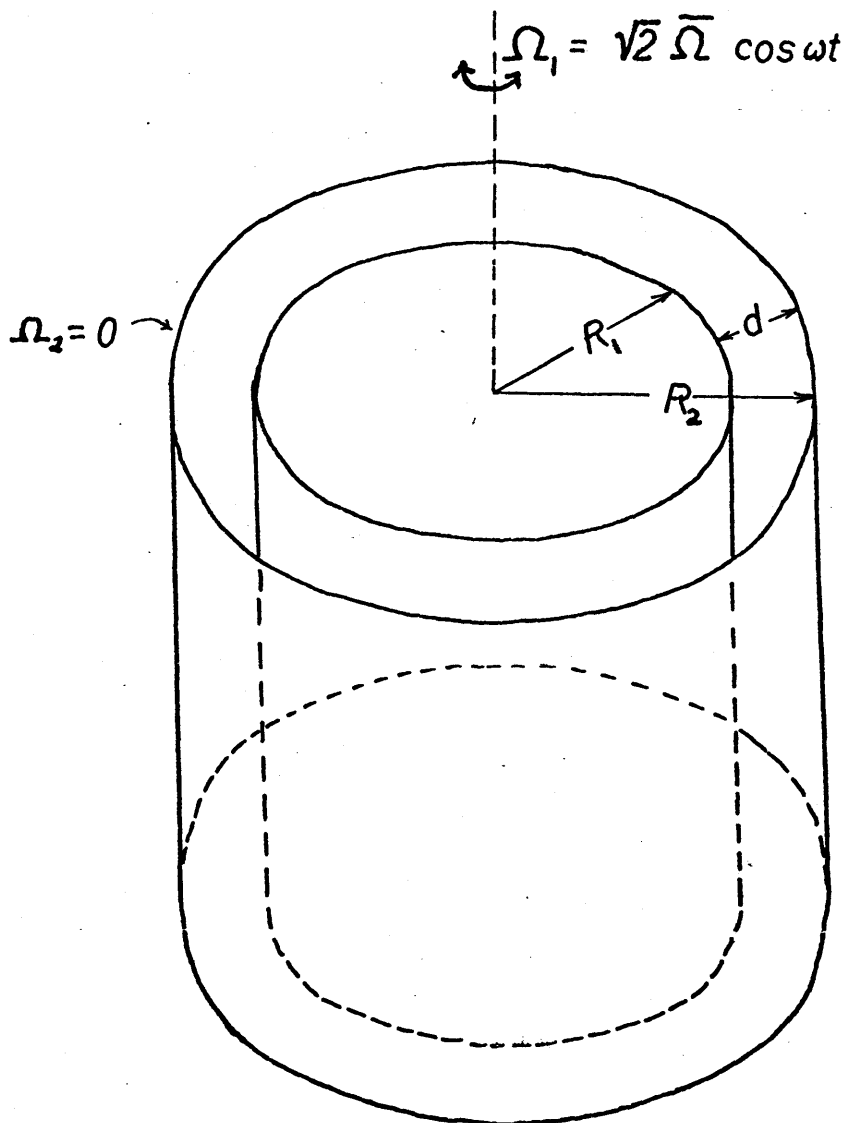


Figure 6. Sketch of basic Taylor apparatus with oscillating inner cylinder.

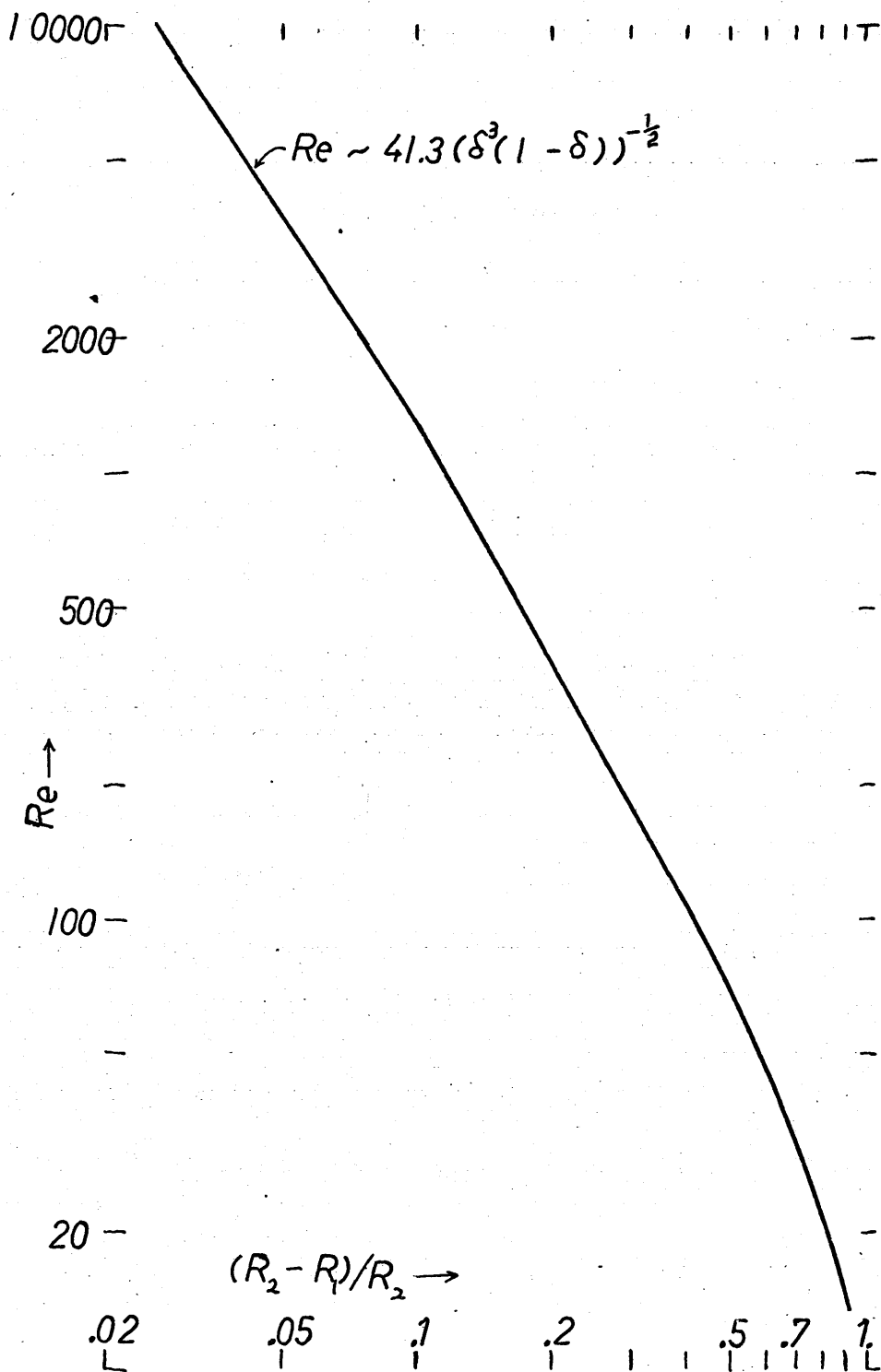
Chapter Two -- Periodic Taylor Problems.

We now consider another problem of periodic, incompressible, laminar fluid motion in an annulus which will involve similar mathematical tools, but which is fundamentally different. This problem is a variant of Taylor's [1923] classical problem of centrifugal instability when the inner cylinder of a concentric pair (as in figure 6) rotates enough faster than the outer. What will be the effects if the rotation speeds depend on time? One still expects centrifugal instabilities if there is enough mean centrifugal potential, or perhaps when the potential is particularly strong. With a view toward Fourier integrals, the obvious motions to consider are periodic and impulsive. This chapter considers periodic torsional movements of the cylinders, with special attention to the interesting limiting case of pure torsional oscillations of the inner cylinder while the outer cylinder is fixed.

Literature Review.

The zero-frequency (steady) problem of centrifugal

Figure 7. Critical Reynold's number $Re = \Omega^2 R_1^2 / \nu$ as a function of gap width for the steady Taylor problem with $\Omega_2 = 0$.



instability was started, and to a remarkable extent finished, by G.I. Taylor (1923) both experimentally and theoretically. It has been pursued extensively since; thorough reviews may be found in Chandrasekhar (1955) and Coles (1967). Coster (1919) considered the two-dimensional flow around a torsionally oscillating cylinder. Winny (1932) tested the theory experimentally and found it good for $Re = \frac{\Omega R^2 \Delta \theta}{\nu} < 600$. Ring vortices were apparently first observed for oscillation of the inner cylinder by Fage (1935), but he presents no theory nor critical parameters. Meister and Münzer (1966) considered the special case $\Omega_1 = 3 + \epsilon \sin \omega t$, $\Omega_2 = 2$ for narrow gap, using Galerkin approximation, and solved numerically for $\epsilon = 1$, and $\omega = 0$ and 10. They found the kinetic energy for fixed t to be less for $\omega = 10$ than for $\omega = 0$.

Carrier and DiPrima (1956) consider the torsional oscillations of a sphere by expanding in the oscillation amplitude. However, the resultant mean flow should not be considered an instability like the vortices around a cylinder, where the generators are parallel to the axis of rotation. Serrin (1959b) used variational techniques to show that if the Reynolds number is below a certain bound, the flow in a volume with periodic forcing is stable. Kirchgässner (1960) gives a time-dependent extension of Rayleigh's principle, that an inviscid flow is centrifugally stable for all $t \geq 0$ if $\frac{\partial v}{\partial r} + \frac{v}{r} \geq 0$ and $v(r, t) \geq 0$. Note this does not cover the case of pure oscillations. Conrad and Criminale (1965) consider sufficient conditions for stability for axisymmetric vortices in a narrow gap for

torsional oscillation of one of the cylinders with or without a superposed steady mean motion of either cylinder. They use Serrin's (1959a) variational equations to give several lower bounds for the critical Reynolds numbers as functions of the shape of the basic flow, assuming it is quasi-steady, perhaps relative to a changing amplitude, but always locally in time. They seem to regard stability as being a local property of a fluid flow rather than asymptotic in time or as a bifurcation of solution forms as functionals of the parameters. However, if the Reynolds number of the basic flow is below the infimum over a cycle of the Reynolds numbers curves they give, then the energy of a perturbation must always decrease. For steady rotation, their critical Taylor number is about two-thirds of Taylor's for $\Omega_2 = 0$ but is a definite improvement on Rayleigh's principle for $0 < \Omega_2 \lesssim \Omega_1$. For pure oscillation, of one cylinder, they get the curious result that the critical Reynold's number for the outer cylinder oscillating is lower than for the inner, though unfortunately they used different Strouhal numbers (or angle of swing.) Conrad and Criminale also find that superposing an oscillation on an outside rotation lowered their Reynolds number bound a lot as the frequency increases. Superimposing an oscillation on the inner cylinder's mean rotation also lowered the bound for large enough amplitude, but actually slightly increased it for small amplitude. They also find that rotation of the outer cylinder lowered the Reynold's number bound for oscillation of the inner cylinder. While these are for

lower bounds, Donnelly (1965) found that small oscillations superposed on a mean rotation of the inner cylinder can stabilize the flow to centrifugal instabilities, though he meant by this that the torque does not increase strongly until higher mean $\bar{\Omega}_1$, even though periodic rolls appeared at lower mean $\bar{\Omega}_1$.

Notation and Discussion.

As sketched in figure 6, we consider concentric cylinders with inner radius R_1 and outer R_2 , with $\eta = R_1/R_2$ and $d = R_2 - R_1$. The angular velocities of the cylinders are $\Omega_1(t)$ and $\Omega_2(t)$. Define non-dimensional parameters:

$$\begin{aligned} \delta &= d/R, \\ \text{Re} &= \frac{\Omega_1 R_1^2}{\nu}, \\ E &= \frac{\omega d^2}{\nu}, \\ N &= \omega/\Omega, \end{aligned} \tag{35}$$

where ω is the angular frequency of oscillation, and $\Omega = \sqrt{\Omega_1^2 + \Omega_2^2}$. As before, $u = dr/dt$, $v = r d\theta/dt$, $w = dz/dt$.

This thesis has a general policy of not spending endless pages in attempting analytic solutions to approximate equations in which the effect of neglecting terms is unknown, when an approximate solution to the exact equations can be found more easily numerically. As an example of this, consider the extensive bibliography and impressive formalism devoted by Taylor through Chandrasekhar to determining the critical parameters for the steady Taylor

problem, i.e., determining the minimum Re (or Taylor number) and associated wave number a for which one may solve

$$\left[\frac{\partial}{\partial r} \left(\frac{\partial}{\partial r} + \frac{1}{r} \right) - a^2 \right]^2 u = 2a^2 Re \left(A + \frac{B}{r^2} \right) v,$$

$$\left[\frac{\partial}{\partial r} \left(\frac{\partial}{\partial r} + \frac{1}{r} \right) - a^2 \right] v = 2 Re A u,$$

with $u = \frac{\partial u}{\partial r} = v = 0$ at $r = \eta$ and $r = 1$.

where $A = (\Omega_2 - \Omega_1 \eta^2) / (1 - \eta^2)$,

$$B = R_1^2 (\Omega_1 - \Omega_2) / (1 - \eta^2).$$

The classical thrashing around with this problem has produced only the asymptotic values as $\eta \rightarrow 1$ (Taylor, 1923), the values for $\eta = \frac{1}{2}$ (Chandrasekhar, 1955), and $\eta = \frac{1}{3}$. While testing a program used below, these values were reproduced for the special case $\Omega_2 = 0$. Upon noticing that the values for other η had not been done, sufficient other points were run off (in about half an hour) to produce figure 7, of the critical Reynolds number for $\Omega_2 = 0$ for $d/R = .02$ to 0.9 . The same program could have worked out Re for $\Omega_2 \neq 0$.

Initial Value Problem.

The equations of motion are already given in equations (1) where the boundary conditions are now

$$u = v = w = 0, \quad V = \Omega_1 R_1 \quad \text{at } r = R_1,$$

$$u = v = w = 0, \quad V = \Omega_2 R_2 \quad \text{at } r = R_2,$$

everything is periodic in z , and the azimuthal velocity is

$$V(r,t) + v(r,\theta,z,t),$$

with $\int \int_0^{2\pi} v \, d\theta \, dz = 0$ defining V .

Following Chandrasekhar (1955), linearize the equations of motion, take the wave number as k , assume axisymmetry, and eliminate p and w to get

$$\begin{aligned} \frac{\nu}{k^2} (DD_* - k^2 - \frac{1}{\nu} \frac{\partial}{\partial t}) (DD_* - k^2) u &= 2 \frac{\nu}{r} u, \\ \nu (DD_* - k^2 - \frac{1}{\nu} \frac{\partial}{\partial t}) v &= (D_* V) u, \\ \frac{\partial V}{\partial t} &= \nu DD_* V, \end{aligned} \quad (36)$$

with boundary conditions as above, and where

$$D \equiv \frac{\partial}{\partial r} \quad \text{and} \quad D_* \equiv \frac{\partial}{\partial r} + 1/r,$$

and the variables are functions of r and t only. Now non-dimensionalize, so

$$k^2 = a^2 / R_1^2, \quad r \rightarrow rR_1, \quad t \rightarrow \omega^{-1} t,$$

where ω is the oscillation angular frequency:

$$\begin{aligned} (DD_* - a^2 - R_2 N \frac{\partial}{\partial t}) (DD_* - a^2) u &= 2 R_2 a^2 V / r, \\ (DD_* - a^2 - R_2 N \frac{\partial}{\partial t}) v &= R_2 (D_* V) u, \\ (DD_* - R_2 N \frac{\partial}{\partial t}) V &= 0, \end{aligned} \quad (37)$$

with $u = v = D_* u = 0$ at $r = 1$ and $r = \eta^{-1}$,

$$v = \Omega_1(t) / \Omega \quad \text{at} \quad r = 1, \quad v = \Omega_2(t) / \Omega \eta \quad \text{at} \quad r = \eta^{-1}.$$

Noting that the main flow V is independent of u and v (since linearized), it seems worthwhile to solve it first, so try the problem with scaled boundary conditions

$$V(1,t) = \sin t, \quad V(\eta^{-1}, t) = 0,$$

and initial conditions $V(r,t) = 0$ for $1 < r < \eta^{-1}$.

This turns out to be easy to solve with the aid of a Hankel transform. Multiply both sides by

$$rB_1(pr) \equiv r[J_1(pr)Y_1(p) - Y_1(pr)J_1(p)],$$

where p is a positive root of $B_1(p\eta^{-1}) = 0$, and integrate over r , solve the resulting ordinary differential equation, and invert, to get

$$V(r,t) = \frac{\pi}{R_0 N} \sum_p \left[\frac{p^2 J_1^2(p\eta^{-1}) B_1(p\eta^{-1})}{J_1^2(p) - J_1^2(p\eta^{-1})} \right] \left[\frac{\cos t - \frac{p^2}{R_0 N} \sin t - \exp\left(-\frac{p^2 t}{R_0 N}\right)}{\left(\frac{p^2}{R_0 N}\right)^2 + 1} \right]. \quad (38)$$

As $t \rightarrow \infty$, this becomes strictly periodic. This V is the solution of a diffusion equation, so cannot have poles in the interior $1 < r < \eta^{-1}$, which makes one curious if the denominators $J_1^2(p) - J_1^2(p\eta^{-1})$ ever are zero. We have $J_1(p\eta^{-1})Y_1(p) = J_1(p)Y_1(p\eta^{-1})$, so this is equivalent to the graphs of $Y_1(x) = Y_1(y)$ and $J_1(x) = J_1(y)$ intersecting. These graphs were sketched, and were found to occupy the whole positive (x,y) quadrant in great wiggles, but to cleverly avoid each other, avoiding any difficulties in the given form (). The asymptotic expression for V can be summed to a closed but complicated form in Kelvin function of the first order, e.g., for $\eta = 0$ [no outside cylinder]

$$V = \left\{ \cos(t) \left[-\ker_1\left(\frac{\lambda}{E^{\frac{1}{2}}}\right) \operatorname{kei}_1(E^{-\frac{1}{2}}) + \operatorname{kei}_1(\lambda E^{-\frac{1}{2}}) \operatorname{ker}_1(E^{-\frac{1}{2}}) \right. \right. \\ \left. \left. + \sin(t) \left[\operatorname{ker}_1(\lambda E^{\frac{1}{2}}) \operatorname{ker}_1(E^{-\frac{1}{2}}) + \operatorname{kei}_1(\lambda E^{-\frac{1}{2}}) \operatorname{kei}_1(E^{-\frac{1}{2}}) \right] \right\} \cdot \left\{ \operatorname{ker}_1^2(E^{-\frac{1}{2}}) + \operatorname{kei}_1^2(E^{-\frac{1}{2}}) \right\}^{-1}.$$

Thus, for $\eta = 0$,

$$2 \overline{V^2} = \left\{ \ker_1^2(\eta E^{\frac{1}{2}}) + \text{kei}_1^2(\eta E^{\frac{1}{2}}) \right\} \left\{ \ker_1^2(E^{-\frac{1}{2}}) + \text{kei}_1^2(E^{\frac{1}{2}}) \right\}^{-1} \\ \sim \frac{1}{\eta} \exp(-E^{-\frac{1}{2}}(\eta-1)),$$

showing the boundary layer structure of the decay due to spreading as well as viscous decay.

Numerical Initial Value Problem.

Since there is no easy analytic method for solving the non-dimensional equations (37), let us try numerical methods for insight. We will use three numeric methods for comparison and exploration of the best methods a second-order solution to the initial value problem, a harmonic system, and a (slightly disguised) spectral method. For the initial value problem, we rephrase the non-dimensional equations so

$$\begin{aligned} \frac{\partial \psi}{\partial t} &= \frac{1}{ReN} (DD_* - a^2) \psi - \frac{2a^2}{N} \frac{vV}{r}, \\ \frac{\partial v}{\partial t} &= \frac{1}{ReN} (DD_* - a^2) v - \frac{1}{N} (D_* v) u, \\ \frac{\partial V}{\partial t} &= \frac{1}{ReN} DD_* V, \end{aligned} \tag{39}$$

where $\psi = (DD_* - a^2) u$,

$$u = D_* u = v = 0 \quad \text{at } r = 1 \text{ and } r = \eta^{-1},$$

$$V(1, t) = \Omega_1(t), \quad V(\eta^{-1}, t) = \eta^{-1} \Omega_2(t).$$

The mean flow is included here because it turns out to be easier to expand the system of ordinary differential equations a little than to evaluate a bunch of Kelvin functions, though the latter are useful for checking. We use the usual second-order difference approximations to D and D_* in the interior, so using superscripts to denote network position out of K [so $r^k = 1 + \frac{k}{K}(\eta^{-1} - 1)$ for $k = 0(1)K$ and $\Delta r = \frac{\eta^{-1} - 1}{K}$],

$$\frac{\partial \psi^k}{\partial t} = \frac{1}{2\lambda^k R N} \left[\left(1 + \frac{\Delta r}{2\lambda^k}\right) \psi^{k+1} - \left(2 + \left(\frac{\Delta r}{\lambda^k}\right)^2 + a^2 (\Delta r)^2\right) \psi^k + \left(1 - \frac{\Delta r}{2\lambda^k}\right) \psi^{k-1} \right] - 2a^2 \frac{v^k v^k}{N \lambda^k},$$

$$\frac{\partial v^k}{\partial t} = \frac{1}{R N (\Delta r)^2} \left[\left(1 + \frac{\Delta r}{2\lambda^k}\right) v^{k+1} - \left(2 + \left(\frac{\Delta r}{\lambda^k}\right)^2 + a^2 (\Delta r)^2\right) v^k + \left(1 - \frac{\Delta r}{2\lambda^k}\right) v^{k-1} \right] - \frac{1}{2(\Delta r) N} \left[\left(1 + \frac{\Delta r}{\lambda^k}\right) v^{k+1} - 2 \frac{v^k}{\lambda^k} - \left(1 - \frac{\Delta r}{\lambda^k}\right) v^{k-1} \right] u^k,$$

$$\frac{\partial v}{\partial t} = \frac{1}{R N (\Delta r)^2} \left[\left(1 + \frac{\Delta r}{2\lambda^k}\right) v^{k+1} - \left(2 + \left(\frac{\Delta r}{\lambda^k}\right)^2\right) v^k + \left(1 - \frac{\Delta r}{\lambda^k}\right) v^{k-1} \right], \quad (40)$$

where

$$\left(1 + \frac{\Delta r}{2\lambda^k}\right) u^{k+1} - \left(2 + \left(\frac{\Delta r}{\lambda^k}\right)^2 + a^2 (\Delta r)^2\right) u^k + \left(1 - \frac{\Delta r}{2\lambda^k}\right) u^{k-1} = (\Delta r)^2 \psi^k, \quad (41)$$

all for $k = 1(1) K-1$. The boundary conditions

$$u^0 = u^K = v^0 = v^K = 0 \quad \text{and} \quad v^0 = \Omega_1(t), \quad v^K = \Omega_2(t) \eta^{-1}$$

are easy enough, but the boundary condition $D_* u = 0$ is more interesting. How can this be imposed when all of the u 's are now defined? One realizes the values ψ^0 and ψ^K are still free and provide the needed two more conditions, through

$$(D D_* - a^2) u = \psi; \quad \text{set}$$

$$\begin{aligned} h^2 \psi^0 &= \left(1 + \frac{\Delta r}{2\lambda^0}\right) u^1 - \left(2 + \left(\frac{\Delta r}{\lambda^0}\right)^2 + a^2 (\Delta r)^2\right) u^0 + \left(1 - \frac{\Delta r}{2\lambda^0}\right) u^{-1} \\ &= \left(1 + \frac{\Delta r}{2}\right) u^1 + \left(1 - \frac{\Delta r}{2}\right) u^{-1}. \end{aligned}$$

Now impose $Du = 0$; the centered second order approximation defines $u^{-1} = u'$, so

$$\psi^0 = \frac{2}{(\Delta r)^2} u' \quad (42)$$

Similarly,

$$\psi^k = \frac{2}{(\Delta r)^2} u^{k-1} \quad (43)$$

These provide the additional constraints needed. If one felt uncomfortable with introducing the artificial u' above, one might think of only defining u from the ψ definition for $k = 2(1)K-2$, then imposing the boundary condition $Du = 0$ as $u' = u^2/4$, $u^{K-1} = u^{K-2}/4$, which then define ψ' and ψ^{K-1} :

$$\psi' = \left[\frac{1}{2(\Delta r)^2} + \frac{1}{(\Delta r)} \frac{1}{2r'} \left(1 - \frac{1}{2r'}\right) - \frac{a^2}{4} \right] u^2,$$

$$\psi^{K-1} = \left[\frac{1}{2(\Delta r)^2} - \frac{1}{(\Delta r)} \frac{1}{2r'} \left(1 + \frac{1}{2r'}\right) - \frac{a^2}{4} \right] u^{K-2}.$$

However, this scheme effectively brings the walls closer together, thereby causing too high a critical Reynolds number, so one should use the centered scheme. So much for ten hours work and experimentation.

For the numeric solution, all variables were initially zero for each run, then the ψ' 's were set with small random numbers. Then over-relaxation was used on (41) for $k = 1(1)K-1$ [with $u^0 = u^K = 0$]. When the error was small enough, ψ^0 and ψ^K were set as in (42) and (43). Now all of the right sides of (40.1) through (40.3) were defined, so a time-step could be taken. A fourth-order Kutta-Merson scheme with automatic error checks and step-size control was used. The curves $u(r)$, $v(r)$, $V(r)$, and $\psi(r)$ were displayed for visual checks, under sense switch control, so it was seen that v had the same period as V (forced to be 2π), and a similar shape, with zero crossings near the same radii. A

typical graph is given as figure 8 . The radial velocity u always had the same sign [after a transient adjustment period in which it occasionally kept a second mode appearance for a while], so had a zero-frequency component. It also grew twice in each V period. Superposed on these cycles was an exponential growth or decay. In figure 9 is a typical graph of the kinetic energies of the perturbation and the mean flow. Two bumps correspond to one basic period, due to the squaring. Note how well the perturbation kinetic energy can be represented as $p(t)e^{\sigma t}$, for p periodic. We thus have a picture of the motion; as the inner cylinder is past the middle of its swing, the centrifugal potential in the V boundary layer builds up enough to encourage u to grow, which advects V to encourage v . Thus, u will pulse on swings either way, whereas the sign of v will change on opposite swings. If the centrifugal potential is enough to cause more growth than the viscous decay over the whole cycle, then each cycle will result in the same proportional growth, once the fastest growing mode is dominant, and until limiting size is reached.

The whole system was run for various parameters Re , a^2 , and N relevant to the experiment with $\eta^{-1} = 1.0444$ described later. The initial value problem was run out far enough to determine whether there was growth or decay. While the

Figure 8. Typical display of u , v , and V during time integration for $\eta^{-1} = 1.0444$, $Re = 8000$.

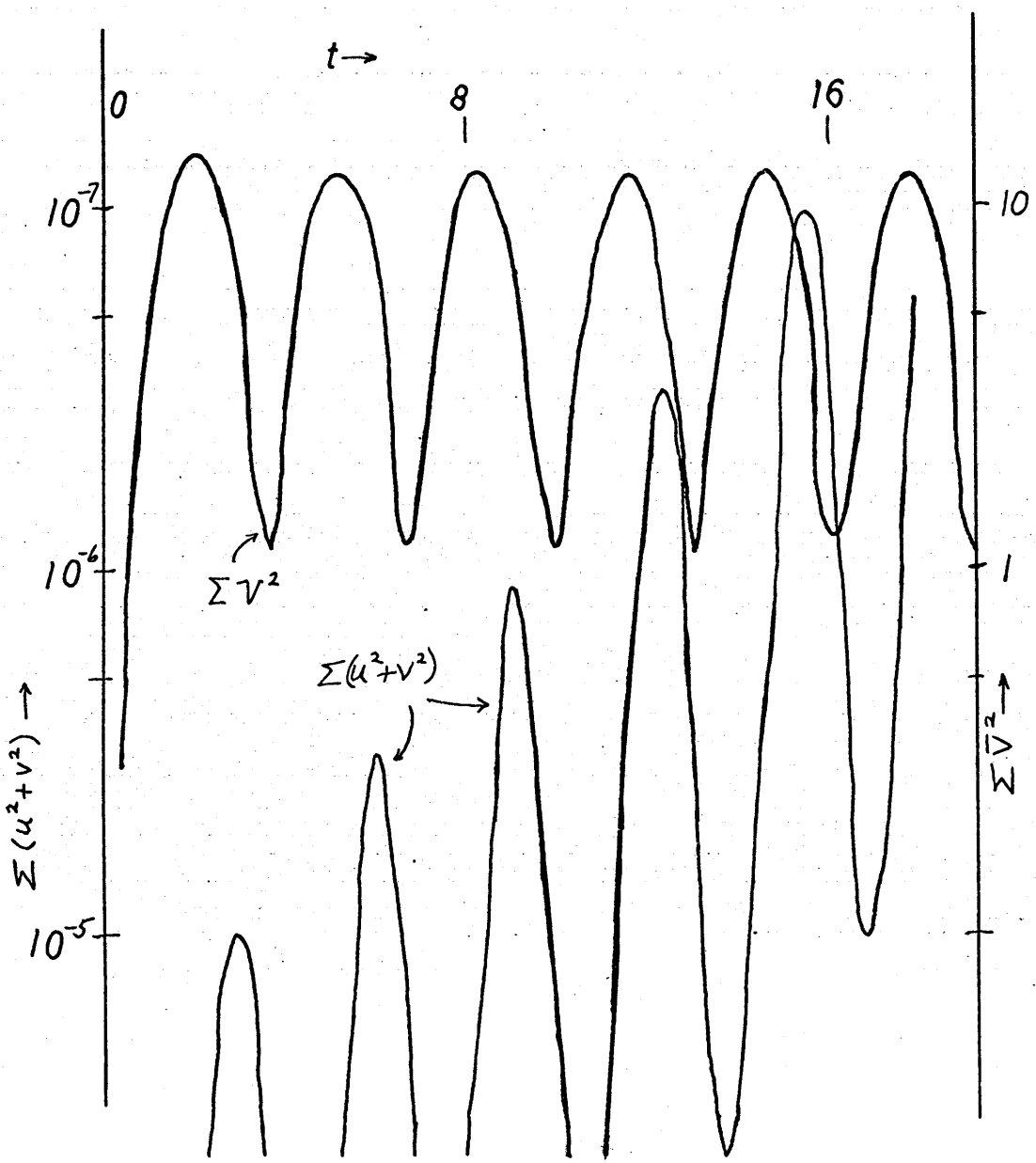
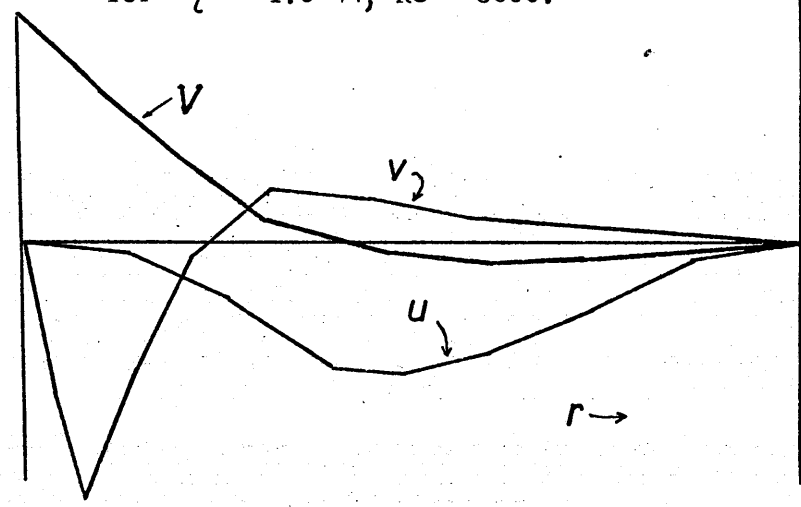


Figure 9. Basic flow and perturbation kinetic energies from time integration for $Re = 83.3$, $\eta = 0.5$, $N = 0.1$.

Oscillations were a handicap, fortunately only a few cycles were necessary, except near marginal growth. This indicates that the fastest growing (or most slowly decaying) mode was always quickly dominant. After the growth or decay was discerned, Re was changed until the value which gave zero growth was found. Then a^2 was changed until the Re found was minimized. The results are plotted for Re versus N in figure 10 and tabulated in table 2. The six points found represent over one hundred hours of computer time. The seventh is the steady limit from Taylor's narrow gap theory or figure 7.

For the smaller N 's (higher frequency, smaller angles), the amplitude of the kinetic energy oscillations were small, suggesting the pulses were rapid compared to the decay time, but not very efficient. For $N < 1$, the kinetic energy oscillations were over several decades, which is a strong 'on-off' behavior, and suggests the feasibility of a quasi-steady approximation, for $N \ll 1$, as discussed later. However, a quasi-steady approximation plainly will not be useful for $N > 1$, though then considerations of a mean-square centrifugal potential may be.

The critical Re was not sensitive to a^2 , explaining the rather large error estimates for a . The growth rate was much more sensitive to Re for small N , so the $KE = 0$ curve is closer to given finite amplitude for small N than large. Conrad and Criminale (1965) claim stability for $\eta^+ = 1.060$ and $N = 1.94$ if $Re \leq 103$ (after translating notation). While

this is the only η^{-1} for which they give a value, the narrow gap approximation translates this to a claim of stability for $\eta^{-1} = 1.0444$ and $N = 1.94$ if $Re < 163$. This point is also entered on the graph. Indeed, there will be stability below that Re .

Quasi-Steady and Rapid Oscillation Limits

When the oscillations are slow enough that the viscous boundary layer $\pi\sqrt{\nu/\omega}$ is thicker than the gap d , one expects a quasi-steady assumption to be realistic. The dimensional equations of motion and boundary conditions are given by (). Let us rescale $t \rightarrow \Omega^{-1}t$, so

$$\begin{aligned} [DD_* - a^2 - Re \frac{\partial}{\partial t}] \psi &= 2a^2 \sqrt{\nu/r}, \\ [DD_* - a^2 - Re \frac{\partial}{\partial t}] v &= (D_* V) u, \\ Re \frac{\partial V}{\partial t} &= DD_* V, \end{aligned} \tag{44}$$

where $\psi = (DD_* - a^2)u$,

$$\begin{aligned} u = v = D_* u &= 0 \quad \text{at } r = 1 \text{ and } r = \eta^{-1}, \\ V &= \sin Nt \quad \text{at } r = 1, \\ V &= 0 \quad \text{at } r = \eta^{-1}, \text{ so} \end{aligned}$$

$$V(r,t) = M(r) \sin Nt + N Re \delta^2 K(r) \cos Nt,$$

where M and K are $O(1)$ and $\delta = d/R$. Thus, V is 'quasi-steady' insofar as $N Re$ is small. Let us use this as an expansion parameter, so $\psi = \psi_0 + N Re \delta^2 \psi_1 + \dots$ etc, and retain the zero-order equations

$$\begin{aligned} (DD_* - a^2 - Re \frac{\partial}{\partial t}) \psi_0 &= 2a^2 M(r) \frac{\sin Nt}{r} v_0, \\ (DD_* - a^2 - Re \frac{\partial}{\partial t}) v_0 &= D_* M (\sin Nt) u_0, \end{aligned} \tag{45}$$

where $\psi_0 = (DD_* - a^2)u_0$,

$$u_0 = v_0 = D_* u_0 = 0 \quad \text{at } r = 1 \text{ and } r = \eta^{-1},$$

$$M = 1, K = 0 \text{ at } r = 1, M = K = 0 \text{ at } r = \eta^{-1}.$$

These are the quasi-steady equations, so one is justified in treating stability as depending only on the current time and not the past if $N \text{Re} \delta^2$ is small, i.e. if the forcing has plenty of time to diffuse. If it is, we have the classical $\text{Re} |\sin Nt| = \sqrt{1700} \delta^{3/2}$ and $a \approx 3.16$, which determine the times at which the rolls will 'switch on', reaching their limiting size in much less than a period of oscillation. They will die just as fast when $|\sin Nt|$ approaches its next zero. Of course, there will be no instability if $\text{Re} < \sqrt{1700} \delta^{3/2}$, at least for $N \ll \frac{1}{41} \delta^{-1/2}$. This guaranteed stability line is entered in figure 10, since it probably holds for larger N also, since it seems clear that the oscillating forcing will always be less destabilizing than steady rotation with the same maximum angular velocity [though quasi-steady results of Currie (1967) suggest this may not be quite true]. But in that case, Taylor (1923) gave a bound which for this η is $\text{Re} < 4710$, independent of N . This line is asymptotic to the results presented here. We see from figure 10 that the experiments were conducted for boundary layer thicknesses comparable to the gap width, and merge smoothly with the quasi-steady prediction to the right, for $N \ll 1$.

When the boundary layer thickness becomes enough less than the gap that even the vertical wavelength is less than

d, the dependence of the parameters on d should drop out. Then $\psi = (DD_* - k^2)u$ gives a ψ scale of $\omega u/\nu$, whereas $\nu(DD_* - k^2)\psi = 2k^2 Vv/r$ gives a ψ scale of $\frac{\Omega}{2}v$, and $\nu(DD_* - k^2)v = (D_*V)u$ gives a v-scale of $\frac{\Omega R}{\nu\omega}u$, which combine to force $\frac{\Omega^2 R (\frac{2}{\omega})^2}{\nu^2} \approx$ constant, much like the classical formula. Since $N = \frac{\omega}{\Omega}$, this can be squared to yield

$$Re = c N^3 \quad (46)$$

for N large. The asymptotic region was not reached in the experiments, for the exponent of N for Re increases from 0 at the right to about 1.9 at N = 1.5 at the left. The thickness of the viscous boundary here is about a third of the gap, and the wave-number has just started to increase, so the balances above still have factors of two and three depending on d as well as $\sqrt{\frac{\Omega}{\omega}}$.

Mean Rotations with Oscillations Superposed

With the equipment available, an obvious extension of the theme of time-dependent centrifugal instabilities was to superpose mean rotations of the outer and inner cylinders on the oscillation of the inner cylinder. This seemed attractive in connecting to the steady problem.

Donnelly (1964) experimentally studied effects on the stability of steady circular Couette flow of a superposed oscillation of the inner cylinder. Meister and Münzer (1966) and Conrad and Criminale (1965) studied this problem theoretic-

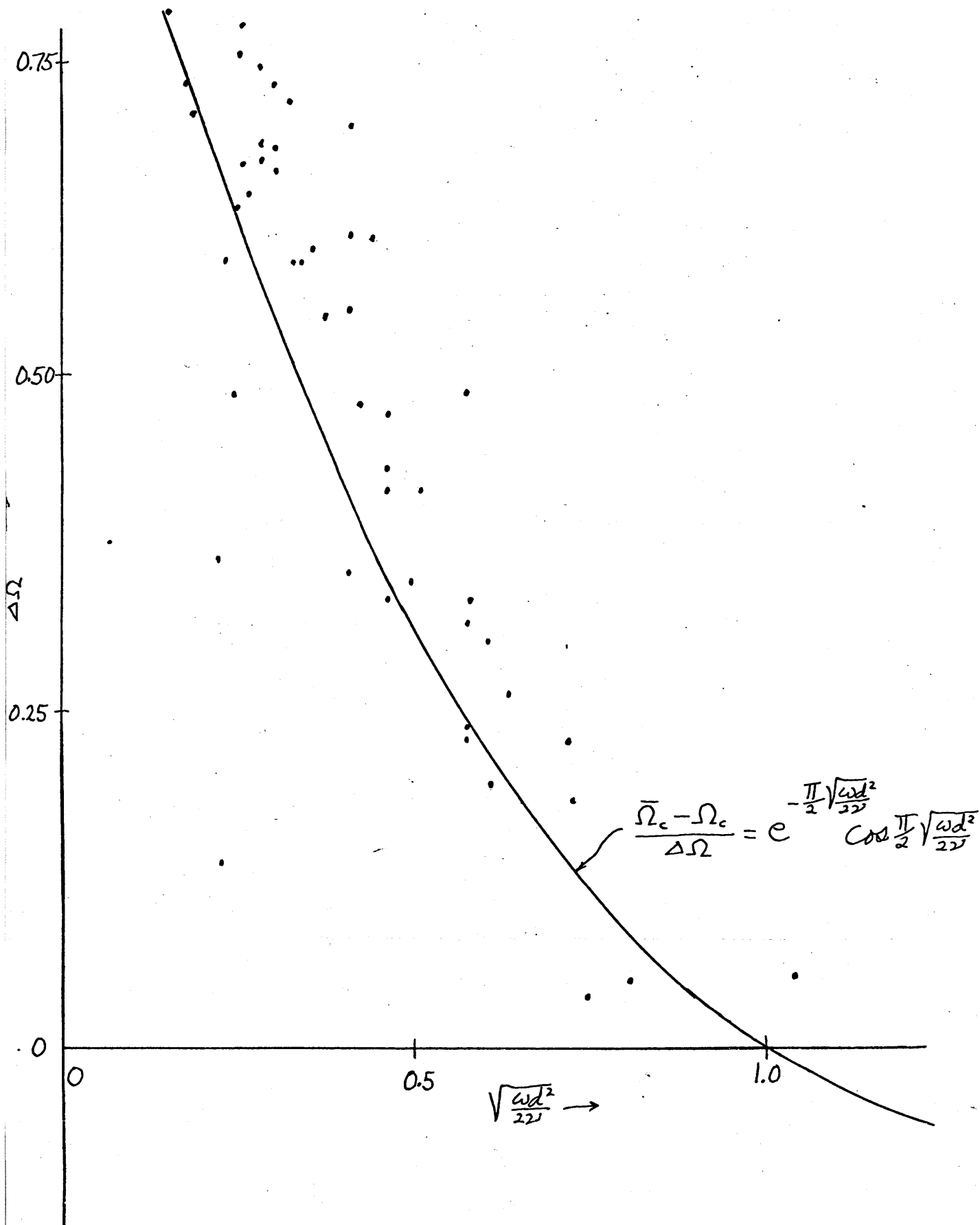


fig. 11 oscillation stabilization vs gap width

tically, and agreed with Donnelly that small amplitude oscillations can stabilize the mean flows. Donnelly's experimental points of onset of sharp increase of mean transmitted torque are replotted in figure 11. His abscissa is inverted to show the number of viscous waves in the gap. This way it seems clearer that the decrease in torque is due to the correlation of the phase of the viscous wave at the outer and inner walls. It even seems clear that the effect has about the same shape as the viscous wave, and if Donnelly had tried higher frequencies, he would have found a weak destabilization.

My observations of the onset of instability were visual rather than by average torque, and indicated the periodic existence of ring vortices about as soon as the maximum velocity exceeded the critical for steady, except for oscillations too fast to be quasi-steady. These did not show up much before the instabilities on the mean flow.

The claim here that oscillations superposed on a mean rotation always destabilize is not contradictory to Donnelly's conclusion, for while Donnelly's definition of instability involves a sudden increase in the torque, here the definition involves the existence of a different asymptotic solution to the equations of motion and boundary conditions than the basic one. Donnelly's own experiments showed the existence of ring vortices with a non-zero mean radial motion below the steady Taylor number.

The periodic ring vortices only appear on the latter

half of the forward swing, and not on the back, when the periodic velocity opposes the mean velocity. This and the possible destabilization for the proper frequency oscillations above suggest an interesting possible resonant instability. If the mean centrifugal gradient is stable, there will be 'inertial-elastoid' oscillations. What will happen if their natural frequency is driven? Clearly, inviscid modes would grow, but viscosity would oppose this.

Since the mean flow here is forced by viscosity, it would be interesting if a resonance could force a harmonic instability with viscosity present. The possible mechanism requires an inner oscillation at twice the natural frequency, so that the forward pulse may correlate with each outward swing of the mode, and the backward decay may match the end of the swing. One suspects that there will be considerable difficulty in getting this mechanism to work, for the high Reynolds number necessary to avoid too much decay on each cycle also makes the oscillatory boundary very thin, so not driving the mode efficiently.

The same program used for the pure oscillation was used, with the boundary conditions on V changed to include a dominant rotation. All runs were for $\eta = 1/2$ and $a^2 = 10$, and for simple rotation of the walls, so $V = 1$ at $r = 1$, $V = \eta^{-1}$ at $r = \eta^{-1}$. The natural frequency was found by setting the viscosity to zero and integrating in time. The solution oscillated very nicely on the scope. The real part of the frequency did not change measurably when viscosity was added. An inner oscillation was superposed on the inner

cylinder at that frequency, twice it, three times it, and several other frequencies. They all decayed fairly rapidly and rather indistinguishably. This suggests that either this viscous harmonic mechanism will not work, or a different mean state is necessary. When the forcing of the mean flow used a smaller Re than the Re of the perturbations, the resonance was quite discernible. Some growth rates are plotted in figure 12. This situation may arise if the mean flow is driven by an azimuthal pressure gradient rather than by the viscous drag of the walls.

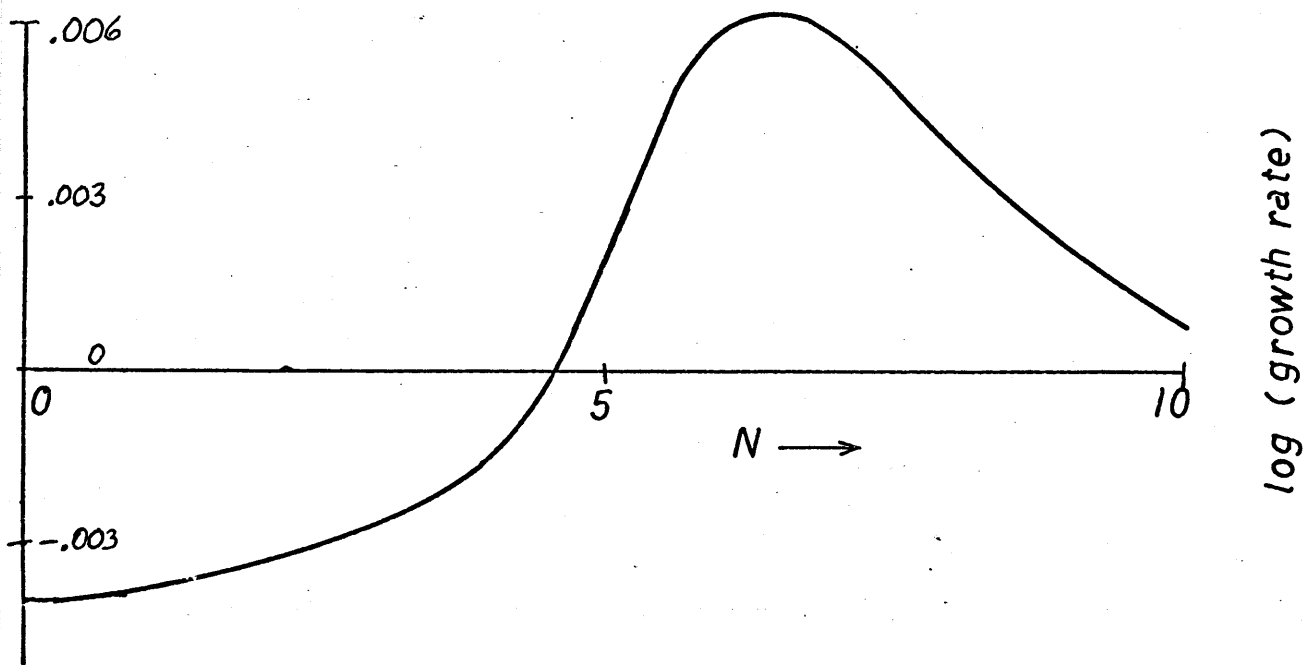


Figure 12.

Growth rate for $Re = 10000$ and $\eta = \frac{1}{2}$ for $\Omega_1 = 1 + 0.5 \sin Nt$, $a^2 = 10$.

Harmonic Decomposition.

Figure 9 and all of the other runs show that the kinetic energy can be well represented by $p(t)e^{\sigma t}$, with p periodic with the frequency of the basic oscillation, or twice it for symmetric oscillations. This reminds one of Floquet's theorem (see Coddington and Levinson, p 78-81, 1955), that the fundamental solution matrix of $\frac{dx}{dt} = F(x, t)$ with F periodic in t can be expressed $X(t) = P(t) \exp(Rt)$, where P is a periodic and R is a constant matrix. By using an L_2 norm, $\|X\| = \|P(t)\| \|\exp(Rt)\|$, where $\|X\|$ is a positive quadratic form like the kinetic energy. When using linear theory, the usual presumption is that the solution can be separated into modes, of which some one will dominate. Thus, $\exp(Rt)$ will normally tend toward a one-dimensional projector $R_\infty e^{\sigma t}$, where R_∞ is of rank 1, and the kinetic energy of any particular solution will tend to that of the dominant mode, or $p(t)e^{\sigma t}$, as observed.

Since this form holds so rapidly here, the presumption of a dominant mode holds. Thus, one might find it profitable to look for such modes, especially for $\sigma = 0$, which corresponds to the marginal stability for a steady basic flow. So, write

$$\psi = \psi_0(r) + \sum_{n=1}^{\infty} (\psi_{1n}(r) \cos nt + \psi_{2n}(r) \sin nt),$$

etc., substitute these into the equations of motion, and separate harmonic coefficients to get

$$\begin{aligned}
-\text{Re} N V_1 &= DD_* V_2 \\
\text{Re} N V_2 &= DD_* V_1 \\
-n \text{Re} N \psi_{1m} &= (DD_* - a^2) \psi_{2m} + \frac{a^2 \text{Re}}{\nu} [-V_1 v_{2,m+1} + V_2 v_{1,m+1}] \\
&\quad - a^2 \frac{\text{Re}}{\nu} [(1 - \delta_m) V_1 v_{2,m-1} + (1 + \delta_m) V_2 v_{1,m-1}], \\
n \text{Re} N \psi_{2m} &= (DD_* - a^2) \psi_{1m} - \frac{a^2 \text{Re}}{\nu} [V_1 v_{1,m+1} + V_2 v_{2,m+1}] \quad (47) \\
&\quad + \frac{a^2 \text{Re}}{\nu} [-(1 + \delta_m) V_1 v_{1,m-1} + (1 - \delta_m) V_2 v_{2,m-1}], \\
-n \text{Re} N v_{1m} &= (DD_* - a^2) v_{2m} + \frac{1}{2} \text{Re} [-(D_* V_1) u_{2,m+1} + (D_* V_2) u_{1,m+1}] \\
&\quad - \frac{1}{2} \text{Re} [(1 - \delta_m) (D_* V_1) u_{2,m-1} + (1 + \delta_m) (D_* V_2) u_{1,m-1}], \\
n \text{Re} N v_{2m} &= (DD_* - a^2) v_{1m} - \frac{1}{2} \text{Re} [(D_* V_1) u_{1,m+1} + (D_* V_2) u_{2,m+1}] \\
&\quad + \frac{1}{2} \text{Re} [-(1 + \delta_m) (D_* V_1) u_{1,m-1} + (1 - \delta_m) (D_* V_2) u_{2,m-1}], \\
\psi_{im} &= (DD_* - a^2) u_{im},
\end{aligned}$$

where $n = 0, 1, 2, 3, \dots$, $i = 1, 2$, and the boundary conditions are $u_{in} = v_{in} = D_* u_{in} = 0$ at $r = 1$ and $r = \eta^{-1}$, for $n = 0, 1, 2, 3, \dots$, and V_i given. Note there are two independent sets of harmonics. The first are the even harmonics for u and the odd for v . These are the ones observed numerically and experimentally. u has a mean and a double frequency component, whereas v has the fundamental. The other set of harmonics with u oscillating at the fundamental and v with a rectified component must require a higher Re .

The obvious method to solve the above system of equations is to follow Galerkin or Lorenz, and to truncate the above system to $n \leq$ constant, setting variables with higher subscripts to zero and solve for the eigenvalue Re . The above equations all have the second-order operator DD_* , and seem quite suitable for relaxation. This system was programmed separately by two programmers in quite different

styles. Overstability in the relaxation was avoided by under-relaxing with a factor $\min(1, (2n\text{Re}n^2)^{-1}, (a^2\text{Re}h^2)^{-1})$. This was necessary, else there was a rapidly-growing oscillatory numerical instability due to the large coefficients, in close analogy to the time-step limitation for parabolic equations such as these arose from. However, even with this under-relaxation, when the second harmonic was added to the system, both programs gave kinetic energies which grew continually for any Re , though not rapidly. This is disturbing, and suggests a new numerical instability, which deserves to be understood.

Let us consider a simple analog: $D^2y + \text{Re}y = 0$, with $y(0) = y(\pi) = 0$. This simple system has non-trivial solutions only if $\text{Re} = n^2$ for some integer n , so has only the trivial solution for $\text{Re} < 1$. What happens when one tries a relaxation for various Re 's? Experiments were run for the usual second-order relaxation scheme,

$$\Delta y^j = \frac{1}{2} [y^{j+1} - 2y^j + y^{j-1} + \frac{\pi^2}{3^2} \text{Re} y^j].$$

For $\text{Re} = 1$, y quickly came to resemble the first arch of a sine, but very slowly decayed, reflecting the slightly different spectral character of the finite-difference operator from the differential operator. For $\text{Re} < 1$, the solutions decayed, and did so more rapidly the smaller Re was. For $\text{Re} = 1.02$, the solution slowly decayed, then grew as the first mode emerged. For larger Re , there was rapid growth. So this works nicely, and suggests the instability may lie in the boundary conditions for ψ .

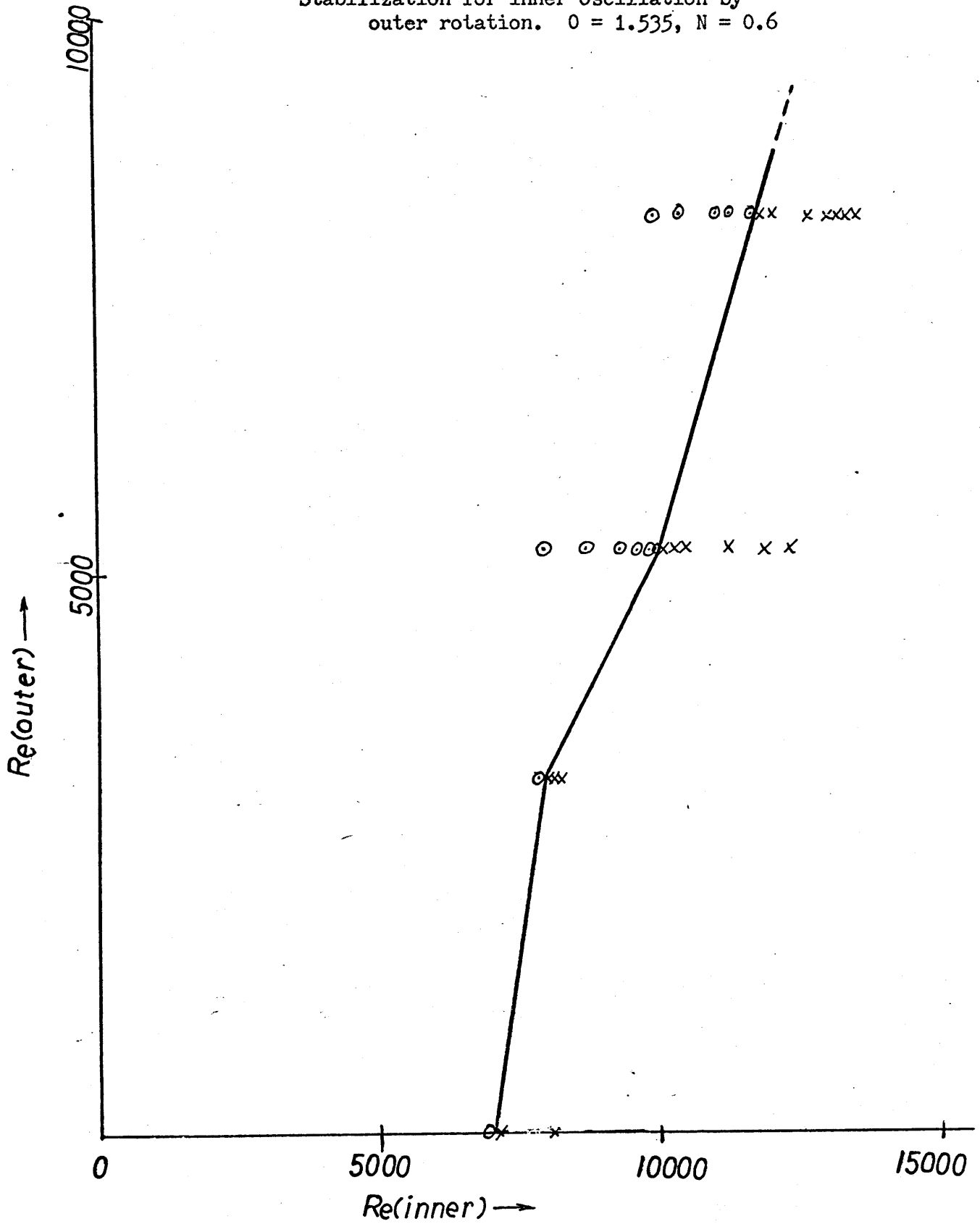
Experiments for Oscillations.

The major piece of apparatus was built by H. Snyder and S.K.F. Karlsson at Brown University, and is described in several places, such as Snyder and Karlsson (1964). It has elaborate circulation and control devices to maintain temperatures, as well as complicated electronic measuring devices. However, the latter rarely worked, so could not be used, so periods were measured with a stop-watch, and existence of the vortices was determined visually. Both the inner and outer cylinders could be oscillated independently, with or without a superposed rotation. Installing a heavy fly-wheel allowed very smooth oscillations. The radius of the inner cylinder is $6.0275 \pm .0003$ cm, with length 90 cm. The radius of the outer cylinder is $6.295 \pm .0003$ cm, so the gap width is $0.267 \pm .0006$ cm, and $\eta = 0.9575$, $\eta^{-1} = 1.0444$. Thermistors at various locations were used to center the inner cylinder by checking that no periodic variation occurred in the output voltages as the cylinders rotated. The voltage from a precision potentiometer on the drive shaft was displayed against a harmonic oscillator at 0.180 cps. The signal was found to be virtually free of harmonics.

The apparatus included ink outlets, but these did not

work. The ring vortices were first visualized using nacromer, but this was found to flocculate. Aluminum powder was tried, but required too large a concentration, settling on the glass and forming slag inside the apparatus. It should never be used in apparatus that cannot be taken apart and washed. The same is true of the artificial nacromer tried next. While washing this out with Ivory Liquid detergent, it was noticed that beautiful vortices formed while the inner cylinder was rotating, even for just a few capfuls in several gallons. Ivory Liquid seems more satisfactory than nacromer generally, for it is cheap, won't settle out, and even helps to clean the apparatus, so was used from then on. The observation procedure was to set the lever arm of the oscillation gear, then to measure the angular amplitude of a half rotation. This did not change during operation, for there was no measurable back-lash. Then any mean rotation was turned on and determined by counting with a stopwatch. Then the oscillation frequency was counted, using the gear arm crossing a slot in the wheel to define a cycle. The temperature of the bath was noted. Then any existence of vortices at any part of the cycle was noted. As soon as vortices were seen, the oscillation frequency was lowered until they could not be, then up again until they could. No hysteresis was noted, so the time could be noted to 0.1 second over a minute or so. The temperature was also measured to 0.01C. Unfortunately, the basic definition of existence was not so accurate, but varied with the condition of the nacromer. It is also often difficult to

Stabilization for inner oscillation by
outer rotation. $\sigma = 1.535$, $N = 0.6$



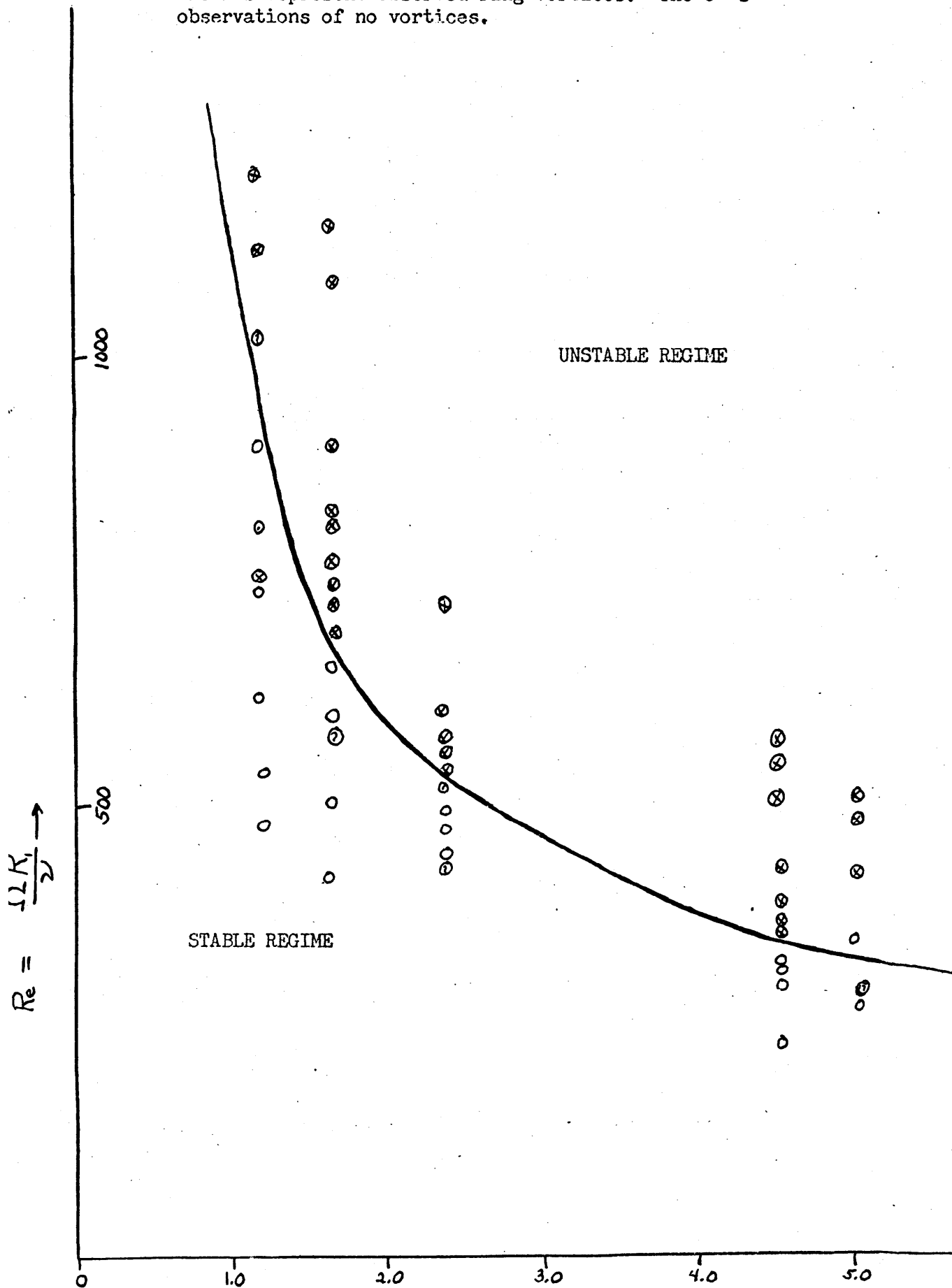
decide if faint, flickering lines are really there. However, wherever they were definitely observed, a '+' is entered in figure . When near critical, the rolls only appear near the ends of the swings. The abscissa is angular amplitude ($\theta = N^{-1}$), and the ordinate is Reynolds number. The data seems satisfactory in lying above the zero-growth line nearly on a constant growth isopleth. The pair of points lying far below the line are undoubtedly a blunder, probably due to measuring the angle between the end-points of oscillation the wrong way around. An attempt at measuring wavelength was made. While parallax made even harder the counting and delimitation of the faint on and off bands near critical, the average at $N = 0.7$ was about 2.1 waves/cm. With $R = 6.3$ cm, the numerical study result of $a^2 \approx 5500$ gives 1.9/cm. For higher N , there were smaller wavelengths observed. Some experiments were run with the outer cylinder rotating while the inner oscillated. Just as one would expect, the outer rotation stabilized. The results are plotted in figure . The necessary oscillating Reynolds number increases approximately linearly in the outer Reynolds number. Some data on oscillation of the inner cylinder with a mean rotation superposed were also gotten before the main bearing wore out. For these, the oscillation amplitude and frequency were set first, then the mean angular velocity to cause instability was found. The rolls only occurred on the forward swing now. Some experiments for inner oscillation only were run in a much smaller and cruder apparatus at M.I.T., for a different gap width. After grinding down the

inner cylinder to be rid of rust spots, the inner radius was 2.08 cm, the outer was 2.57 cm, so $\eta = .807$, and the height of the cylinders was 15 cm. The oscillation amplitude could only be set at six angles, and the range of constant frequency for the small motor was discrete and rather limited. However, water and mixtures of Dow-Corning 200 silicone oil allowed several viscosities, so further Reynolds numbers. The results are plotted in figure 13. The results seem reasonably consistent over two orders of magnitude in ν , considering that a secretary laughed when she saw the experimental set-up.

EXPERIMENTAL RESULTS OSCILLATION OF THE INNER CYLINDER

WITH $\eta = .807$

The x's represent observed ring vortices. The o's observations of no vortices.



Coda.

In the final stages of preparing this thesis, a very relevant paper by Rosenblat (1968) appeared. Rosenblat notes the importance, yet neglect, of the effects of time-dependence on instabilities, then considers centrifugal instabilities of inviscid, periodic flows between coaxial cylinders. He linearizes and assumes axisymmetry, and also discusses what instability might mean.

For rigid oscillations of the mean flow, he finds the time-dependence of the disturbances to be $\cos(\frac{\gamma}{\omega} \cos \omega t)$, where γ is the exponent for the corresponding steady (Rayleigh) problem. If this be complex, and ω is small, the disturbance will increase $\exp(\frac{\gamma}{\omega})$ -fold during growth, which may take it out of the linear range.

He next considers nearly rigid oscillations. He finds the phase-differential in the radial direction, however small, is sufficient to cause instability. This conclusion certainly does not extend to viscous flows. It also does not hold for $N \ll 1$, which is exactly the requirement for nearly rigid oscillations when the mean flow is driven by wall oscillations.

Rosenblat shows that small oscillations on a stable steady mean flow will be stable, except in a band around twice the natural frequency of an inertial-elastoid oscillation, though he suppresses the dependence of this

frequency on vertical wave-number. This seems to mean that for all driving frequencies below 2π , some wave-numbers will be subharmonically unstable.

When the steady mean flow is unstable, Rosenblat finds a second-order, inviscid decrease in the linear growth rate, which he takes to explain the reduction in limiting amplitude found by Donnelly (1964). This seems questionable.

Chapter Three - Suddenly Twisted Cylinder.

We now consider another time dependent flow on which centrifugal instabilities may arise, that of suddenly starting the inner cylinder rotating, with a view toward meaning and methods, rather than just the problem at hand. The equations of motion are already given in (1.1). As soon as the cylinder starts, a thin boundary layer on it will form, of thickness $\approx \sqrt{\nu t}$. When this grows thick enough, the centrifugal potential will be great enough to pay radial motions. We first are interested in the margin between decay and growth. Mallick (1957) considers the mean flow around a suddenly twisted cylinder, but gets no closed expression, and does not consider the instabilities. The impulsively started sphere has been considered by Barrett (1967), expanding in $\delta = \sqrt{\frac{\nu t}{R_1^2}}$ and using boundary layer theory, but instabilities are not involved. A similar problem of a suddenly applied temperature in the Benard problem has been considered by Lick (1965) and repeated by Currie (1967), but using an assumption of quasi-steadiness, as well as a broken-line approximate mean temperature gradient. Robinson (1965) also considers this Benard problem, using an erfc profile, and devotes some attention to when the quasi-steady approximation may be valid. His results bear a resemblance to the numeric initial-value results of Foster (1965).

Why should one be able to make such an assumption as quasi-steadiness when the mean is changing so much? The

usual argument is that the perturbations have a much shorter time scale than the mean, and then they consider the marginal state ($\sigma=0$) of zero growth rate. This seems a contradiction, especially since no perturbation time-scale is produced. Consider a simple example $\frac{dy}{dt} = ty - Ey$. The quasi-steady approximation gives $0 = ty - Ey$ or $t = E$ as a stability bound. The actual solution is $y = y(0) \exp(\frac{t^2}{2} - tE)$, which has a minimum of $y = y(0) \exp(-E^2/2)$ at $t = E$, so the approximation does give the division between decay and growth. However, $y(2E) = y(0)$, so y cannot grow past its initial perturbation size until $y = 2E$. It can be made to have arbitrarily large $\frac{dy}{dt}$ at $y = 2E$, by large E , so is not $2E$ the bound past which initial perturbations grow? This sort of definition would be operationally more meaningful, in requiring a finite size large enough to be detectable. However, it is usually inconvenient theoretically, since it requires considerations of limiting size, as well as depending on the particular detection device.

The axisymmetric linearized equations for the started cylinder are

$$\begin{aligned} \frac{\partial u}{\partial t} &= -\frac{\partial p}{\partial z} + 2\frac{\nu}{r}v + \nu\left[\frac{\partial}{\partial r}\left(\frac{1}{r}\frac{\partial(ru)}{\partial r}\right) + \frac{\partial^2 u}{\partial z^2}\right], \\ \frac{\partial v}{\partial t} &= -\frac{1}{r}\frac{\partial(rv)}{\partial r}u + \nu\left[\frac{\partial}{\partial r}\left(\frac{1}{r}\frac{\partial(rv)}{\partial r}\right) + \frac{\partial^2 v}{\partial z^2}\right], \\ \frac{\partial w}{\partial t} &= -\frac{\partial p}{\partial z} + \nu\left[\frac{1}{r}\frac{\partial}{\partial r}\left(r\frac{\partial w}{\partial r}\right) + \frac{\partial^2 w}{\partial z^2}\right], \\ \frac{1}{r}\frac{\partial(ru)}{\partial r} + \frac{\partial w}{\partial z} &= 0, \end{aligned} \quad (48)$$

where

$$\frac{\partial v}{\partial t} = \nu \frac{\partial}{\partial r} \left(\frac{1}{r} \frac{\partial(rv)}{\partial r} \right),$$

and $u = v = w = 0$ at $r = R$, $V = \begin{cases} 0, & t < 0 \\ \Omega R, & t > 0 \end{cases}$ at $r = R$,

all $\rightarrow 0$ as $r \rightarrow \infty$, all $\rightarrow 0$ as $t \rightarrow 0$ ($r \neq R$).

We are interested in the margin between decay and growth. Assume the r scale is $\sqrt{\nu t} = \delta R$ and the z scale is L, to be found. Look at $\frac{\partial}{\partial t} = 0$ (quasi-steady margin), i.e., balance generation and dissipation. The scales are

$$\frac{P}{\delta R}, \quad \Omega V, \quad \frac{u}{t}$$

$$\frac{P}{L}, \quad \frac{\Omega u}{\delta}, \quad \frac{v}{t}$$

$$\frac{W}{L}, \quad \frac{u}{\delta R}$$

$$\Rightarrow W \sim \frac{L}{\delta R} u, \quad P \sim \frac{LW}{t} \sim \frac{L^2 u}{\delta R t}, \quad V \sim \frac{\Omega t}{\delta} u$$

so the scales in the first equation are

$$1 : \frac{\Omega^2 t^3 \nu}{\delta L^2} : \frac{\nu t}{L^2}.$$

In the experiments, $\Omega t \gtrsim 30 \gg 1$, so the last term is much smaller than the second, giving scale $L \sim \Omega t \delta R \gg \delta R$, or even R. This is the sort of wave-length one expects first to go unstable. Note the sharpening of Robinson's quasi-steady conclusion of wave-number zero in scale R being the most unstable. This small but non-zero wavenumber matches the numerical results better. Another conclusion is that the scale of generation/dissipation is $\Omega^2 t^2 \delta^{-1}$, so one expects growth for t_0 such that $\Omega t_0 \delta^{-1/2} > \text{critical}$, or:

$$\frac{\Omega R^2}{\nu} = c * \left(\frac{\nu t}{R^2} \right)^{-3/4}, \quad (49)$$

just as observed. Thus, balancing generation and dissipation gives the right form; quantitative considerations will also yield the constant c. First one might remark that this problem with a V boundary layer with one rigid surface condition and one open is similar enough to the classical convection problem with one rigid and one free boundary to

suggest that c in the last equation is about $\sqrt{1100}$. This works beautifully in figure 13, so now to find out why.

Writing $r = R(1+\delta x)$, and using δR for the z -scale for simplicity, the dimensionless equations of motion are

$$\begin{aligned} \frac{1}{\tau_a} \frac{\partial u}{\partial t} &= -\frac{\partial p}{\partial x} + 2\tau_a \frac{v}{1+\delta x} + \frac{1}{\tau_a} \left(\frac{\partial^2 u}{\partial x^2} + \frac{\delta}{1+\delta x} \frac{\partial u}{\partial x} - \frac{\delta^2 u}{(1+\delta x)^2} + \frac{1}{\tau_a} \frac{\partial^2 u}{\partial z^2} \right), \\ \frac{\partial v}{\partial t} &= -\left(\frac{\partial v}{\partial x} + \delta \frac{v}{r} \right) u + \frac{\partial^2 v}{\partial x^2} + \frac{\delta}{1+\delta x} \frac{\partial v}{\partial x} - \frac{\delta^2 v}{(1+\delta x)^2} + \frac{1}{\tau_a} \frac{\partial^2 v}{\partial z^2}, \\ \frac{\partial w}{\partial t} &= -\frac{\partial p}{\partial z} + \frac{\partial^2 w}{\partial x^2} + \frac{\delta}{1+\delta x} \frac{\partial w}{\partial x} + \frac{1}{\tau_a} \frac{\partial^2 w}{\partial z^2}, \\ \frac{\partial u}{\partial x} + \frac{\partial w}{\partial z} + \frac{\delta}{1+\delta x} u &= 0. \end{aligned} \tag{50}$$

Note that the coefficient $\tau_a = \Omega^2 t^2 / \delta$ depends on t , as does the shape of V . We see that when δ is small, the only $O(1)$ parameter is τ_a , so it is natural that it is the critical parameter, as argued above. Since it will be independent of δ for small δ , a boundary layer argument will yield the constant.

Quasi-Steady Approach

The quasi-steady approach is to assume the basic flow changes slowly, so there is exponential time-dependence, then to set the growth-rate to zero. Perhaps a more consistent approach is to assume that one mode is dominant and find when the generation exactly balances the dissipation, so leaving zero growth rate. This view has no explicit dependence on slow change for the basic state,

hiding this assumption under the assumption of one mode dominating. Either case uses the equations (48) with $\frac{\partial}{\partial x} = 0$. One can eliminate p and w to get

$$0 = (DD_* - a^2)\psi - 2a^2 \text{Re} V v / r,$$

$$0 = (DD_* - a^2)v - \text{Re}(D_* V)u,$$

$$\text{where } \psi = (DD_* - a^2)u,$$

$$u = v = D_* u = 0 \text{ at } r = 1 \text{ and as } r \rightarrow \infty.$$

This is solved by 'shooting'. Write

$$\begin{aligned} y_1 &= u & \text{so } Dy_1 &= y_2 - y_1 / r, \\ y_2 &= D_* u & \text{so } Dy_2 &= y_3 + a^2 y_1, \\ y_3 &= \psi & \text{so } Dy_3 &= y_4 - y_3 / r, \\ y_4 &= D_* \psi & \text{so } Dy_4 &= a^2 y_3 + 2a^2 \text{Re} V y_5 / r, \\ y_5 &= v & \text{so } Dy_5 &= y_6 - y_5 / r, \\ y_6 &= D_* v & \text{so } Dy_6 &= a^2 y_5 + \text{Re}(D_* V) y_1, \end{aligned} \tag{51}$$

here $y_1(1) = y_2(1) = y_5(1) = 0 = y_1(\infty) = y_2(\infty) = y_5(\infty)$. This is a two-point boundary value problem, which is solved similarly to that of the bottom boundary in Chapter One: solve for three sets of initial conditions $(y_3, y_4, y_6) = (1, 0, 0), (0, 1, 0), \text{ and } (0, 0, 1)$. The system of equations above is linear, so the outer boundary conditions can be satisfied if the determinant of (y_1, y_2, y_5) for the three solutions goes to zero as r goes to infinity. One actually solves by finding that the determinant changes sign somewhere for large enough Reynolds number, but does not at a lower Reynolds number. One deduces that there is an intermediate value for which the determinant is asymptotically zero from continuity of the solutions with respect to the initial conditions.

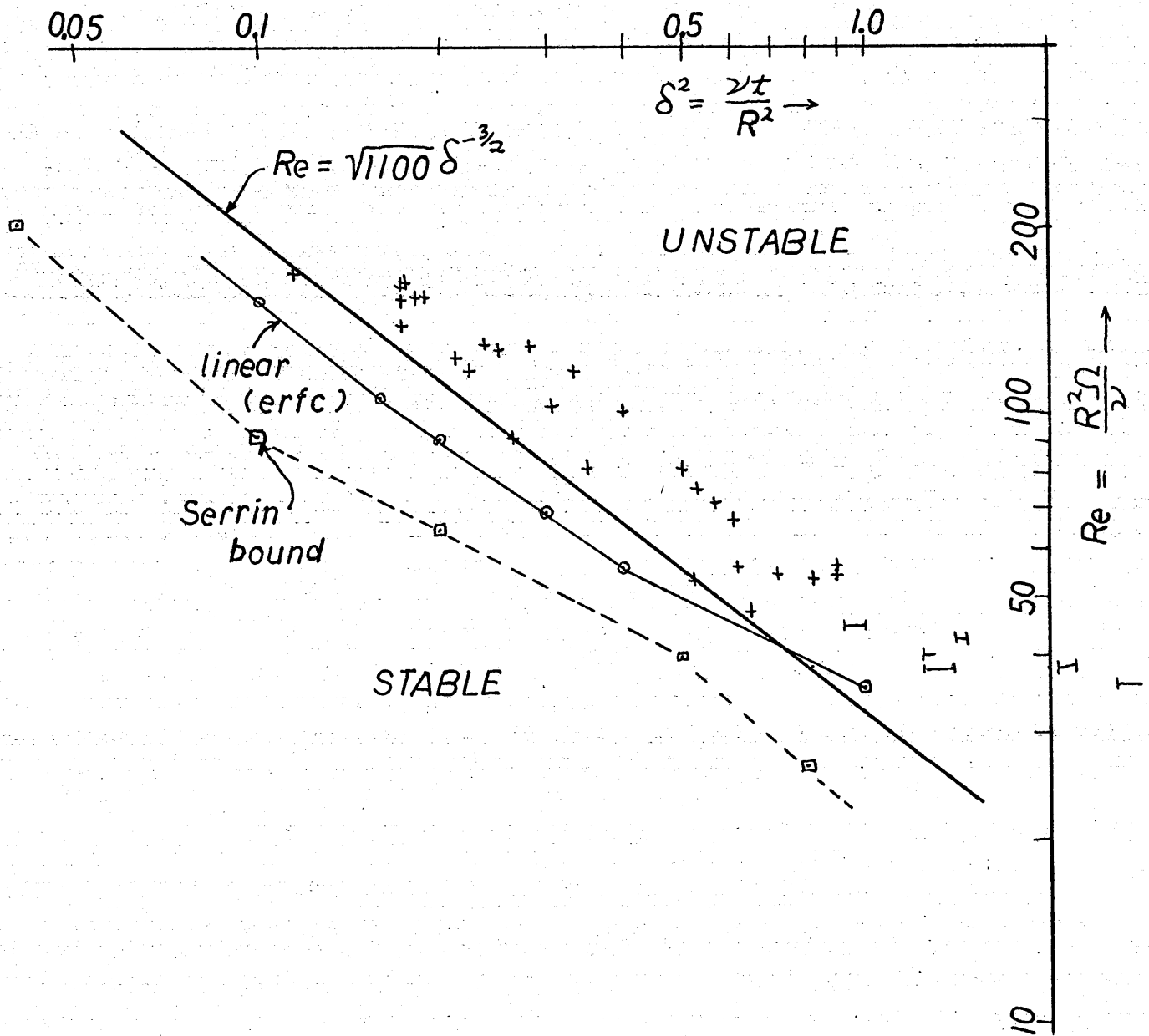
This numerical integration was carried out for the approximation $V = \operatorname{erfc}((r-1)/\delta)$. This should be an excellent approximation for small δ . The results are plotted in figure (13), and form a reasonable lower bound for the observed instabilities, suggesting that this 'quasi-steady' method here gives a good approximation to the time of minimum energy, as in the simple example at the beginning of this chapter.

One discrepancy of this quasi-steady approach is that the wave numbers come out higher than for the fastest growing waves found from the initial-value integrations, which are presented in figure 14. These curves are even shaped rather like the simple example considered at the beginning of this chapter -- they grow back to their original perturbation size about as long after zero growth rate as it took to get there, and some of those that dropped more slowly also grew more slowly and were passed. There is a correlation between those wavelengths which started growing first and those which grew most rapidly later, which explains some of the success of the quasi-steady method.

Numerical Methods.

Because the equations of motion are the same for this problem as for the oscillating cylinder of the last chapter,

Figure 13. Predicted stability boundaries and observed instabilities for the started cylinder.



it is first worthwhile to try this initial value problem with the inner boundary condition changed to

$$V(1,t) = 1,$$

and the outer boundary changed to $r = 4$, where the boundary conditions were changed to free slip, $u = Dv = DD_x u = 0$, since this seemed to work heuristically quite well in figure 13. $R = 4$ was far enough out that imposing a virtual mass from the exterior solution would not be worth while.

The most obvious feature of the solutions was that while v had the same r -scale as did V , u and w had a much wider scale. This suggests the value of a boundary treatment, and made difficult a grid representation. The number of grid points was increased to 36, which gave smooth enough curves on the screen to indicate that both scales were adequately handled.

Reynolds numbers of 50, 100, and 150 were run for various wave-numbers designed to be near maximum growth. The kinetic energies of the disturbances as functions of the non-dimensional time from starting are given in figure 14. To compare these results with the quasi-steady theory and the experimental results discussed later, some level must be selected at which the disturbances have become 'unstable'. The quasi-steady theory essentially finds the points at the bottoms of the curves, where the kinetic energy growth is zero. Examining these curves, we see that the time to this point is not very dependent on the wave-number, and is not necessarily related to the wave-number which grows most rapidly later.

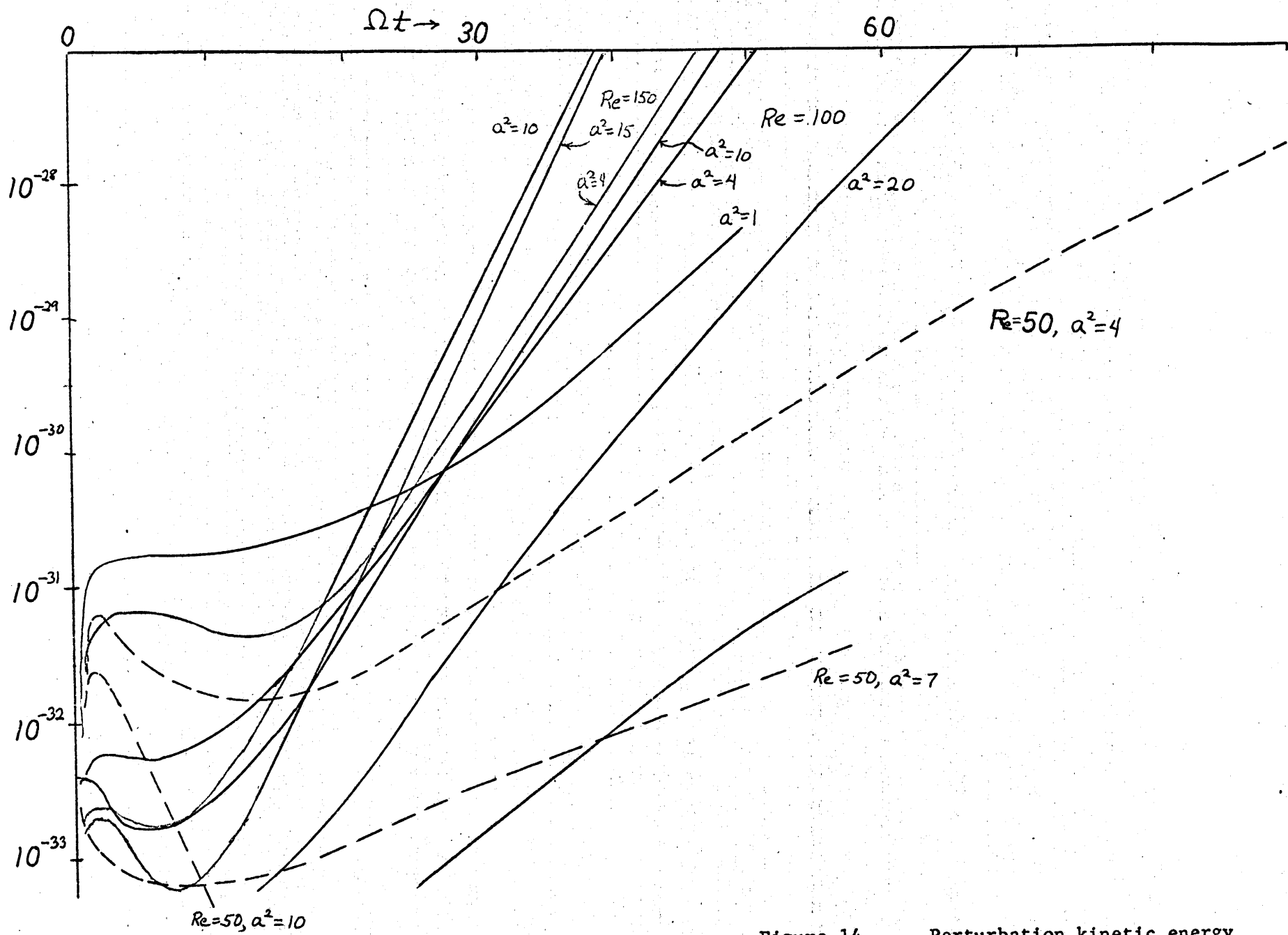


Figure 14. Perturbation kinetic energy versus time after cylinder starts.

The initial peaks are adjustment of the energy from potential, where it is put initially, to kinetic. The declining parts represent viscous decay before the main boundary layer grows thick enough to yield energy. Note that the higher wave-numbers decay more during this period, though they may start drawing energy earlier. The wave number of maximum growth increases with Reynolds number, and with a nearly linear in Re , which is to say, their wavelength remains nearly proportional to the boundary thickness. The growth rates are exponential with log-slopes very nearly constant over the period run, and increase with Re , perhaps at a $4/3$ power rate.

Finite-Difference forms.

So far, the conventional second-order finite-difference approximations have been used, largely because they are relatively easy to program, especially at boundaries. Now let us consider what finite-difference forms ought to be used. Most of the computations essentially involve parabolic terms, for which

$$\frac{\partial v}{\partial t} = \frac{\partial^2 v}{\partial x^2}, \quad v(0) = v(\pi) = 0 \quad (52)$$

is the prototype; non-zero boundary conditions can be absorbed in interior forcing. Let us consider how this might be accurately computed with a special view toward eliminating the purely computation restriction on step size

$\Delta t \leq \frac{(\Delta x)^2}{2}$, which can be very inconvenient for fine grids necessary to look at boundary layers, such as in present problem. Arakawa showed the value of preserving quadratic integral forms. Here we have

$$\frac{\partial}{\partial t} \int_0^{\pi} \frac{v^2}{2} dx = - \int_0^{\pi} \left(\frac{\partial v}{\partial x} \right)^2 dx,$$

so let us force a finite-difference approximation to this, where the integrals are approximated by sums. Let us use three-point finite-difference approximations for illustration:

$$\left. \frac{\partial v}{\partial x} \right|^k = a v^{k-1} + b v^k + c v^{k+1}$$

$$\left. \frac{\partial^2 v}{\partial x^2} \right|^k = d v^{k-1} + e v^k + f v^{k+1},$$

and require these to hold exactly for $v = 1$ and $v = x$, i.e., to be of first-order accuracy. Now impose the integral energy condition in the form

$$\frac{\partial}{\partial t} \sum \frac{v_k^2}{2} = - \sum \left(\frac{\partial v^k}{\partial x} \right)^2,$$

or, using the boundary conditions $v^0 = v^m = 0$,

$$(d + f) \sum v^k v^{k+1} + e \sum (v^k)^2 = -(a^2 + b^2 + c^2) \sum (v^k)^2 - 2(a+c)b \sum v^k v^{k+1} - 2ac \sum v^k v^{k+2}.$$

Above we imposed four conditions on the six coefficients, so we may impose the zero and first order conditions here. There are two solutions to these six equations:

$$a = 0, b = -\frac{1}{\Delta x}, c = \frac{1}{\Delta x}, d = \frac{1}{(\Delta x)^2}, e = -\frac{2}{(\Delta x)^2}, \text{ and } f = \frac{1}{(\Delta x)^2},$$

which is an Euler approximation

$$\left. \frac{\partial^2 V}{\partial x^2} \right|^k = \frac{V^{k-1} - 2V^k + V^{k+1}}{(\Delta x)^2}, \quad \left. \frac{\partial V}{\partial x} \right|^k = \frac{V^{k+1} - V^k}{\Delta x}.$$

The other is the backward Euler, $\left. \frac{\partial V}{\partial x} \right|^k \approx (V^k - V^{k-1}) / \Delta x$. Note that the centered approximation $\left. \frac{\partial V}{\partial x} \right|^k \approx (V^{k+1} - V^{k-1}) / 2\Delta x$ would not be consistent with this energy equation. Also note that $0 = 2ac$ and $f + d = 2/(\Delta x)^2$, so this approximation is actually second order in the energy and second derivative approximations.

Thus, using an Arakawa style approach, the Euler scheme

$$V^k(t + \Delta t) = V^k(t) + \frac{\Delta t}{(\Delta x)^2} [V^{k-1} - 2V^k + V^{k+1}]$$

is derived as 'energy preserving'. Yet if $\Delta t > (\Delta x)^2/2$, the energy grows rapidly. The trouble is that the energy requirement was imposed with $\frac{\partial}{\partial t}$, but the computation is done with $\Delta/\Delta t$. The above scheme would be stable on an analog computer, but only digital computers can handle systems of the necessary complexity.

Since the equation (52) is linear, let us use a spectral viewpoint. We are committed to a discrete grid $\{X^k\}$ by use of a digital computer, so cannot handle anything with finer scale, if such are important, a finer grid must be used. Thus, we can regard V as band-limited, so

$$V = \sum_{p=1}^{m-1} a_p \sin px, \quad \text{where } a_p = \frac{2}{m} \sum_{k=1}^{m-1} V\left(\frac{k\pi}{m}, t\right) \sin \frac{pk\pi}{m}$$

by the Sampling Theorem, even between the gridpoints. Thus,

$$\nabla^2 V = - \sum_{p=1}^{m-1} p^2 a_p \sin px, \quad (53a)$$

$$\text{so } \frac{\partial a_p}{\partial t} = -p^2 a_p \quad \text{and } a_p(t + \Delta t) = a_p(t) \exp(-p^2 \Delta t) \quad (53b)$$

for arbitrary Δt . Combining (53a) and (53b) gives

$$V\left(\frac{k\pi}{m}, t + \Delta t\right) = \sum_{j=1}^{m-1} C(k, j) V\left(\frac{j\pi}{m}, t\right), \quad (53)$$

where $C(k, j) = \frac{2}{m} \sum_{p=1}^{m-1} \sin\left(\frac{pk\pi}{m}\right) \exp(-p^2 \Delta t) \sin\left(\frac{pj\pi}{m}\right)$. (54)

These give the exact solution to the equations as a finite-difference stepping formula. The matrix $C(\Delta t)$ can be worked out once at the beginning. To combine this idea with non-linear forcing is easy enough; instead of using a Runge-Kutta or whatever scheme to evaluate $\frac{\partial v}{\partial t} = \nabla^2 v + F$, we use it to evaluate $(\frac{\partial}{\partial t} - \nabla^2)v = F$, with a time step as usual, followed by the above (53) transformation. In fact, there seems considerable merit in bringing all of the linear parts of the equation to the left, on a general philosophy of using everything one knows. In this case, for the price of having $n-1$ interactions to handle instead of 3, we get exact answers (nth order), which allows arbitrary time-step size. This must be at least $(n-1)/3$ times as large to pay off. However, if a fast Fourier Transform is used to find $\{a_p\}$ and back, the ratio is only $\approx \log_2(n)/3$, which can be much smaller for the fine grids visualized. We follow N.A. Phillips in considering a prototype equation

$$\frac{\partial v}{\partial t} = \nu \frac{\partial^2 v}{\partial x^2} + \bar{u} \frac{\partial v}{\partial x} \quad (52m)$$

where \bar{u} is a stream velocity representing the non-linear terms. The second term on the right imposes a time-step limit like $\Delta t < \frac{\Delta x}{\bar{u}}$, whereas for conventional schemes the first imposes $\Delta t < \frac{(\Delta x)^2}{2\nu}$. This will be more restrictive than the first if

$$\Delta x < \frac{2\nu}{\bar{u}}, \quad (55)$$

where the right side represents a viscous boundary thickness. Thus, this new disguised spectral scheme may well be useful for looking at a boundary layer structure, as we are doing here. A few evaluations of the matrix $C(\Delta t)$ showed it to be near block-diagonal for Δt small, and in fact, clearly $C(n,k)$ represents the influence of each region on the others; for small time, only nearby vorticity can diffuse over. We note that

$$C_n(k,m) = \frac{2}{\pi} \sum_{p=1}^{m-1} \exp\left\{-\frac{\pi^2 p^2 (\nu \Delta t m)}{\pi^2}\right\} (\sin k \frac{p\pi}{n}) (\sin m \frac{p\pi}{n}) (\frac{\pi}{m})$$

and write $\Delta x = \pi/n$, $x = p\pi/n$, $\alpha \equiv \frac{\nu \Delta t}{(\Delta x)^2}$ to see this is a partial sum for an integral

$$C(k,m) \approx \frac{2}{\pi} \int_0^\pi \exp\{-\alpha x^2\} \sin kx \sin mx \, dx.$$

Now, $\exp(-\pi^2) \ll 1$ and we are interested in $\alpha \gtrsim 1$ (otherwise, old formulas are stable), so may change the upper limit of integration and use trigonometric addition formulas to get

$$C(k,m) \approx \frac{2}{\pi} \int_0^\infty \exp\{-\alpha x^2\} [\cos \frac{(k-m)x}{2} - \cos \frac{(k+m)x}{2} - \cos \frac{(2n-k-m)x}{4}] dx$$

$$= \frac{1}{4\sqrt{\pi\alpha}} [2 \exp\{-\frac{(k-m)^2}{4\alpha}\} - \exp\{-\frac{(k+m)^2}{\alpha}\} - \exp\{-\frac{(2n-k-m)^2}{\alpha}\}] \quad (56)$$

from (1.4.11) p 15 of Erdelyi, et al (1954), Vol. 1. The latter two terms represent reflection in the walls. Higher order reflections have been (properly) suppressed in the approximation. Numerical experiments show this to hold well even for $n = 5$, and it considerably eases the work of evaluating C , and may even be more accurate than the sum (54), since there will be no round-off error. The $\exp\{-x^2\}$ behavior shows how far one needs to evaluate; there is no

use going beyond the accuracy of the machine or data.

While Cartesian coordinates were clearer for exposition, we are interested in cylindrical coordinates, where

$$\frac{\partial V}{\partial t} = \frac{\partial}{\partial r} \left(\frac{\partial}{\partial r} + \frac{1}{r} \right) V, \quad (52a)$$

so write $B^m(r) = Y_1(\lambda_m) J_1(\lambda_m r) - J_1(\lambda_m) Y_1(\lambda_m r)$, where λ_m is such that $B^m(\lambda_m \eta^{-1}) = 0$. For wide gap, one needs to numerically invert the matrix B to form C, which hardly pays. For narrow gap, one can use the asymptotic formulas (9.2.9) and (9.2.10) of Abramowitz and Stegun (1965) to get

$$B^m(r) = \frac{1}{\sqrt{r}} \sin\left(\frac{(1-\eta^{-1})m\pi}{\eta^{-1}-1}\right) + O\left[\frac{(1-\eta^{-1})^{5/2}}{10m^{3/2}}\right].$$

Proceeding now exactly as for the Cartesian case, we get

$$\begin{aligned} C(k,m) &\sim \frac{2}{\pi \sqrt{\lambda^k}} \int_0^\pi \sqrt{1 + \frac{(\eta^{-1}-1)}{\pi}} \exp(-\alpha y) \sin(ky) \sin(my) dy \\ &\sim \frac{(1 + \frac{1-\eta^{-1}}{2})}{4(\alpha\pi)^{1/2} \sqrt{1 + (\eta^{-1}-1) \frac{k}{2\pi}}} \left[2 \exp\left\{-\frac{(k-m)^2}{\alpha}\right\} - \exp\left\{-\frac{(k+m)^2}{\alpha}\right\} - \exp\left\{-\frac{(2m-k+m)^2}{\alpha}\right\} \right]. \end{aligned} \quad (56a)$$

This provides a good approximation for narrow gap which ought to speed the numeric integration of parabolic schemes on fine grids in cylindrical coordinates.

The system of equations (51) requires $D_* V$ as well as V .

This can be found in the same disguised spectral fashion as

$$D_* V \approx \sum_{m=1}^{n-1} V(r^m) \sqrt{\frac{\lambda^m}{\lambda^j}} \frac{1}{\pi(\eta^{-1}-1)} \left[\frac{1 - (-1)^{j-m}}{(j-m)^2} (1 - \delta_{mj}) + \frac{\pi^2}{2} \delta_{mj} - \frac{1 - (-1)^{m+j}}{(m+j)^2} \right].$$

Experimental Comparison.

Christensen [see Chen and Christensen (1967)] gathered data on the instability for started cylinder with radius $1/4$

inch in distilled water. Christensen's original data is reproduced in Table 3, along with the corresponding δ'_a and N 's. This data consists essentially of the time at which instability was first observed, as Ω varied, and are plotted in non-dimensional form in figure 13. Thus, all of the points marked are in the unstable region, and it is satisfying how well they all fall just above the marginal lines given in the last section.

After the critical time.

In the similar problem of Görtler cells on a concave surface, Lin (1966) neglects the viscous terms. His student D'Arcy (1951) used a broken line approximation to the basic flow to compute the first and second modes, and found patterns very close to Görtler's. Let us look at how this might work.

The axisymmetric linearized equations of motion are

$$\begin{aligned}
 \frac{\partial u}{\partial t} &= -\frac{\partial p}{\partial r} + 2\frac{v}{r}v + \nu \left(\frac{\partial^2 u}{\partial r^2} + \frac{1}{r} \frac{\partial u}{\partial r} - \frac{u}{r^2} + \frac{\partial^2 u}{\partial z^2} \right) \\
 \frac{\partial v}{\partial t} &= -u D_* v + \nu \left(\frac{\partial^2 v}{\partial r^2} + \frac{1}{r} \frac{\partial v}{\partial r} - \frac{v}{r^2} + \frac{\partial^2 v}{\partial z^2} \right) \\
 \frac{\partial w}{\partial t} &= -\frac{\partial p}{\partial z} + \nu \left(\frac{\partial^2 w}{\partial r^2} + \frac{1}{r} \frac{\partial w}{\partial r} + \frac{\partial^2 w}{\partial z^2} \right) \\
 D_* u + \frac{\partial w}{\partial z} &= 0
 \end{aligned} \tag{57}$$

Let us look for an appropriate growth time-scale T so

$$\frac{\partial}{\partial t} \rightarrow \frac{1}{T}, \frac{\partial}{\partial r} \rightarrow \frac{1}{\delta R}, \frac{\partial}{\partial z} \rightarrow \frac{\alpha}{R}, r \rightarrow R(1+\delta x), v \rightarrow \Omega R.$$

The continuity equation forces scales $W \sim U/\alpha\delta$, and (57.4)

becomes

$$\left(\frac{\partial u}{\partial x} + \delta \frac{u}{r}\right) + \frac{\partial w}{\partial z} = 0.$$

The vertical momentum equation forces a pressure scale

$$P = \frac{RU}{\alpha^2 \delta T}, \text{ and (57.3) becomes}$$

$$\frac{\partial w}{\partial t} = -\frac{\partial p}{\partial z} + \frac{T}{t_0} \left(\frac{\partial^2 w}{\partial x^2} + \frac{\delta}{1+\delta x} \frac{\partial w}{\partial x} + \alpha^2 \delta^2 \frac{\partial^2 w}{\partial z^2} \right). \quad (58)$$

Now the quasi-steady assumption is that the perturbation time scale T is much smaller than the basic time scale t_0 . Thus, the viscosity in (58) is precisely as negligible as the quasi-steady assumption is good, once past the initial marginal stability. Thus, just as Lin suggests, (and Lamb before him), the viscosity may be neglected, so

$$\frac{\partial w}{\partial t} = -\frac{\partial p}{\partial z}.$$

Substituting the pressure scale found above into the u-momentum equation forces scales $|u| \sim |v| \alpha^2 \delta^2 N(T/t_0)$, and shows the viscosity here to be $O(\alpha^2 \delta^2 T/t_0)$, even more negligible. We get a curious quasi-centrifugal balance

$$\alpha^2 \delta^2 \frac{\partial u}{\partial t} = -\frac{\partial p}{\partial x} + 2Vv/r.$$

We earlier found that the first α 's to emerge have scales $\alpha \sim \frac{1}{\Omega t_0}$ evaluated at that time, so $\alpha^2 \delta^2$ is certainly small. However, it happens to have been preserved throughout.

Putting the u/v scale into the v equation forces the growth time scale

$$T/t_0 = \frac{1}{\alpha \Omega t_0 \delta^2}. \quad (59)$$

For this to be small, either t_0 must be several times the marginal growth time, or else α must be large. In fact, it

is found below that the larger wave numbers do grow more rapidly at this time. This fits Foster's picture of the growth of disturbances in the analogous started Benard problem: the long disturbances start growing first, but do not grow as rapidly as shorter disturbances starting later.

It also fits the observation that the wavelengths are quite random when at finite size.

Again dropping the viscosity as being $O(T/t_0)$,

$$\frac{\partial v}{\partial t} = -\left(\frac{\partial v}{\partial x} + \delta v/r\right)u.$$

Writing the variables with $e^{\sigma t}(\sin z, \cos z)$, the equations are

$$\begin{aligned} \frac{\partial u}{\partial x} + \delta \frac{u}{\lambda} &= w \\ \sigma w &= -p \\ \alpha^2 \delta^2 \sigma^2 u &= -\frac{\partial p}{\partial x} + 2\frac{v}{\lambda} \\ \sigma v &= -\left(\frac{\partial v}{\partial x} + \delta \frac{v}{\lambda}\right)u, \end{aligned} \quad (60)$$

from which w , p , and v may be eliminated:

$$\frac{\partial}{\partial x} \left(\frac{\partial}{\partial x} + \frac{\delta}{1+\delta x} \right) u - \left[\frac{2}{\sigma^2} \frac{v}{1+\delta x} \left(\frac{\partial v}{\partial x} + \delta \frac{v}{1+\delta x} \right) + \alpha^2 \delta^2 \right] u = 0, \quad (60b)$$

with $u(0) = 0$, $u \rightarrow 0$ as $x \rightarrow \infty$, and $\frac{\partial u}{\partial x} = 1$ at $x = 0$, to normalize. This defines an eigenvalue problem for $\sigma^2(\delta)$, since $v = v(\delta)$. It is worth noting that the other two viscous boundary conditions ($v = w = 0$) can both be taken care of in a thinner boundary $O((T/t_0)^{\frac{1}{2}})$ without affecting this boundary.

Let us first consider the broken line model

$$v = \begin{cases} 1 - x, & \text{for } 0 < x < 1 \\ 0, & \text{for } x > 1 \end{cases} \quad (61)$$

as do D'Arcy, Lick and Currie. This gives exponential

solutions for u in the two regions, which must match continuously at $x = 1$, must be 0 at $x = 0$ and as $x \rightarrow \infty$.

This requires

$$u = A \sin(x \sqrt{\frac{1}{\sigma^2} - \delta}) \quad \text{for } x < 1,$$

$$u = B K_1(\alpha \delta x) \quad \text{for } x > 1,$$

which requires [to $O(\delta)$]

$$\sqrt{\frac{\sigma^2}{1-\delta\sigma^2}} \tan \sqrt{\frac{1}{\sigma^2} - \delta} = -\frac{1}{\alpha} \tanh \alpha(1-\delta). \quad (62)$$

For given α and δ , this determines σ^2 , if it exists. We see that there are an infinite number of modes for which the sine is just enough past a peak to smoothly match the declining K , so $\sqrt{\frac{1}{\sigma^2} - \delta} \approx (n + \frac{1}{2})\pi$, and $\sigma \approx \frac{1}{(n + \frac{1}{2})\pi}$, so the lowest mode grows fastest. The n th mode has n rolls stacked radially, with the outer one stretching from inside $x = [r - 1 = \delta]$ to ∞ . This corresponds to D'Arcy's results and illuminates the following.

Let us now consider the better approximation $V = \operatorname{erfc}(x/2)$, so $\frac{\partial V}{\partial x} = \frac{\delta}{\sqrt{\pi}} \exp(-x^2/4)$. To facilitate wave-number comparisons, let us temporarily take α out of the time-scale, so $T/t_0 = (N\delta^2)^{-1}$, and consider

$$\frac{\partial^2 u}{\partial x^2} + \frac{\delta}{1+\delta x} \frac{\partial u}{\partial x} - \left[\frac{\alpha^2}{\sigma^2} \frac{\delta}{\sqrt{\pi}} \exp(-x^2/4) \operatorname{erfc}(x/2) + \alpha^2 \delta^2 \right] u = 0, \quad (63)$$

where $u(0) = 0$, $\left. \frac{\partial u}{\partial x} \right|_0 = 1$, and $\sigma(\alpha, \delta)$ is such that $u \rightarrow 0$ as $x \rightarrow \infty$. This is an ordinary differential equation with non-constant coefficients, so seemed well suited to solution on an analog computer.

The function multiplying u must be generated by the analog computer. We note that the erfc satisfies the differential equation

$$\frac{d^2}{dx^2} [\operatorname{erfc}(x)] + 2x \frac{d}{dx} [\operatorname{erfc}(x)] = 0, \quad (63b)$$

with $\text{erfc}(0) = 1$ and $\frac{d}{dx} \text{erfc}(0) = 2/\sqrt{\pi}$.

This was first generated from equation (63b) using a circuit

where standard notation is used. Adjusting the coefficients a little brought erfc to within .0003 of its exact value at several points, and brought erfc to zero as x increased. Naturally, x must be restricted, usually to $x \leq 5$ here and below.

With erfc well approximated, the whole equation can now be solved. The whole circuit, in one of its forms, including some necessary debiasing, used is shown in figure 15. This circuit grew considerably from the initial conception, the lower right corner represents the equation.

The solution $u(x; \sigma, \alpha, \delta)$ behaves very like a line $a + bx$ once $x \gg 1$. We want to find when both a and b match the exterior solution $K_1(\alpha r)$, which requires

$$a + bx = cK_1(\alpha) + c K_1'(\alpha) \approx K_1(\alpha(1+\delta x))$$

using a Taylor expansion. A c can be found iff

$$\frac{b}{a} \frac{K_1(\alpha)}{\alpha K_1'(\alpha)} = \delta \tag{64}$$

For each α , σ , and δ , the equation (63) was integrated and ramp $a + bx$ was also. This latter was adjusted until asymptotic to the solution u , and the a and b were recorded.

Figure 15 -- An analog circuit used.

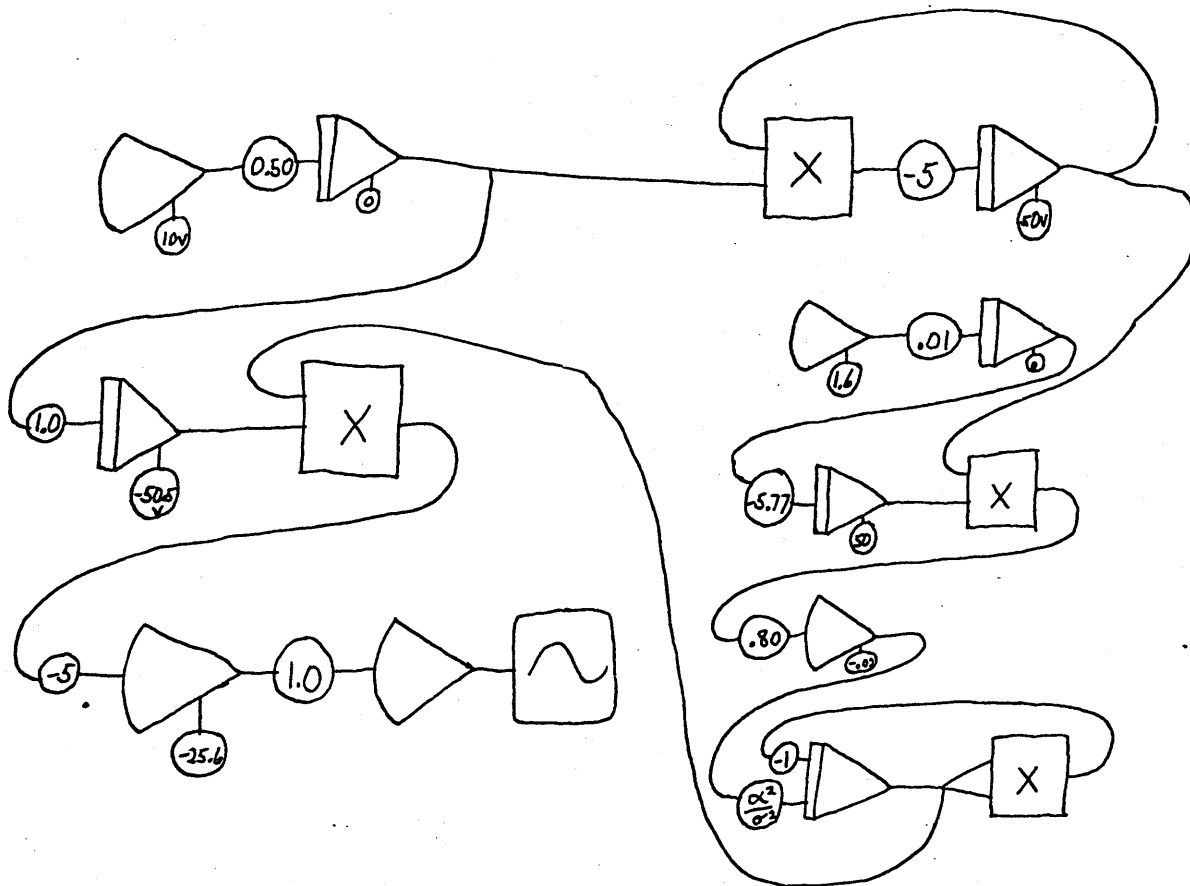


TABLE 4

Eigenvalues σ^2 to satisfy $DD_x u - \left(\frac{2}{\sigma^2} \frac{V}{N} D_y V + \alpha^2 \delta^2 \right) u = 0$,
with boundary conditions $u(0) = 0$, $u(\infty) = 0$.

wave #	σ_1^2	σ_2^2
for $\delta = 0.1$:		
5.0	0.4099	
4.0	0.44965	0.109
3.0	0.49514	
2.0	0.548	
1.0	0.6079	0.1205
0.7	0.6280	
0.5	0.6426	
0.3	0.6578	
0.1	0.6708	0.129
for $\delta = 0.6$:		
1.0	0.2195	0.0563

growth rate $\sigma \rightarrow$

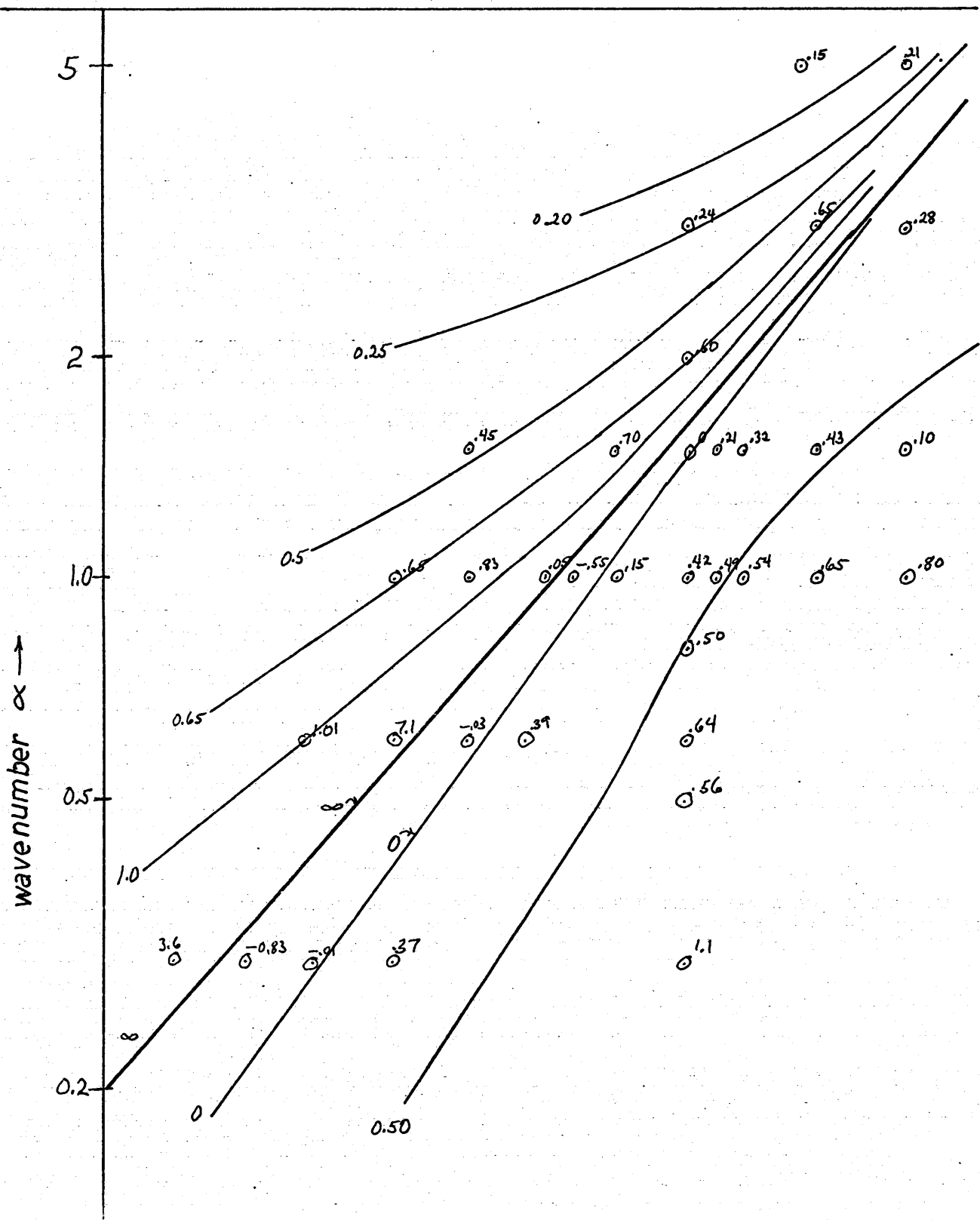


Figure 16. Contours of $\frac{b K_1(\alpha)}{a \alpha K_1'(\alpha)}$

The ratio $\frac{b}{\alpha} \frac{K_1(\alpha)}{K_1'(\alpha)}$ is recorded and contoured in figure 16 for $\delta = 0.1$. Plainly the contour for $\delta = 0.1$ [the intersection for (64)] is close to the zero contour, and $\sigma \approx 0.8 \alpha^{3/4}$. Thus, long waves grow more slowly than short in this quasi-steady range. Actually viscosity would come into play as α increases, stabilizing short waves and causing a most unstable α , which will change with time. For a check, this problem was also integrated on the digital computer for a few cases presented in Table 4. The results are very similar.

Energy Bounds for Stability

A guaranteed stability bound can be gotten from the energy equation for the full non-linear, time-dependent incompressible Navier-Stokes equations, if we assume axisymmetry. The formulas follow Serrin's (1959a), though here we are interested in the minimum time at which there may be growth, rather than the minimum Reynold's number for a steady basic flow. If we maximize $\frac{\partial}{\partial t} KE$ of the perturbation kinetic energy over smooth perturbations (u,v,w) which satisfy the boundary conditions, and find the time that this maximum becomes positive, no perturbation kinetic energies can grow before this time. Following Serrin, we find a stationary value of the generation minus dissipation, subject to the constraint of continuity. The variational equations are similar to the quasi-steady equations in form:

$$\begin{aligned}
\text{Re } v \lambda \frac{\partial(\frac{V}{\lambda})}{\partial r} &= -\frac{\partial \lambda}{\partial r} + 2 \left\{ (DD_* + \frac{\partial^2}{\partial z^2} + \frac{\partial^2}{r^2 \partial \theta^2}) u - \frac{2}{r^2} \frac{\partial V}{\partial \theta} \right\} \\
\text{Re } u \lambda \frac{\partial(\frac{V}{\lambda})}{\partial r} &= -\frac{\partial \lambda}{r^2 \partial \theta} + 2 \left\{ (DD_* + \frac{\partial^2}{\partial z^2} + \frac{\partial^2}{r^2 \partial \theta^2}) v + \frac{2}{r^2} \frac{\partial u}{\partial \theta} \right\} \\
0 &= -\frac{\partial \lambda}{\partial z} + 2 \left\{ (DD_* + \frac{\partial^2}{\partial z^2} + \frac{\partial^2}{r^2 \partial \theta^2}) w, \right.
\end{aligned} \tag{65}$$

with $\frac{\partial(uw)}{r \partial r} + \frac{\partial v}{r \partial \theta} + \frac{\partial w}{\partial z} = 0$, and $u = v = w = 0$ at $r = 1$ and as $r \rightarrow \infty$.

The interesting feature here is that these equations give a rigorous bound, and do not include a vague 'quasi-steady' assumption. Thus, given the time, and hence the shape V , the eigenvalue Re of these equations provides an absolute bound. Unfortunately, they are very difficult to solve, even numerically. If one relies on the observation that the perturbations are axisymmetric in the experiments under consideration, the equations can be simplified to

$$\begin{aligned}
(DD_* - a^2)^2 u &= -\frac{1}{2} \text{Re } a^2 \left(\frac{\partial V}{\partial r} - \frac{V}{r} \right) v \\
(DD_* - a^2) v &= \frac{1}{2} \text{Re} \left(\frac{\partial V}{\partial r} - \frac{V}{r} \right) u,
\end{aligned} \tag{66}$$

with $u = v = Du = 0$ at $r = 1$ and as $r \rightarrow \infty$. These are just like the quasi-steady equations already integrated, with slightly different V coefficients. These were integrated for several values of δ with a 'broken-line' profile

$$V = \frac{1}{\delta(2+\delta)} [-r + (\delta+1)^2/r],$$

$$\text{so } DV = -\frac{1}{\delta(1+\frac{\delta}{2})}$$

for $1 < r < 1 + \delta$, and both 0 for $r > 1 + \delta$. The Re 's found are plotted on figure 13 also. They are not as far below the actual critical values as one might expect from such a general criterion. An interesting feature of the integrations was that the wave-number a for minimum Re increased very rapidly as δ became small, and Re was quite sensitive to a^2 for δ near 1.

Thus, the picture seems fairly complete; After the

cylinder starts, a viscous boundary layer forms and thickens until the Reynolds number based on its thickness is about 30, when generation can match dissipation for certain long rolls. After this, the importance of viscosity for the perturbations decreases, and shorter waves may grow, and faster than the long rolls. As the mixture of rolls reaches finite amplitude, they will take over the transmission of angular momentum from the basic flow, discouraging the growth of further rolls. The first mode will grow fastest, so all of the rolls will have a structure which intensifies out to $r - 1 \approx \delta^-$, then decays on a scale $\propto R$, which can be several radii for the longer rolls. Ink in the inner boundary will be drawn out in disks between the rolls, just as observed.

Acknowledgments

I acknowledge my particular indebtedness to:

Professor L. N. Howard, for being an encouraging thesis advisor.

The Electrical Engineering Department, J. McKenzie in particular, for allowing me to use the PDP-1 computer to do the extensive computations, draw graphs, and even type this thesis. In this connection Charles Landau did some of the programming, Luella Thompson did most of the typing, and W. B. Ackermann helped when the machine would not cooperate. Many other computer hackers also willingly offered advice.

Prof. S. K. F. Karlsson of Brown University Engineering Department for allowing me access to the Taylor apparatus, and having patience when accessories ground down, pipes clogged, and a flood awakened him at 2 A.M. Colin Hackett for helping me with the maze of pipes and valves.

Prof. C. Rooth at Woods Hole Oceanographic Institution for the original problem in Chapter One, and for use of the equipment used in those experiments.

Prof. G. Veronis and the National Science Foundation for providing two pleasant summers at the Woods Hole

Oceanographic Institution Geophysical Fluid Dynamics summer seminars among some of the most stimulating people of the field, and where this thesis was started and finished. Professors F. Busse and W. V. R. Malkus, for encouraging discussions there.

Prof. C. S. Chen for providing the original data for the started cylinder.

The Mechanical Engineering Department of M.I.T. for use of their analog computer.

Professors E. Mollo-Christensen, E. N. Lorenz, and the rest of the Meteorology Department, for doing interesting things. M.I.T., for providing a nice office overlooking the Charles and other facilities.

The Hertz and Ford Foundations, for providing a comfortable standard of living.

BIBLIOGRAPHY

- Abramowitz, M., and Stegun, I. A., (Eds), (1964), Handbook of Mathematical functions with formulas, graphs, and math tables., Wash., U.S. Govt. Printing Office, XIV, 1046p.
- Aldridge, K. D., (1967), An experimental study of axisymmetric inertial oscillations of a rotating liquid sphere., Ph.D. Thesis, Massachusetts Institute of Technology.
- Allen, E. E., (1954), Analytical approximations., Math. Tables Aids Comp., 8, 240-241.
- Baines, P. G., (1967), Forced oscillations of an enclosed rotating fluid., J. Fluid Mech., 30, 533-546.
- Barrett, K. E., (1967), On the impulsively started rotating sphere., J. Fluid. Mech., 27, 779-788.
- Benjamin, T. B., and Ursell, F., (1954), The stability of a plane free surface of a liquid in vertical periodic motion., Proc. Roy. Soc., A 225, 505.
- Betchov, R., and Criminale, W. O., Jr., (1967), Stability of Parallel Flows., Academic Press, New York, 330p.
- Busse, F., (1967), Shear flow instabilities in rotating systems., Abstract in Geophysical Fluid Dynamics Notes. 11, 221-222.

Carrier, G. F., and DiPrima, R. C., (1956), On the torsional oscillations of a solid sphere in a viscous fluid., J. Appl. Mech., 23, 601.

Chandrasekhar, S., (1958), The stability of viscous flow between rotating cylinders., Proc. Roy. Soc., A, 246, 301-311.

Chandrasekhar, S., (1961), Hydrodynamic and hydromagnetic stability., Oxford Univ. Press, London.

Chen, C. F., and Christensen, D. K., (1967), Stability of flow induced by an impulsively started rotating cylinder., Physics of Fluids, 10, No. 8, 1845-1846.

Coddington, E. A., and Levinson, N., (1955), Theory of ordinary differential equations., McGraw Hill, New York.

Coles, D., (1965), Transition in circular Couette flow., J. Fluid Mech. 21, 385-425.

Conrad, P. W., and Criminale, W. O., Jr., (1965), The stability of time-dependent laminar flow with curved streamlines. Z. Angew. Math. Phys., 16, 569-581.

Coster, D., (1919), The rotational oscillations of a cylinder in a viscous fluid., Phil Mag., No. 6, 37, 587-594.

111

Crow, S., (1965), Geophysical Fluid Dynamics Student Lectures, Woods Hole Oceanographic Institution.

Currie, I. G., (1967), The effect of heating rate on stability of stationary fluids., J. Fluid Mech., 29, 337-348.

D'Arcy, D., (1951), Studies in vertical flow., M.S. Thesis, Massachusetts Institute of Technology.

Donnelly, R. J., (1958), Experiments on the stability of viscous flow between rotating cylinders. I. Torque Measurements., Proc. Roy. Soc., A 246, 312-325.

Donnelly, R. J., (1964), Experiments on the stability of viscous flow between rotating cylinders. III. Enhancement of stability by modulation., Proc. Roy. Soc., A 281, 130-139.

Edmunds, D. E., (1963), On the uniqueness of viscous flows., Arch. Rational Mech. Anal., 14, 171-176,

Erdelyi, A., (1954), Tables of Integral Transforms., McGraw Hill, New York.

- Fage, A., (1938), The influence of wall oscillations, wall rotation, and entry eddies on the breakdown of laminar flow in an annular pipe., Proc. Roy. Soc., A 165, 501-529.
- Foster, T. D., (1964), Some comments on hydrodynamic stability theory when nonlinear temperature profiles are present., unpublished.
- Foster, T. D., (1965), Stability of a homogeneous fluid cooled uniformly from above., Phys. Fluids, 8, 1249-1257.
- Fultz, D., (1959), A note on overstability and the elastoid-inertia oscillations of Kelvin, Solberg, and Bjerknes., J. Meteor., 16, 199-208.
- Fultz, D., (1965), Lecture given at Midwestern Mechanics Conference.
- Fultz, D., and Murty, T. S., (1968), Effects of the radial law of depth on the instability of inertial oscillations in rotating fluids., submitted.
- Greenspan, H. P., and Howard, L. N., (1963), On the time-dependent motion of a rotating fluid., J. Fluid Mech., 17, 385-404.
- Hammerlin, G., (1955), Über das eigenwertproblem der drei-dimensionalen Instabilität laminarer Grenzschichten an konkaven Wänden., J. Rat. Mech. Anal., 4, 279-321.

Hastings, C. B., (1955), Approximations for digital computers.,
Princeton Univ. Press, Princeton, New Jersey.

Helmholtz, H., (1868), Über diskontinuierliche Flüssigkeitsbewegungen
Monats. Könige. preuss. Akad. Wisc. Berlin, 215-228.

Howard, L. N., (1968), Geophysical Fluid Dynamics Lecture Series
Notes, Woods Hole Oceanographic Institution.

Howard, L. N., (1963), Heat transport by turbulent convection.,
J. Fluid Mech., 17, 405-432.

Ito, S., (1961), The existence and uniqueness of regular
solutions of the non-stationary Navier-Stokes equations,
J. Fac. Sci. Univ. Tokyo, Sect. 1, 9, 103-140.

Johnson, J. A., (1963), The stability of shearing motion in
a rotating fluid., J. Fluid Mech., 17, 337-352.

Johnson, L., (1967), Geophysical Fluid Dynamics Student Lectures,
Woods Hole Oceanographic Institution.

Kelly, R. E., (1965), The stability of an unsteady Kelvin-Helmholtz
flow., J. Fluid Mech., 22, 547-560.

Kelly, R. E., (1967), On the stability of an inviscid shear layer which is periodic in space and time., J. Fluid Mech., 27, 657-689.

Kirchgässner, K., (1961), Die Instabilität der Strömung zwischen zwei rotierenden Zylindern gegenüber Taylor-Wirbeln für beliebige Spaltbreiten., Z. Angew. Math. Phys., 12, 14-30.

Lick, Wilbert, (1965), The instability of a fluid layer with time-dependent heating., J. Fluid Mech., 21, Part 3, 565-576.

Lin, C. C., (1955), The theory of hydrodynamic stability., Cambridge Univ. Press, Cambridge.

Lin, C.C., (1966), The theory of hydrodynamic stability., Cambridge Univ. Press, Cambridge, (sec. ed.).

Longuet-Higgins, M. S., (1953), Mass transport in water waves., Phil. Trans., A, 245, 535-581.

Longuet-Higgins, M. S., (1960), Mass transport in the boundary layer at a free oscillating surface., J. Fluid Mech., 8, 293-306.

McDonald, B. E., and Dicke, R. H., (1967), Solar Oblateness and Fluid spin-down., Science, 158, 1562-1564.

- Mallick, D. D., (1957), Nonuniform rotation of an infinite circular cylinder in an infinite viscous fluid., Z. Angew. Math. Mech., 37, 385-392.
- Meister, B., and Munzer, W., (1966), Das Taylorsche Stabilitätsproblem mit modulation., Z. Angew. Math. and Phys., 17, 537-540.
- Miles, J. W., (1964), Free-surface oscillation in a slowly rotating liquid., J. Fluid Mech., 18, 187-194.
- Orr, W. McF., (1907), The stability or instability of the steady motions of a liquid., Proc. Roy. Irish Acad., A27, 9-138.
- Phillips, N. A., (1963), Geostrophic Motion, Reviews of Geophysics, 1, No. 2, 123-176.
- Rayleigh, Lord, (1884), On the circulation of air observed in Kundt's Tubes, and on some allied acoustical problems., Phil. Trans. Roy. Soc., 1-22.
- Rayleigh, Lord, (1916), On the dynamics of revolving fluids., Scientific Papers, Vol. 6, 447-453, Cambridge Univ. Press, London.
- Reynolds, O., (1883), An experimental investigation of the circumstances which determine whether the motion of water shall be direct or sinuous, and of the law of resistance in parallel channels., Scientific Papers, 2, 51-105, Cambridge Univ. Press, London.

Robinson, J. L., (1966), Two problems in convection; Thermal instability in an infinite region, and finite amplitude convection cells., Ph.D. Thesis, Massachusetts Institute of Technology, Department of Mathematics.

Rosenblat, S., (1968), Centrifugal instability of time-dependent flows. Part 1. Inviscid, periodic flows., J. Fluid Mech., 33, 321-336.

Schlichting, H., (1968), Boundary Layer Theory., J. Kestin, Ed., McGraw Hill, New York.

Serrin, J., (1959a), On the stability of viscous fluid motions., Arch. Rational Mech. Anal., 3, 1-13.

Serrin, J., (1959b), A note on the Existence of periodic solutions of the Navier-Stokes equations., Arch. Rational Mech. Anal., 3, 120-122.

Snyder, H. A., and Karlsson, S. K. F., (1964), Experiments on the stability of Couette motion with a radial thermal gradient., Phys. Fluids, 7, 1696-1706.

Soberman, R. K., (1959), Onset of convection in liquids subject to transient heating from below., Phys. Fluids, 2, 131-138

- Sorger, P., (1966), Über ein Variationsproblem aus der nichtlinearen Stabilitätstheorie zäher, inkompressibler Strömungen., Z. Angew. Math. Phys., 17, 201-216.
- Sparrow, E. M., Munro, W. D., and Jonsson, V. K., (1964), Instability of the flow between rotating cylinders: the wide-gap problem., J. Fluid Mech., 20, 35-46.
- Stokes, G. G., (1886), On the effect of the rotation of cylinders or spheres about their own axes in increasing the logarithmic decrement of the arc of vibration., Math. and Phys. Pap., 5, 207-14
- Taylor, G. I., (1923), Stability of a viscous liquid contained between two rotating cylinders., Phil. Trans., A, 223, 289-343.
- Tranter, C. J., (1956), Integral transforms in mathematical physics., John Wiley and Sons, New York.
- Turner, J. S., and Frazel, R., (1958), Construction of a one-meter turntable., unpublished report.
- Urabe, M., (1965), Galerkin's procedure for non-linear periodic systems., Arch. Rational Mech. Anal., 20, 120-152.
- Winney, H. F., (1932), Rotary oscillation of a long circular cylinder in a viscous fluid., Phil. Mag., (7), 14, 1026-1032.

BIOGRAPHICAL SKETCH

Rory Thompson was born 10 May 1942 in Seattle, Washington of Alix Saunders and Richard Cuthbert Thompson. He attended his mother's kindergarten, then five elementary schools, a junior and two senior high schools, all in the San Diego, California area, and graduated with honors from Will C. Crawford High School there in 1959. He married Luella Hallas Thomas in 1960. Subsequently, he graduated with high honors from San Diego State College in 1962, majoring in maths, with a minor in physics, then received an M.S. in mathematics from San Diego State College in 1964. He received a Ford Fellowship to M.I.T. and later a Hertz Fellowship and a post-doctoral to the Canadian Meteorological Service. Earlier, he had gotten research and teaching assistantships at San Diego State College, as well as four minor scholarships, including one from the Folk Dance Federation of California. He has worked as a minor hardware installator, a flower salesman, a trainee at the U.S. Navy Electronics Laboratory in San Diego, a teacher of computer programming, a dishwasher, and a programmer. His publications so far include:

'Goodness of Fit for Two-Sample Tests', Annals of Math. Statist., Feb. 1966, with C. B. Bell and J. M. Moser.

'Bias of the Cramer -von Mises Test', J. Amer. Statist. Assoc., Mar. 1966.

'Evaluation of $I_m(b) = 2\pi^{-1} \int_0^{\infty} (\sin(x)/x)^m \cos(bx) dx$ and Similar Integrals', Math. Comput. April 1967.

'Antipodality of Continents and Oceans', Science, Sept. 1967.

'Distribution and Power of the Absolute Normal Scores One-Sample Test', J. Amer. Statist. Assoc. Feb. 1968, with Z. Govindarajulu and K.A. Doksum